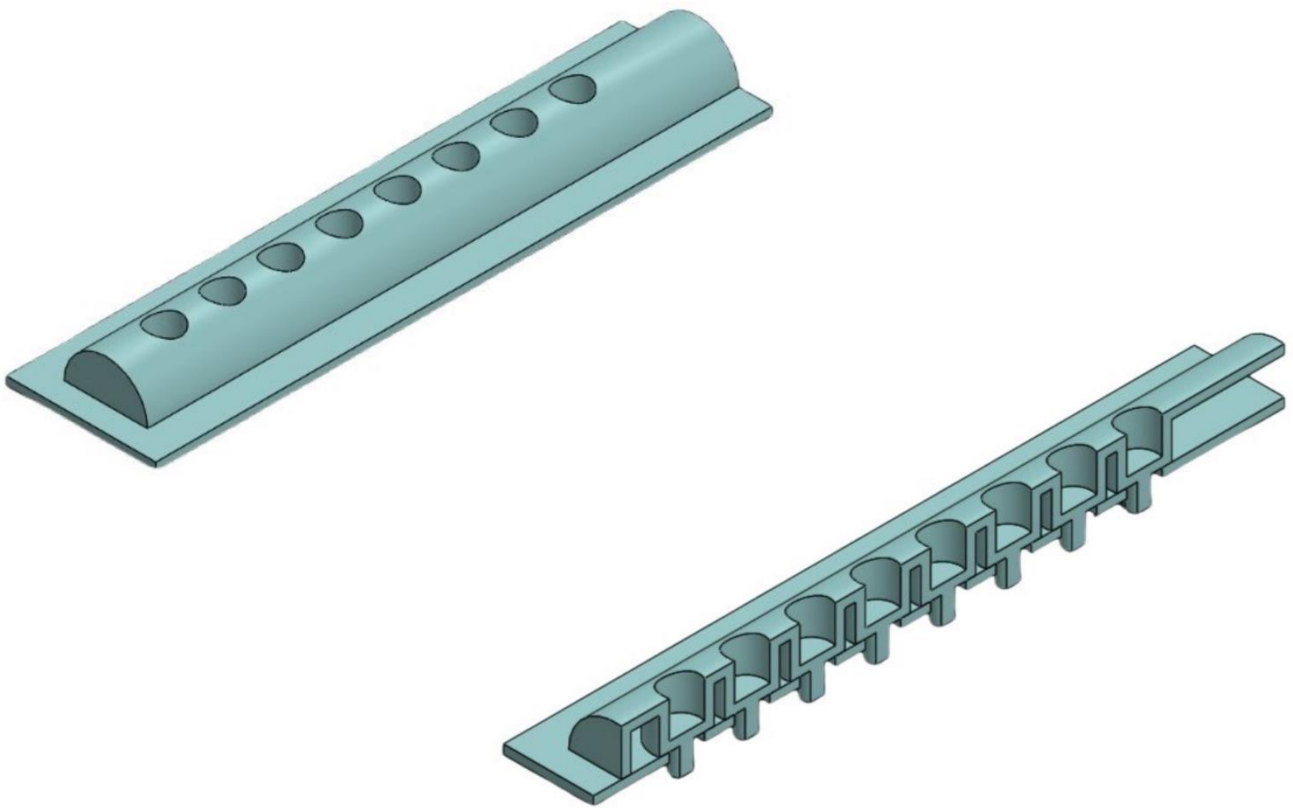


The ProSTATIC – a Suction based Stabilisation Instrument for the Prostate

A Design and Experimental study

- Güven Aydın -



The ProSTATIC – a Suction based Stabilisation Instrument for the Prostate

A Design and Experimental Study

By

Güven Aydın

In partial fulfilment of the requirements for the degree of

**Master of Science (MSc)
in Mechanical Engineering**
at the Delft University of Technology,

to be defended publicly on Thursday February 9, 2023 at 13:45

Student number:	4297725	
Project duration:	September 14, 2021 – February 9, 2023	
Supervisors:	Dr.ir. P. Breedveld	
	E. de Kater	
	J. Bloemberg	
Thesis committee:	Dr.ir. P. Breedveld	TU Delft
	E. de Kater	TU Delft
	J. Bloemberg	TU Delft
	Dr.ir.ing T.Horeman	TU Delft

An electronic version of this thesis is available at <http://repository.tudelft.nl/>.

Preface

As a young lad, I started my academic journey at the Delft University of Technology (TU Delft), not knowing the incredible adventures, valuable knowledge, and interesting people I would meet along the way. It is bittersweet to say, but my TU Delft journey has come to an end: I finished my Master's thesis. The research conducted in this study was performed within the BioMechanical Engineering department at the TU Delft, located in the Faculty of Mechanical, Maritime, and Materials Engineering (3ME). This study focussed on designing and testing an instrument that could stabilise the prostate gland during brachytherapy, which is a radiation method to treat prostate cancer by inserting needles with radioactive seeds into the prostate. The study resulted in the development of the ProSTATIC, which is a unique modular suction cup with self-regulating valves that can attach to different types of prostate surfaces to generate a grip force when a needle is inserted.

During the research study, I enjoyed learning the process of developing an instrument from a theoretical problem statement to an actual prototype. I acquired knowledge through manufacturing methods such as casting, new solutions, and in experimenting.

I would like to thank certain people, who helped me throughout my project. First of all, I want to thank Esther de Kater and Jette Bloemberg for their guidance, support, and valuable feedback throughout the project. Furthermore, I want to thank Paul Breedveld for putting in the effort and time for photographing the prototypes of my instrument, which was not easy at all. Last but not least, I want to thank my loved ones for the given love and support, not only during this project but throughout my life. What left to say is that I hope you will enjoy reading my project and be inspired in some way.

Güven Aydın

Delft, February 2023

Contents

1	Introduction	1
1.1	Prostate brachytherapy	1
1.2	Target deviation error	2
1.3	Stabilisation needles	4
1.4	Problem statement	5
1.5	Objective of the study	5
1.6	Structure of the study	5
2	Design direction	5
2.1	Anatomical analysis of the prostate	5
2.2	Mechanical analysis of needle insertion	6
2.3	Stabilisation methods for the prostate	6
2.4	State of the art: the Octopus heart stabiliser TM	6
2.5	Theoretical analysis suction	7
3	Design	8
3.1	Design requirements	8
3.2	Design process of the ProSTATIC	9
3.3	Final design of the ProSTATIC	10
4	Prototype	13
4.1	Material choice	13
4.2	Manufacturing method: Mould casting	13
4.3	Assembly of the ProSTATIC	14
5	Experimental evaluation	15
5.1	Experiment I: Self-regulating valves	15
5.2	Experiment II: Footprint grip	16
5.3	Experiment III: Prostate displacement	18
5.4	Data analysis	20
6	Experimental results	20
6.1	Experiment I: Self-regulating valves	20
6.2	Experiment II: Footprint grip	21
6.3	Experiment III: Prostate displacement	22
7	Discussion	22
7.1	Main findings & interpretation	22
7.2	Limitations & recommendations	25
7.3	Future work	26
8	Conclusion	28
9	References	28
	Appendices	33

The ProSTATIC – a Suction based Stabilisation Instrument for the Prostate

A Design and Experimental study

Güven Aydın 4297725

Abstract— Treatment of prostate cancer can be done by performing brachytherapy, where radioactive seeds are transperineally implanted in the prostate via needles. A known problem during treatments with needles is the risk of targeting errors caused by the deviation of the needle from the planned path in the prostate. One of the main sources of this error is the displacement of the prostate due to insertion of the needle. Often, stabilisation needles are used to stabilise the prostate, however, stabilisation needles alter prostate properties, damage tissue, and do not fully reduce prostate displacement. Therefore, in this study, we propose and evaluate an alternative solution that stabilises the prostate without additional tissue damage. The stabilisation solution is a modular suction cup referred as the ProSTATIC, which can be transperineally inserted via a 5 mm incision to attach to the prostate within the rectoprostatic space. The ProSTATIC has a multi-holed design consisting of three structural layers with their functionality; (1) the top to maintain the pressure inside of the suction cup and provide for structural stability, (2) the footprint to adapt and form a closed seal with the prostate surface, and (3) the self-regulating valves to increase the attachment reliability on irregular surface textures. For the footprint, we experimented with micro-patterns and suction hole sizes to increase the overall grip force. The prototype was completely fabricated out of biocompatible and ultrasound-compatible silicone rubber using mould casting. An experimental evaluation showed that the self-regulating valves work only on healthy prostate phantom. On healthy-tumorous and full tumorous tissue phantoms the suction holes deform, hindering the optimal working of the valves and leading to air leaks. Furthermore, only the prototype with the base footprint with enlarged suction holes (from 2 mm to 3.2 mm diameter) and radial ridges was able to generate a maximum grip force higher than the required 5 N for stabilisation and demonstrated that prostate displacement was reduced by 75% during needle insertion without the use of the ProSTATIC. The prototype proposed in this study forms an initial breakthrough in safe and reliable volumetric stabilisation of the prostate during brachytherapy.

Keywords— Suction cup – brachytherapy – prostate – stabilisation – medical- mould casting

1 INTRODUCTION

1.1 Prostate brachytherapy

Prostate cancer is with prostatitis and prostatic hyperplasia one of the most common and well-known diseases of the prostate [1]. In 2020 it was estimated that prostate cancer was the second most frequent cancer among men and responsible for being the fifth-highest cause of male mortalities [2]. The prostate is a doughnut-shaped gland about the size of a peach pit located underneath the bladder, surrounding the prostatic urethra as can be seen in Figure 1 [3, 4]. The gland is enclosed by a tough capsule consisting of dense irregular connective tissue [3]. The prostate itself is made of tubuloalveolar glands

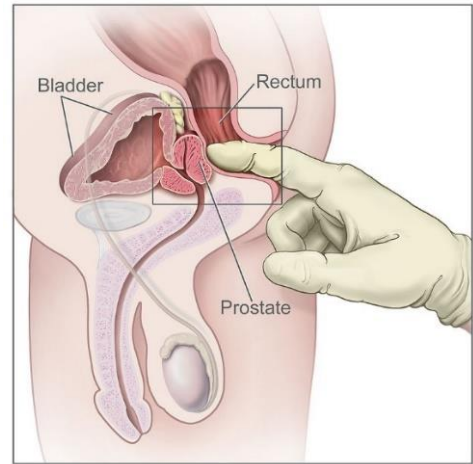


Figure 1: Visual representation of the male pelvic cavity during a rectal prostate examination [4].

embedded in a mass of smooth muscle and dense connective tissue. The prostate plays a role during male ejaculation where it releases a milky secretion to activate sperm.

Effective treatment of prostate cancer can be done by performing surgical methods. Brachytherapy is such a well-known method, in which small radioactive seeds are transperineally inserted in the prostate to kill cancerous cells via radiation as shown in Figure 2 [5, 6]. Other treatment methods are prostatectomy, where a part of or the entire prostate is removed [7], and external beam radiotherapy, where the prostate is treated with x-ray beams from outside of the body [8]. However, compared to brachytherapy the risk

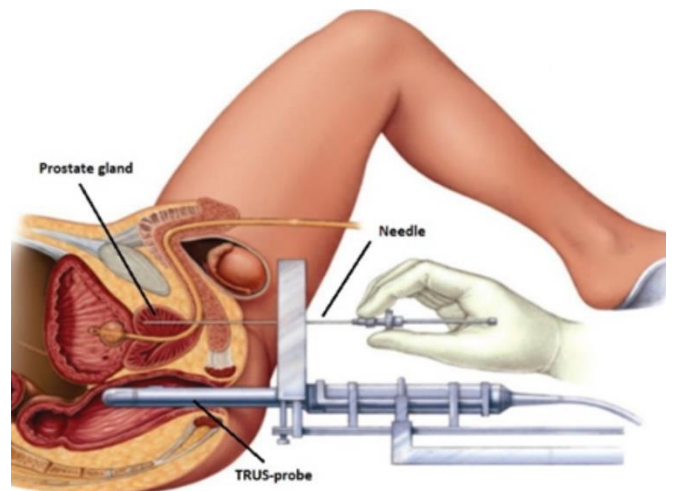


Figure 2: Schematic image of the pelvic cavity during a brachytherapy procedure of the prostate [6].

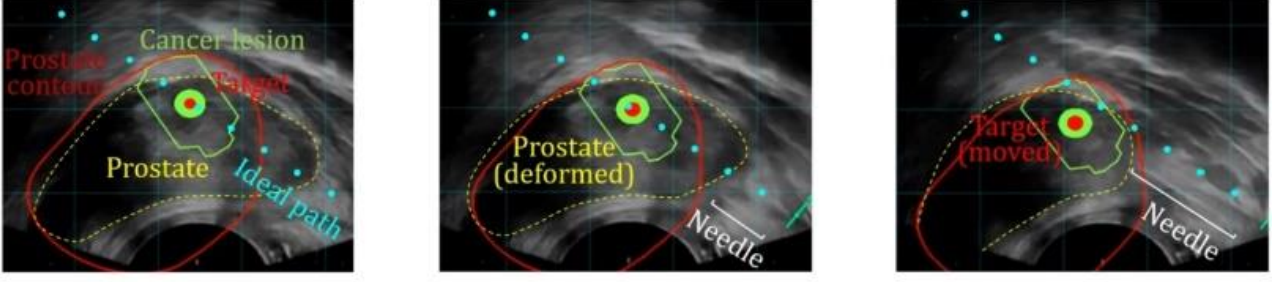


Figure 3: Ultrasound images of the insertion of a needle in the prostate. The needle (white) causes the prostate (yellow) to displace and deform, resulting in a deviation of the target (red) from the ideal insertion path (blue) [15].

of erectile dysfunction and urinary incontinence is much greater with these methods due to the more aggressive approach [9, 10].

Transperineal brachytherapy utilises needles for the insertion of the seeds within the prostate [5]. Also, during the diagnosis of cancer, needles are used to perform core biopsies, where a tissue sample is taken for laboratory research [11]. In medical practice, needle insertion is seen as puncturing tissue using a needle and advancing the needle through tissue [12]. However, in practice, needle insertions can have certain drawbacks concerning the needle-tissue interaction. Referring back to the prostate, a common experienced and well-documented drawback is an error in reaching the target location within the prostate due to deviation of the needle tip from the desired insertion path [13-16]. When referring to this error, the term target deviation

error will be used, where it is defined as the overall error in the three-axis of motion. Figure 3 gives a representation of the target deviation error [15]. Podder *et al.* [17] quantified in an *in-vitro* experiment that the target deviation error, measured as the distance between the actual needle tip location and the ideal location, was roughly 1.55 mm. This error can lead to ineffective treatment of prostate cancer and even unwanted damage to the surrounding tissue [18].

1.2 Target deviation error

Classification target deviation error

The target deviation error can be divided into intrinsic and extrinsic errors [19]. An intrinsic error is an error caused by the needle during the insertion into the prostate, whereas an extrinsic error is caused by other sources than the needle [19]. Figure 4 gives a categorised overview of the different types

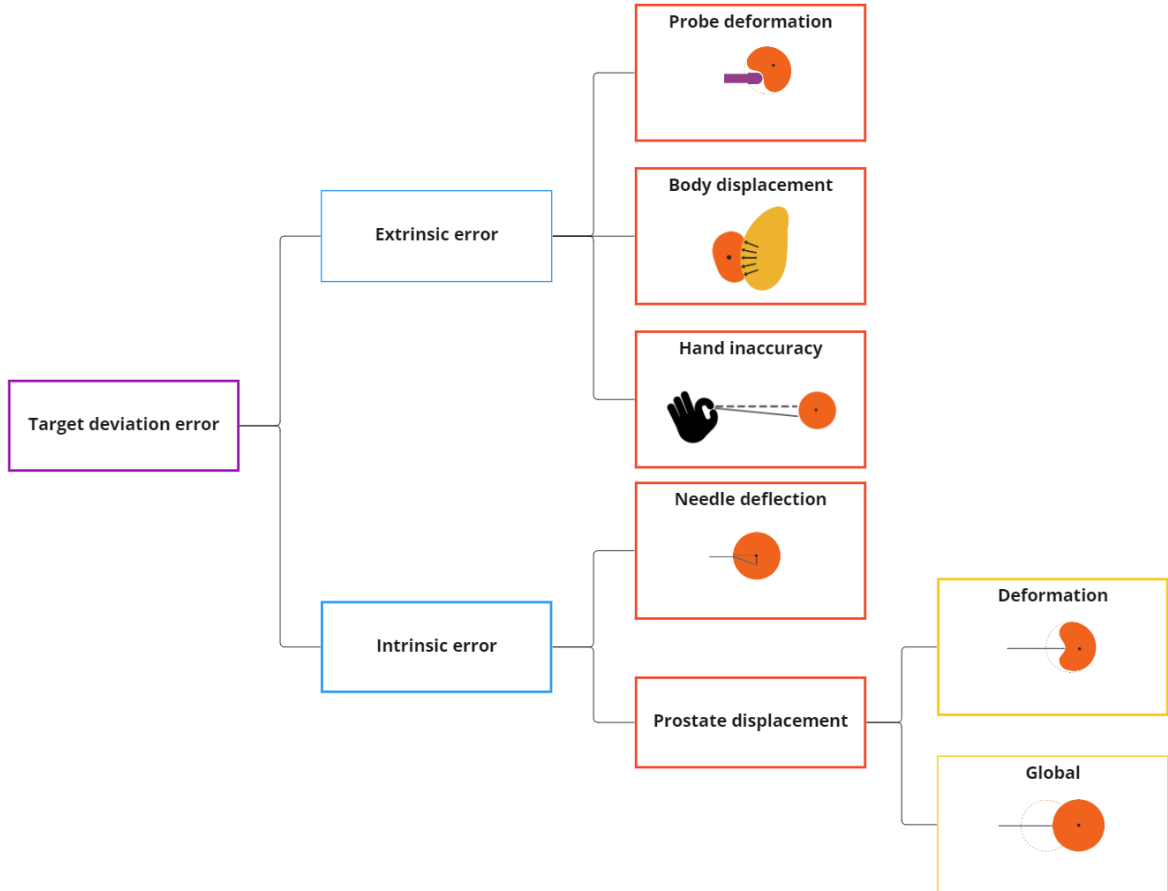


Figure 4: Overview of the components of the target deviation error. The overview shows the two components of the target deviation error (blue) and the different types of errors corresponding with these components (orange & yellow).

of intrinsic and extrinsic errors. The main types of intrinsic errors are prostate displacement by needle-induced forces [20] and needle deflection [21]. Prostate displacement itself can be divided into global displacement and displacement caused by deformation [20].

The main extrinsic errors are the inaccuracies of the physician's hand [22], the deformation of the prostate caused by the transrectal ultrasound (TRUS) probe in the rectum [23], and displacement of the prostate induced by the body such as during respiration [24], pelvic muscle contractions [25], and the volume of the bladder [24].

Extrinsic errors

The impact of extrinsic errors is hard to measure and plan [26]. The occurrence and magnitude of each extrinsic error can differ for every needle insertion, making them unpredictable and non-systematic [26]. This makes it difficult to develop solutions to prevent or reduce extrinsic errors pre-insertion. There are some used strategies such as anesthetising the human body within a short time frame [19] and shortening the overall procedure time to reduce the occurrences of prostate displacement induced by the human body [19]. However, these strategies do not prevent or reduce prostate displacement, rather it reduces the odds of happening. Also, these strategies can be stressful for the physician or increase the workload when time is a limiting factor. Furthermore, teleoperation is considered as a solution, where the needle insertion is done by a robot controlled by a human to remove inaccuracies caused by the physician's hand such as hand tremors [27]. However, the use of teleoperation can introduce a new type of error corresponding with the robotic system [19]. Therefore, the most common solution to deal with extrinsic errors is to compensate for this error while advancing the needle in the tissue during the intervention by using ultrasound or Magnetic Resonance (MR) imaging [28]. However, usually a preventive approach is a preferred way to deal with these errors, rather than compensating for them [29]. Especially in the medical field where a single error can lead to catastrophic complications for a patient. So reducing the overall target deviation error via extrinsic errors is a difficult approach, whereas intrinsic errors are caused by the limitations of the instrument design and insertion method, which makes it easier to predict the behaviour of the needle and to control the magnitude of the error by improving the design and/or insertion method. Therefore in this study, we will focus on dealing with the intrinsic errors.

Intrinsic errors

Needle-induced prostate displacement is a common intrinsic error, where the displacement is seen as the in plane translations and rotations of the centroid of the prostate due to the pushing of the needle on the prostate [20]. As mentioned, a main component of prostate displacement is the global displacement, which is the volumetric movement of the entire prostate. The prostate is a moving organ, which means that it can move from its initial position to another [30]. Therefore, when the needle tip contacts the prostate, it will displace and/or rotate the prostate along the axes and planes as presented in Figure 5. After puncturing, when the needle advances in the prostate, the tissue will induce a resistance force on the needle [31]. At low insertion

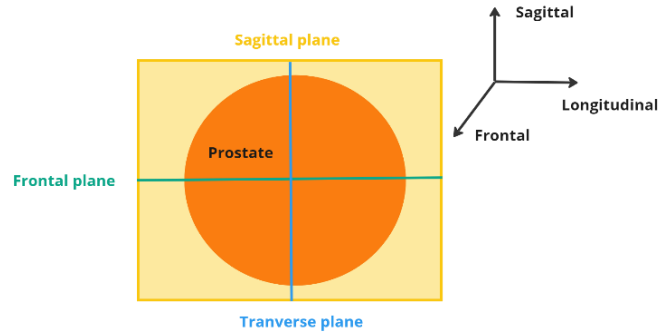


Figure 5: Schematic image of the anatomical axes and planes of a prostate.

velocities, this resistance force will be harder to overcome causing the tissue to stick to the needle, which can result in additional prostate displacement [32]. Podder *et al.* [17] measured the in-plane motion of the prostate being averagely 13.5 mm along the longitudinal axis, 6 mm along frontal axis, and 4.5 mm along sagittal axis. Lagerburg *et al.* [33] measured the range of the rotation of the prostate in the frontal plane being between -11.2 and 13.8 degrees and in the sagittal plane between -8.5 and 10.2 degrees.

Besides global displacement, the needle can also cause displacement of the centroid by deforming the prostate [20]. The prostate tissue has elastic properties [34], which means that a force induced on the prostate will cause the prostate to change its shape. In the case of a needle insertion, deformation is caused by pushing the prostate surface away [20]. This compresses the prostate and results in a change in shape. This change in shape will displace internal tissue and therefore the centroid of the prostate. The capsule of the prostate, which is stiffer than the inner tissue, increases the deformation and makes it harder for the needle to directly puncture the prostate without pushing the prostate surface [13, 35]. Stone *et al.* [20] quantified during *in-vivo* experiments the prostate deformation as the change in maximum dimension of the prostate gland at the plane, through the sagittal and longitudinal axis. It was measured that the average deformation was 6.8 mm along the longitudinal axis and 3.6 mm along the sagittal axis of the prostate.

In addition to prostate inherent errors, the needle tip can deflect during the movement of the needle in the tissue [21]. During transperineal interventions, the needle is pushed through the perineum to reach the prostate. To perform this a force is needed at the needle tip [36]. This force allows the tissue to be cut and separated to create an opening. This separated tissue will induce a force on the needle tip when the needle advances through the tissue. When this force exceeds the critical load of the needle, the needle will buckle, leading to an arched deviation from its original path [37]. This can result in an inaccurate insertion of the needle in the prostate. Especially with single-bevel needles this deflection is significant, because of the non-equal force distribution on the asymmetric needle tip [36]. Podder *et al.* [13] quantitatively measured that needle deflection was averagely 4.0 mm along the sagittal axis during *in-vivo* experiments of prostate brachytherapy.

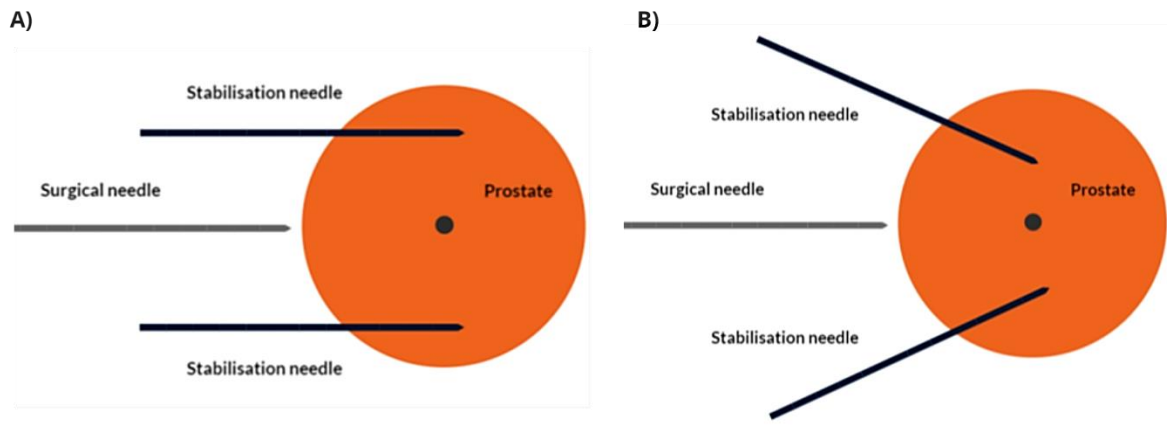


Figure 6: Schematic representation of the method of stabilisation needles in A) the parallel and B) the convergent configuration shown in the frontal plane (top view).

Impact of intrinsic errors

It is important to understand which error contributes the most to the target deviation error. This understanding can lead to the development of new methods and/or instruments to reduce or even prevent this error. Phee *et al.* [38] tried to quantify the contribution of needle deflection and prostate displacement to the overall target deviation error during transperineal prostate biopsies. The error was measured between the actual position and desired location of the needle tip using x-ray imaging. The first nine trials were performed using a standard biopsy needle. After the ninth trial, a thicker and stiffer needle was used to minimise the error caused by needle deflection. The difference showed that the average absolute target deviation error of the first nine trials was roughly 4.3 mm. After using the thicker and stiffer needle, the absolute error was reduced to 2.5 mm. These results showed that needle deflection contributed to roughly 40% of the target deviation error. The remaining 60% was assumed to be caused by prostate displacement. From this study, we can say that prostate displacement is the main contributor to target errors caused by the needle.

In literature, there is an emphasis on studies concerning needle deflection and corresponding solutions. There are preventive and compensative solutions to reduce needle deflection. A common and simple preventive method is using a symmetric needle tip [21, 39]. A symmetric needle tip allows the force on the tip to be distributed equally on all sides, preventing a single side to experience more force. Also, the use of a thicker needle is a preventive solution to counter needle deflection. A thicker needle increases the critical load of the needle, resulting in an increase of the resistance to buckling [38]. Another solution is needle steering [40]. Needle steering allows a flexible needle to be directional controlled within the tissue [40]. Needle steering can compensate for needle deflections caused in the tissue and account for a more accurate needle insertion. Certain insertion techniques can also reduce needle deflection. Needle spinning is such an insertion technique [41]. The insertion is performed by constantly rotating the needle, resulting in a constant switch of orientation of the needle tip in the tissue [41]. This reduces, especially for an asymmetric needle tip, the unequal distribution of the force on the tip.

Prostate displacement in comparison with needle deflection is to our knowledge less discussed within literature while having quantitatively more contribution on the target deviation error. It seems that compensating for displacement and deformation of the prostate, rather than preventing them is an easier solution. Therefore, this study will focus on the impact of prostate displacement and the solutions to deal with this problem.

1.3 Stabilisation needles

In literature, there have been studies addressing possible solutions for prostate displacement. These solutions vary from insertion techniques to mathematical models to predict the prostate's behaviour during needle insertion [42-44]. However, the current used solution is to physically stabilise the prostate using stabilisation needles [45, 46]. The method of stabilisation as shown in Figure 6 is performed by inserting needles in the prostate prior of insertion of the brachytherapy needles [46]. The working principle is that the stabilisation needles will constrain the prostate by reducing the degrees of freedom. The insertion of the stabilisation needles is done via a grid of holes referred as an implantation template, which is commonly used to allow the needles to be inserted at the desired angle and location relative to the perineum [31]. The most common configuration of the stabilisation needles is by inserting two needles parallelly at two opposite sides of the prostate gland as shown in Figure 6 [31]. Another configuration is by converging the tips of the needles towards each other [31]. This configuration allows the prostate to be more effectively constrained in longitudinal direction by using the physical properties of the needles. The stabilisation needles are standard 17 or 18 gauge needles, which are comparable in dimensions with the needles used during brachytherapy [31].

The efficacy of stabilisation needles was tested in multiple experiments. It was found that the effect of stabilisation needles was mainly seen in restricting motion along the sagittal and frontal axes and rotation in the transverse and frontal planes [31, 33, 45]. Wallner *et al.* [45] concluded during *in-vivo* experiments that the frontal displacement of the prostate was reduced from 10 mm to 0.20 mm. Podder *et al.* [31] validated this by showing in an *in-vitro* experiment that the frontal displacement was reduced from 6.0 mm to 1.1 mm and the sagittal displacement was

reduced from 4.5 mm to 0.90 mm. Podder *et al.* also found that there was a small reduction of the longitudinal displacement of the prostate, respectively from 13.5 mm to 11.4 mm. This was mainly caused by the friction forces of the tissue acting on the stabilisation needles. Lagerburg *et al.* [33] found that stabilisation needles had reduced rotation in the coronal plane, from 25 to 12 degrees. However, rotational displacement in the sagittal plane was not significantly reduced by the presence of stabilisation needles. Rotational displacement in the transverse plane was not significant in measurements with and without stabilisation needles.

1.4 Problem statement

Having positive effects on prostate displacement, the method of using stabilisation needles also has considerable limitations. One of these limitations is that stabilisation needles do not significantly reduce displacement along longitudinal axis i.e., the insertion direction. When inserting the needle in the prostate, the largest displacement occurs in the direction of the needle [31]. Furthermore, stabilisation needles decrease the available workspace for the brachytherapy needles and obstruct the view of the physician when using ultrasound imaging [31].

Another noticeable limitation is that stabilisation needles do not prevent prostate deformation [45]. As mentioned in **Section 1.2 Target deviation error**, it was found that prostate deformation is the other main cause of prostate displacement. Tascheau *et al.* [18] even documented that depending on the level of influence of the factors causing target deviation error, the effect of stabilisation needles at reaching the desired location within the prostate can be negligible.

Besides the functional limitations, stabilisation needles unwantedly effect the prostate properties and damage the tissue [47]. Stabilisation needles pierce through the healthy regions of the prostate, damaging the tissue. This brings additional trauma to the prostate, which can lead to an increase in recovery time of the prostate. Furthermore, the risk of oedema bleeding might be increased, causing the tissue to be torn and swollen up [47]. Oedema can also increase the volume of the prostate, which can affect the treatment and diagnosis of prostate cancer due to shifting and/or stretching of the malignant tissue within the prostate [48].

1.5 Objective of the study

The method of stabilisation needles has some positive effects on prostate displacement. However, important limitations do not fully justify the usage of them. Therefore the main objective of this study is:

“To design and experimentally evaluate an innovative instrument that can stabilise the prostate gland during brachytherapy.”

The main objective consists of multiple sub-objectives:

- To design an instrument that stabilises the prostate by constraining the global displacement in longitudinal direction i.e., direction of the needle insertion
- To design an instrument that prevents trauma done to the prostate by the stabilisation operation.

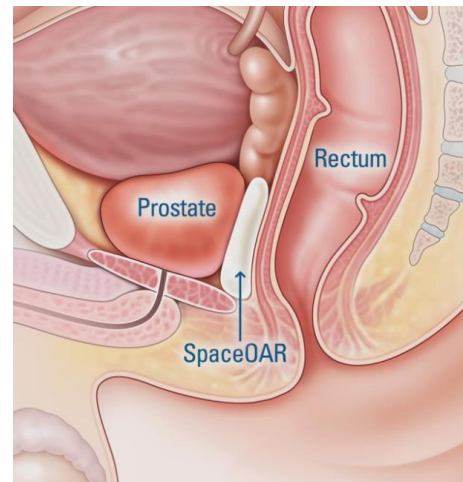


Figure 7: Schematic image of the male pelvic cavity, where a prostatic spacer of the brand SpaceOAR is placed between the prostate and rectum [52].

- To design an instrument that can be percutaneously inserted at an opening in the male perineum and guided to prostate.

The design of the instrument should be applicable for functionalisation of prostatic brachytherapy and not hinder it in any way.

1.6 Structure of the study

To reach the design objective of this study, first in **Section 2 Design direction** we discuss the chosen design path and state of the art of stabilisation instruments. Thereafter, in **Section 3 Design** the design requirements, the design process and final design of our instrument are described. In **Section 4 Prototype**, the manufacturing process of the prototype is described. Furthermore, in **Section 5 Experimental evaluation**, the performance and functionality experiments conducted in this study are explained. Thereafter, in **Section 6 Experimental results** the results of the experiments are presented. In **Section 7 Discussion**, we discuss the findings, limitations, and the future of our stabilisation instrument. Lastly, in **Section 8 Conclusion**, we give our conclusions about this study and the developed stabilisation instrument.

2 DESIGN DIRECTION

2.1 Anatomical analysis of the prostate

The prostate gland is located in the pelvic cavity (see Figure 1). It lies directly against the bladder on the superior side and the external urethral sphincter muscle on the inferior side [49]. The gland is covered with sensitive nerves and vascular plexus from the base to the apex at both transversal sides. Anteriorly, it is in contact with the pubic symphysis, while posteriorly it is in a close relationship to the rectum [49]. The gland is separated from the rectum by a space called the rectoprostatic space [50]. This space is often used for the insertion of spacers during brachytherapy to elevate the prostate from the rectum to reduce exposure to radiation on the rectum as shown in Figure 7 [51, 52]. The spacers are biodegradable hydrogels or balloons and allow for a separation of roughly 15 mm from the rectal wall [51, 53, 54]. Therefore, the rectoprostatic space seems a suitable space to

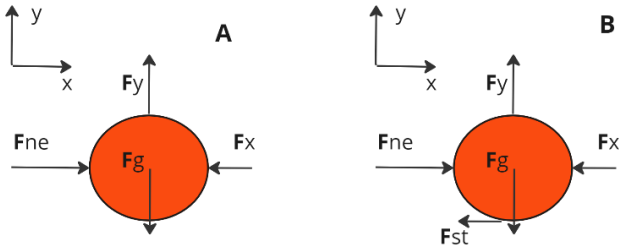


Figure 8: Schematic representation of A) the forces acting on a prostate (orange) during needle insertion without and B) with the stabilisation instrument, where F_{ne} is the needle force, F_g the gravitational force, F_y & F_x the surrounding tissue forces in respectively sagittal (Y-axis) & longitudinal (X-axis) direction, and F_{st} the force of the stabilisation instrument.

insert an instrument and apply a countermeasure on the prostate to establish stabilisation without damaging the surrounding tissue. In continuation of this study, the rectoprostatic space will be used as workspace for the stabilisation instrument.

2.2 Mechanical analysis of needle insertion

During needle insertion, the prostate experiences forces in different directions. Figure 8 shows the Freebody diagram of the prostate with the forces acting on it during needle insertion. In the sagittal direction, the gravitational force of the prostate and the force of surrounding tissue such as the pelvic symphysis are acting on the prostate, forming a force equilibrium. In the longitudinal direction, the force of the needle and the force of surrounding tissue such as the bladder are acting on the prostate. Unlike in the sagittal direction, there is no force equilibrium; the magnitude of the surrounding tissue force is relatively small (neglectable) compared to the force of the needle, leading to displacement of the prostate in the longitudinal direction.

To still establish a force equilibrium as shown in Figure 8, an additional force, which is equal in magnitude, but opposite in direction of the needle is needed. This force will be provided by our stabilisation instrument in the rectoprostatic space to prevent the displacement of the prostate.

2.3 Stabilisation methods for the prostate

As discussed in **Section 2.3 Mechanical analysis of needle insertion**, the stabilisation is seen as creating a force balance by applying a reaction force on the prostate in opposite direction of the pushing force by the needle. The stabilisation

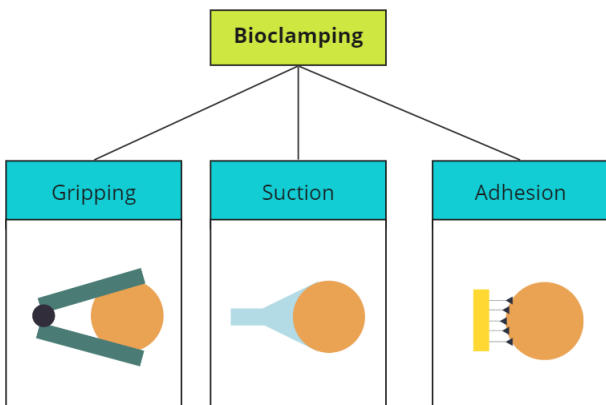


Figure 9: Overview of the main clamping methods found in nature.

can therefore be seen as a way of clamping the prostate, where clamping is defined as holding an object in place using an instrument. In nature, there are three main types of clamping methods, namely gripping, suction, and adhesion as shown in Figure 9 [55, 56]. Each clamping method consists of multiple sub-methods that utilise different working principles by different animals in nature. The clamping methods and their categories are discussed in more detail in Appendix A. Over the years, engineers have invented technical counterparts of these biological clamping methods in different industries as surgical forceps in the medical domain and suction based grippers in industrial production.

Gripping is a popular method in the medical field to hold tissue in place during an intervention via an instrument by applying normal forces. A well-known example of such instruments is the metal forceps. However, the fluid film and irregular shape of the tissue make it difficult for the gripper to establish a sufficient grip [57]. To compensate for this, often a higher normal force is applied on the tissue. However, this leads to higher stresses within the delicate tissue, increasing the risk of tissue damage such as rupturing [58].

In contrast with gripping, adhesion methods such as capillary and Van der Waals adhesion require bonding bridges between the instrument and tissue to establish clamping [59]. However, multiple scientific studies conclude that the clamping proportionally reduces on wet surfaces due to the insufficient forming of the bonding bridge between the tissue and adhesive [59, 60]. In comparison with gripping and adhesion, suction has great usability on slippery delicate surfaces by merely using the surface as application point for clamping. Suction based stabilisation seems therefore a suitable method for our instrument to stabilise the prostate gland within the rectoprostatic space. The other clamping methods can still be applied as secondary stabilisation mechanisms.

2.4 State of the art: the Octopus heart stabiliser™

In this section we will look at the Octopus heart stabiliser™ from Medtronic as shown in Figure 10 [61, 62], which is a well-known suction based stabilisation instrument. The Octopus heart stabiliser™ is used to stabilise the epicardium of a beating heart during coronary artery bypass surgery via suction. The instrument consists of two suction pads that are placed parallel on either side of the heart, where each pad consists of 6 mm sized suction domes. The pads are connected to an external vacuum system and have a mutual air chamber, where a vacuum pressure of 50 kPa is applied. This pressure is proven to be safe on heart tissue [61, 63]. In



Figure 10: Image of the Octopus heart stabiliser™ [62].

practice having a mutual air chamber can sometimes result in attachment failures of the Octopus heart stabiliser when a suction dome fails to make contact with the tissue [63]. This makes the usage of Octopus heart stabiliser™ somewhat unreliable.

The Octopus heart stabiliser™ can be used as inspiration for the design of our instrument. There are many more suction based instrument designs that can be found in literature.

2.5 Theoretical analysis suction

Suction cup

To establish suction, a cup-shaped instrument referred to as suction cup is often used. The general design of a suction cup consists of an air chamber, an outer layer, and a footprint as shown in Figure 11 [64]. The air chamber is used to regulate the vacuum pressure. This can be done by removing the air by squeezing the suction cup against a surface or via an external system that removes the air at the top side. The outer layer of the suction cup provides for the structural strength and airtightness of the cup. The footprint provides for the contact interface between cup and object's surface. This interface needs to be an airtight seal to prevent any leakages.

Suction force

For understanding the working principle of suction, it is fundamental to know the principle of pressure. Pressure is the force applied perpendicular to the surface of an object per unit area N/m^2 as presented in Equation 1.

$$P = \frac{F}{A} \quad (1)$$

Where P is the pressure in kPa, F is the force in N, and A is the corresponding surface area in m^2 . The applied force is the result of molecules colliding on a surface. An example of this is shown in Figure 12 [65]. Here a closed container contains molecules that collide on the inner walls. These molecules exert a force on each wall of the container by colliding with them. If the container becomes smaller i.e., surface area becomes smaller, the molecules will collide more frequent and therefore increase the pressure [66].

On earth, objects experience a constant pressure from the molecules in the atmosphere. This is referred to as the atmospheric pressure and is equal to 101 kPa (1 atm) at sea level [67]. If we take a suction cup with a lower pressure than 1 atm, a pressure difference as shown in Equation 2 will occur at the sides; for a vacuum the pressure inside of the suction cup can never be greater than the atmospheric pressure [65],

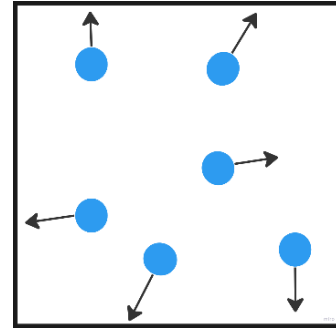


Figure 12: Schematic image of pressure generated as a result of colliding molecules against the walls of a closed container.

$$\Delta P = P_{atm} - P, \text{ where } P < P_{atm} \quad (2)$$

where ΔP is the pressure difference, P_{atm} is the atmospheric pressure, and P is the pressure of the suction cup all in kPa. The vacuum generates a force at the suction cup sides. If the suction cup forms a closed contact area with an object, the surface of the object will experience a pulling force referred to as the suction force presented in Equation 3 (see Figure 13),

$$F_{Suction} = \Delta P * A \quad (3)$$

where $F_{Suction}$ is the suction force in N, ΔP is the pressure difference in kPa, and A is the corresponding surface area in m^2 . The lower the pressure inside of suction cup, the higher the suction force. In theory a suction cup containing zero colliding molecules, which is called a perfect vacuum, will generate the highest possible suction force.

Friction force

A suction cup generates a friction force when the cup experiences a load in shear direction i.e., suction force is orthogonal to the load on the object [68, 69]. In our case, this friction force resembles the gripping force of the suction cup to stabilise the prostate during needle insertion as shown in Figure 14. This friction force $F_{Friction}$ in N (= the grip force F_{Grip}) of the suction cup is determined by the friction μ coefficient of the material, the preload $F_{Preload}$ in N, and the suction force $F_{Suction}$ in N as shown in Equation 4. The preload is the perpendicular force applied on the suction cup to form a sealed contact with the surface [69]. For our suction cup, the preload is generated by a prostatic spacer on a 300 cc tumorous prostate, resulting in a preload of roughly 3 N [70].

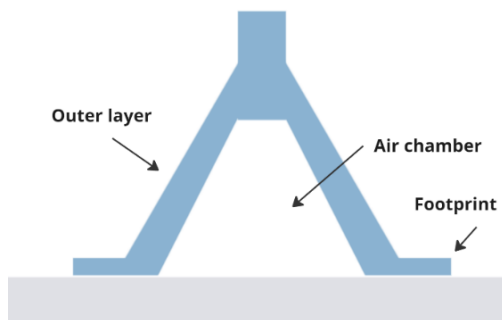


Figure 11: Schematic image of the components of a general suction cup.

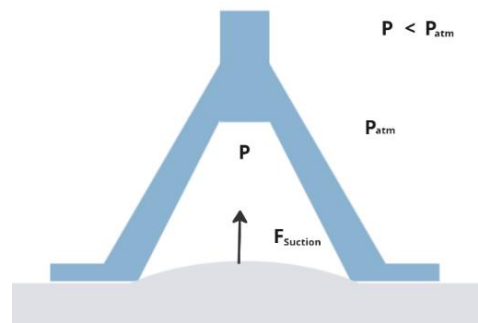


Figure 13: Schematic image of the generation of a suction force $F_{Suction}$ due to the pressure difference between the suction cup and atmosphere.

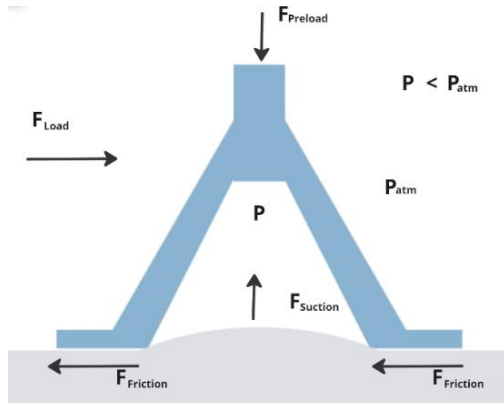


Figure 14: Schematic image of the generation of a friction force $F_{Friction}$ as a result of the suction force $F_{Suction}$ and preload $F_{Preload}$ when a load F_{Load} in shear direction is applied.

$$F_{Friction} = F_{Grip} = \mu * (F_{Suction} + F_{Preload}) \quad (4)$$

Generally, a suction cup is made out of a flexible material such as rubber. The deformable nature of rubber allows the formation of a large contact area with the object's surface. Also, rubber has typically a high friction coefficient of roughly 1 on most materials [71]. The friction coefficient can be increased by adding micro-structures on the footprint of the suction cup to allow for better gripping of the object's surface [57, 72].

The suction force as stated in Equation 3 is determined by the pressure difference between the atmospheric pressure and pressure inside of the suction cup and the contact area of the suction hole with the surface. As mentioned in the previous section, a pressure of 50 kPa is widely used in medical applications and has proven to be safe on heart tissue. With a pressure level of 50 kPa, preload of 3 N, and friction coefficient of 1, the suction cup needs to generate at least an additional grip force of 2 N. This leads, according to Equation 1, to a required suction area of 40 mm². This area can be attained for our suction cup by taken the size, number, and shape of the suction hole into account during the design process.

Seal generation

To perform a successful suction grip on the surface of an object, the suction cup must form a sealed contact with the surface. The ability to form a seal depends on the adaptability of the suction cup on the surface, where surface properties such as roughness, stiffness, and shape play a crucial role [71, 73]. On an object with an irregular and curved surface, it becomes more difficult for the suction cup to form a seal. As a result, air leaks at the rim can occur, which can lead to attachment losses. The main properties that influence seal forming are the stiffness and length of the rim of the suction cup [73]. The more elastic the rim, the better it can adapt on surfaces, and the longer the length of the rim, the farther the suction hole is located from the rim. These parameters should be taken in consideration for the design of our suction cup.

3 DESIGN

3.1 Design requirements

Demands

Demands are requirements that the suction cup must have based on the objective and scope of this design study in order to achieve the desired performance.

Functionality

- 1) **Generate grip force of 5 N:** A needle exerts averagely 5 N force on the prostate. To counter this, the suction cup should able to generate a grip force of at least 5 N with a vacuum pressure of 50 kPa [17].
- 2) **Limit prostate displacement:** A brachytherapy needle can displace the prostate averagely 14 mm in longitudinal direction. The vacuum gripper should prevent the displacement by restricting the movement in longitudinal direction [15].
- 3) **Transperineally insertion:** The suction cup should able to be transperineally inserted 90 mm deep from the perineal wall into the rectoprostatic space [17]. Transperineal insertions minimise the risk of infectious complications in comparison with transrectal insertions[74].
- 4) **Seal generation & pressure maintenance of 50 kPa:** The vacuum gripper should able to form a seal with the prostate's surface and maintain a pressure of 50 kPa when in operation. The seal should be universally formed on all types of prostate surfaces varying from surface texture, shape, and wetness. The mentioned pressure level of 50 kPa is clinically used by commercialized instruments as the Octopus heart stabiliser on delicate heart tissue [75-77]. Therefore this pressure is also seen as safe to utilise on prostate tissue.
- 5) **Manual control:** A physician should able to manually guide and actuate the suction cup using a vacuum system without the need of any assistance.
- 6) **Compatibility with needles and prostatic spacer:** The suction cup should be compatible with the brachytherapy needles and prostatic spacers used during brachytherapy. The spacer is used to separate the rectal fascia from the prostate, to reduce exposure to radiation [53]. The functionality of the spacers should not be hindered in any way.
- 7) **Damage control:** During attachment, operation, and detachment, the suction cup should not inflict any permanent trauma to the tissue of the prostate and surrounding structures, including the nerves and veins located on both lateral sides. Haemorrhages can occur when the used vacuum pressure within the suction tip becomes too high leading to accumulation of blood within the affected tissue, which can cause tissue rupture and scarring of the prostate [78].

Dimensions

- 8) **Fit in 5 mm incision:** During brachytherapy, a 5 mm incision is made through the perineum to insert a prostatic spacer [53]. The suction cup should be able to fit within this space without increasing the incision size and shape.
- 9) **Fit in rectoprostatic space:** The suction cup should be able to fit in the rectoprostatic space together with a prostatic spacer, having an average size of 43 mm x 30 mm x 11 mm [79].

Wishes

Wishes are requirements that are nice to have, but are not obligatory. The wishes can be implemented in future iterations of the suction cup, closer to clinical use. The final design presented in this study must not hinder the implementation of these wishes in future design versions.

- 9) **Single-use:** The suction cup should be a single-usable instrument, that can be disposed after the procedure is done [80]. Single-usable instruments prevent the risk of infections caused by remaining tissue on the instrument compared to re-usable instruments. Furthermore, single-usable instruments are immediately disposed after the procedure, so there is no need of time consuming post-processes such as (dis)assembly, sterilisation, and, disinfection according to ISO 17664 [81, 82].
- 10) **MR-compatible:** The instrument should meet the standards of ASTM F2119 [83] and ASTM F2503[84] when used in combination with a MR-device i.e., MR-imaging scanner. The used material and mechanical components should not hinder the imaging quality, interfere with the

radiofrequency signal, and be safe for patient and surgeon when using MR.

- 11) **Ultrasound compatible:** The instrument should meet the standard of IEC 60601-2-37 [85] when used in combination with an ultrasonic device i.e., transrectal ultrasound (TRUS) probe. The used material and mechanical components should not hinder the imaging quality, interfere with the ultrasonic frequency, and be safe for the patient and physician when using ultrasound.
- 12) **Biocompatible:** The used materials for components intended for internal body use must meet the standards of ISO 10993-1 [72]. Biocompatible material do not produce toxic or immunological response when exposed to the body or bodily fluids by an instrument.

3.2 Design process of the ProSTATIC

The suction cup was designed via an iterative procedure. An iterative process allows to reach the design goal by improving and refining the design till the requirements are met. A summary of the iterative process leading to the final design is discussed in this section.

We started with a design of a bell-shaped suction cup. The bell shape is the most utilised design for suction cups found in literature [86, 87]. The benefit of a bell shape is that it has a circular contact area on a surface. As known, a circle has the largest surface area to perimeter ratio, meaning that the bell shape will theoretically provide the largest area of suction on the prostate [88]. The needed effective suction area for our suction cup was at least 40 mm². This meant that if we wanted to use a bell-shaped design, an inner diameter of at least 7.2 mm was needed. To fit a 7.2 mm diameter sized suction cup in the 5 mm incision size, a folding mechanism such as origami for the suction cup was needed. We tested different origami folding patterns and deployment

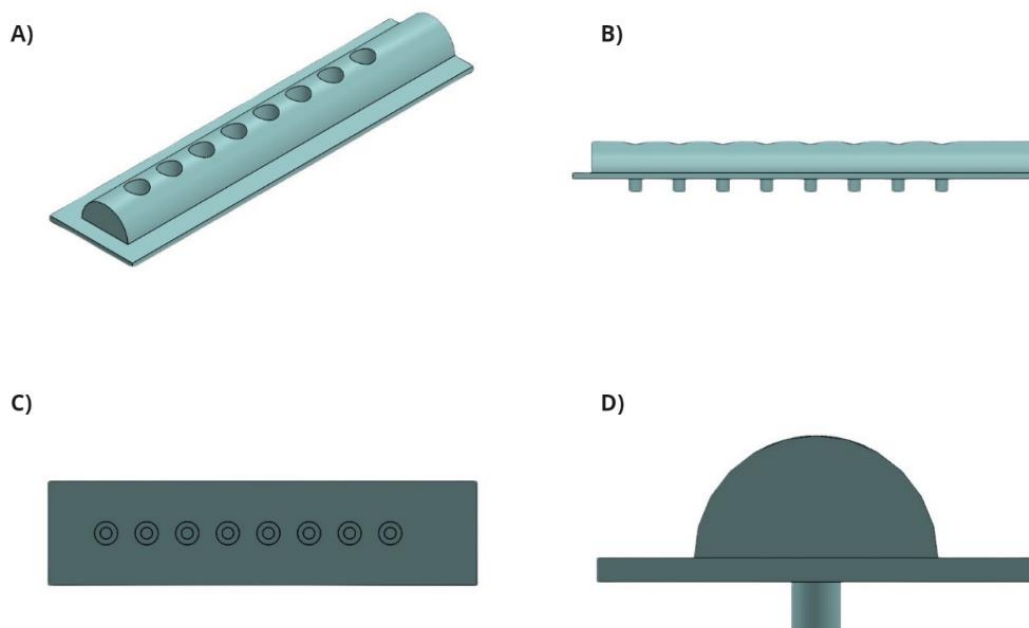


Figure 15: Illustrations of the ProSTATIC shown in A) 3D-view, B) side view, C) bottom view, and D) front view. The ProSTATIC is a semi-cylindrical modular suction cup with self-regulating valves.

configurations using prototypes made of baking paper. The prototypes showed that origami at small scale led to inaccurate folding of the suction cup and therefore incorrect deployment. Other folding mechanisms such as the umbrella mechanism were also considered, however adding the umbrella mechanism at a small scale would increase the size of the suction cup, not provide enough mechanical strength, and be too complex.

Therefore, a design alteration was to remove the need for foldability, while maintaining the needed contact area for suction. By analysing the insertion space through the perineum more thoroughly, we concluded that this space is technically a thin long cylindrical hole. Researching in nature for inspiration, it was found that the shape and functionality of the tentacle of an octopus is quite compliant for what we want for our suction cup; a slender design that fits in a small cylindrical insertion space, while providing a sufficient contact area for suction. This inspiration resulted in the design of our suction cup as shown in Figure 15, which is called the ProSTATIC. The following section will describe the functionality and design of the ProSTATIC.

3.3 Final design of the ProSTATIC

The ProSTATIC is a slender flexible suction cup, also referred to as a suction pad. The stabilisation method of the ProSTATIC is to generate a friction force between the ProSTATIC and prostate surface to establish a grip. The design itself is a semi-cylindrical modular pad consisting of individual suction holes. The unique shape consists of a flat side, which forms the contact area with the prostate. The benefit of the flat side is the ability to form a much larger contact area with the surface when compared to a full-cylindrical suction cup, while still able to compliantly fit in the incision made in the perineum. This design as briefly mentioned was inspired by the tentacle of an octopus. A tentacle is a long flexible limb consisting of multiple independent suckers at one side as shown in Figure 16 [89]. The limb is long and flexible enough to fit in small openings such as cracks between rocks [90]. The suckers are used to grip prey and keep the octopus in place by lashing on surfaces [91]. Each sucker works autonomously by having its own air chamber controlled by the tendon muscles of the octopus [92, 93]. Compressing these chambers allow the inside air to be pushed out, creating a vacuum within the suckers.

The selling-point of the ProSTATIC is that the suction holes

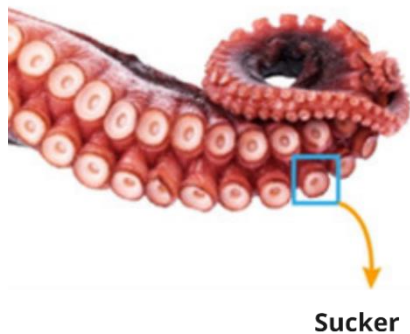


Figure 16: Image of a limb of an octopus with its suckers [89].

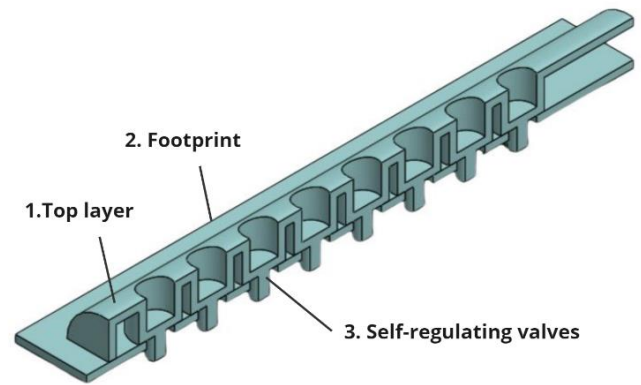


Figure 17: Schematic image of the cross-section of the ProSTATIC with its three structural layers.

are controlled by an unique self-regulating valves mechanism. This allows each suction hole to work independently as the suckers of an octopus. In the following subsections, the design will be discussed in more detail.

Top layer

The ProSTATIC consists of three structural layers as shown in Figure 17: (1) the top, (2) the footprint, and (3) the self-regulating valve mechanism. The top functions as an airtight layer that maintains the vacuum pressure during the stabilisation procedure. Furthermore, the top layer provides the dimensional stability of the suction cup, preventing it from collapsing during vacuum generation and deforming in shear direction.

For the top layer silicone rubber is used as material. Silicone rubber is a well-known material in the medical sector, often used for surgical devices and implants e.g., catheters, shunts, grippers, and pacemakers due to its beneficial properties of being highly biocompatible and having elastomeric behaviour [94, 95]. **Section 4 Prototype** describes the choice of using silicone rubber for the ProSTATIC in more detail.

The top as shown in Figure 18 has a length of 35.5 mm, a radius of 2.5 mm, and a wall thickness of 0.5 mm. The length of the top was based on the perimeter segment of a healthy prostate located within the rectoprostatic space [96]. The radius was based on the 5 mm incision made in the perineum for insertion of the prostatic spacer. The wall thickness was chosen based on the thickness range of other comparable-sized silicone suction cups found in literature [87, 97].

Base footprint

The footprint is the layer where the ProSTATIC forms a sealed contact area with the prostate surface and generates the

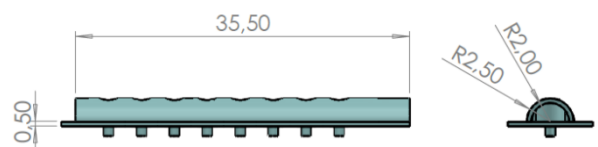


Figure 18: Schematic image of the top layer of the ProSTATIC with the dimensions.

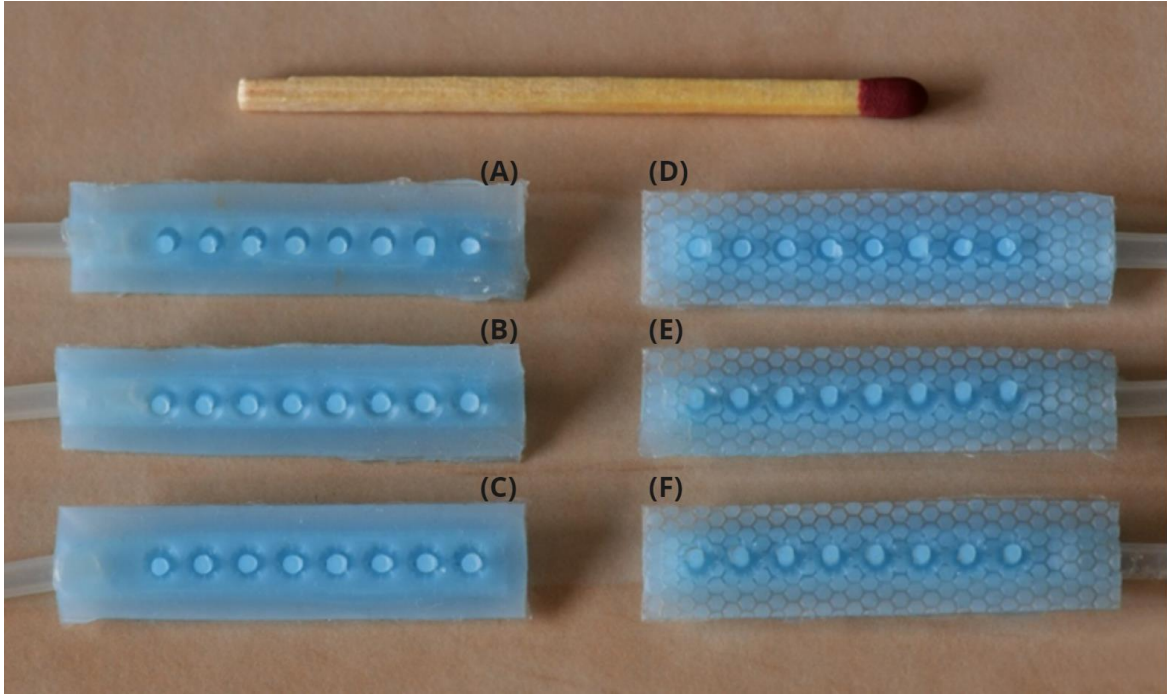


Figure 19: Images of the footprint designs containing (A) the base footprint, (B) base footprint with enlarged suction holes, (C) base footprint with enlarged suction holes and radial ridges, (D) hexagon micro-patterned footprint, (E) hexagon micro-patterned footprint with enlarged suction holes, and (F) hexagon micro-patterned footprint with enlarged suction holes and radial ridges.

gripping force. Therefore, it is important for the footprint to be flexible, allowing to adapt on the curved and irregular surface of the prostate. Different footprints as shown in Figure 19 were designed based on the friction coefficient and suction hole size.

(A) The base footprint is the first design without any added features to the footprint. The base footprint has a smooth surface and a multi-holed design. The multiple suction holes divide the suction force over these holes, reducing the stress in the tissue and therefore lowering the risk of tissue damage when compared to a single larger suction hole. Furthermore, the multi-holed design also enables the possibility of autonomously workable holes.

The footprint as shown in Figure 20 has a length of 37 mm and a width of 9 mm. The thickness of the footprint has the same 0.5 mm value as the top. Each suction hole has a diameter of 2 mm and is spaced 3.5 mm spaced from each other, allowing eight of these suction holes to fit on the footprint. The suction cup can theoretically generate a suction force of 1.3 N when a 50 kPa pressure is applied according to Equation 1.

For the fabrication of the footprint, we used silicone rubber as material due to its flexibility, allowing to adapt and form a closed contact area with the curved irregular prostate

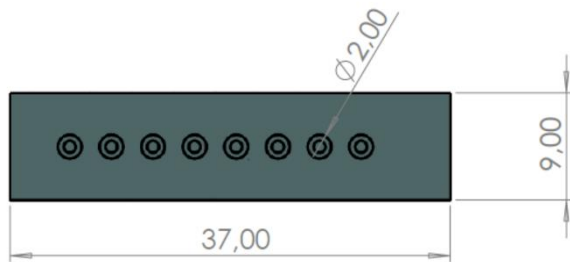


Figure 20: Schematic image of (A) the base footprint design with the dimensions.

surface. Also, the great bonding capability between silicone rubbers was taken into account making the assembly of the layers with each other easier. Furthermore, the soft nature of silicone rubber induces low normal loads on the prostate to establish grip reducing the risk of damage to the tissue. Also, silicone rubber is naturally tacky, resulting in general high friction coefficients on most types of materials including viscoelastic materials as tissue [71].

Footprint with enlarged suction holes

To increase the gripping force, a (B) footprint with enlarged suction holes as truncated holes was designed as shown in Figure 21. The benefit of using truncated holes is that the diameter of the top remains the same as that of the suction holes of (A) the base footprint, maintaining the same functionality with the self-regulating valves while still able to increase the area for suction at the base side and therefore also the suction force according to Equation 1.

Additionally, (C) a third footprint was designed by adding eight radial ridges at the interior of the suction holes of the (B) footprint as shown in Figure 22 [98]. This was done merely as precaution to maintain the effective area for

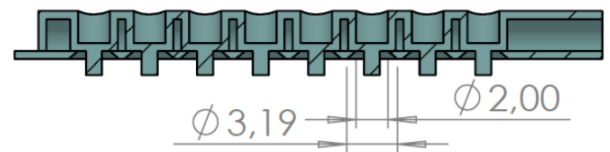


Figure 21: Schematic image of the cross-section of the ProSTATIC with (B) the footprint with enlarged suction holes, where the holes are designed as truncated holes with a base diameter of 3.2 mm and a top diameter of 2 mm.

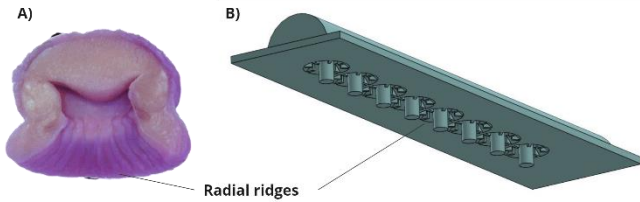


Figure 22: Images of A) The radial ridges inside the sucker of an octopus [98] and B) the radial ridges inside the suction holes of (C) the footprint with enlarged suction holes and radial ridges.

suction. The use of radial ridges is also seen in nature by suckers of cephalopods as octopuses, cuttlefishes, and squids Figure 22. These suckers contain a multitude of radial ridges in the interior to prevent substrate to be pushed in[93].

Each truncated suction hole has a top diameter of 2 mm and a base diameter of 3.2 mm. Each radial ridges has a length of 0.59 mm, a width of 0.2 mm, and is spaced 45 degrees from another. Other dimensions and the number of suction holes are the same as that of the (A) base footprint.

Eight of these truncated suction holes can theoretically generate a suction force of 4 N when a 50 kPa pressure is applied according to Equation 1, which is three times larger than the suction force of the holes of the (A) base footprint.

Footprint with micro-pattern

In literature, it was studied that adding a pattern of micro-structures on the pads of a gripper could increase the friction coefficient depending on the applied substrate [57, 99, 100]. For application on slippery tissue, it was found that a hexagon micro-pattern had shown to have the greatest friction coefficient when compared to other patterns such as teeth and dimple patterning [57, 100]. As the name indicates, the hexagon patterning is a motif of hexagon-shaped pillars, where every side of a pillar is connected to a channel. These channels allow for fluid drainage, which can lead to the increase of dry friction between the footprint and the prostate surface. Furthermore, it was found that when the corners of the hexagon pillars where facing the load direction more fluid on the tissue was drained. This configuration allows the fluid on the tissue to be more easily branched, allowing the fluid to reach more channels. Appendix B describes the effect of other micro-patterns on slippery tissue. In nature, the hexagon micro-pattern is found on the toepads of tree frogs as shown in Figure 23 [59, 99]. This pattern allows tree frogs to grip and climb on slippery substrates such as wet leaves and tree barks. The hexagon micro-pattern was applied on the three (A-C) current footprints, to increase the friction coefficient, yielding in three additional footprint designs as shown in Figure 19: (D) the hexagon micro-patterned footprint, (E) the hexagon micro-patterned footprint with enlarged suction holes, and (F) the hexagon micro-patterned footprint with enlarged suction holes and radial ridges.

A hexagon pillar has a 0.30 mm height with six 0.68 mm long sides. The channel width is 0.20 mm. The dimensions were chosen based on the dimensional ratio of 1:2.3:0.66 (height: side length: channel width) found in literature and based on the minimal available print size of 0.20 mm to create the micro-structures from a 3D-printed mould without losing any detail [57]. In theory, the hexagon micro-pattern can increase the friction coefficient of the footprint by approximately 1.5 times compared to a smooth footprint [57].

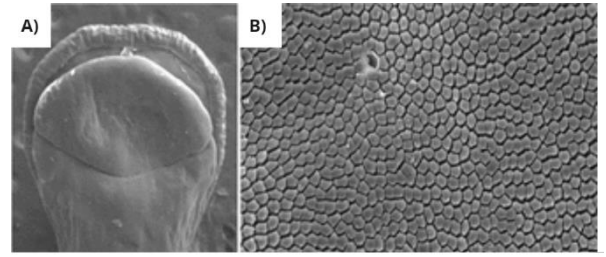


Figure 23: Images of A) the toepad of a tree frog [57], B) the zoomed-in part of the toepad showing the hexagon micro-pattern [57], and C) the hexagon micro-pattern applied on the footprint of the ProSTATIC.

Self-regulating valves

The ProSTATIC has a unique built-in self-regulating valves mechanism that allows each suction hole to work independently, while being connected to a single air chamber. This removes the need for multiple separate air chambers, which would have increased the size and complexity of the tubing. Furthermore, the valves make the usage of the ProSTATIC more reliable by reducing the risk of complete attachment failures caused by contact loss of a suction hole. Also, the built-in feature eliminates the need for additional systems to detect air leakages and the activation of the mechanism. The self-regulating valves were inspired by other suction based grippers, which utilise a self-regulating

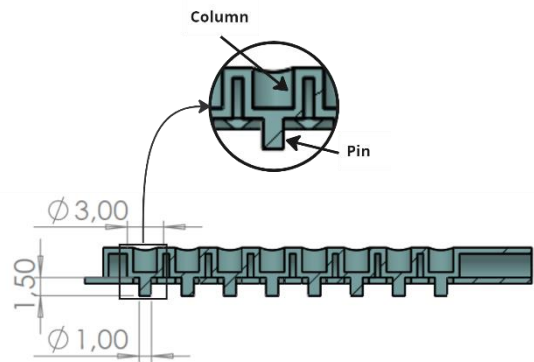


Figure 24: Schematic image of the cross-section of the ProSTATIC showing the pin- and column components of the self-regulating valves with their dimensions.

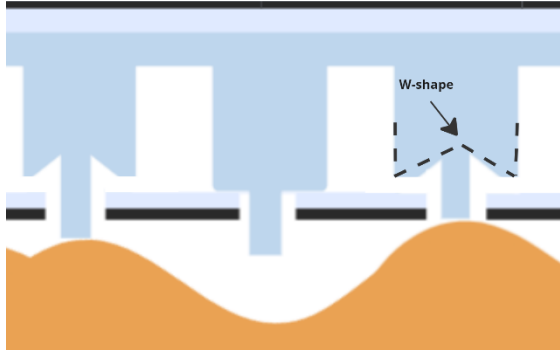


Figure 25: Schematic representation of the deformation of the column in a W-shape when the pin is pushed against the prostate surface (orange). The W-shape creates gaps at the sides to establish airflow inside the air chamber.

mechanism as well [101, 102]. These mechanisms are described in Appendix C. The design of the self-regulating valves as shown in Figure 24 is a module of rigid pins connected to columns. The pins form the contact point with the prostate surface, whereas the columns cover the suction holes, blocking the airflow into the air chamber. The columns are designed as thin-walled cylinders with an open top. When the ProSTATIC is pressed against the prostate surface, the normal force will allow the pins to be pushed back, causing the column to be compressed in a W-shape as can be seen in Figure 25. Being thin-walled allows the column to be easier compressed in comparison with a solid column. The W-shape of the columns creates a gap to establish an airflow to the air chamber. When contact is lost and/or not formed between the prostate and a suction hole, the column will decompress and return/stay to its default configuration. This will cover the corresponding hole and block the airflow. Furthermore, the open top prevents the upper part of the column to extend above the top layer. Another interesting feature of the self-regulating valves is that the pins can also provide micro-gripping by interlocking with the tissue surface, which could contribute to prostate stabilisation

As for the top layer and footprint, silicone rubber was used for the self-regulating valves as well. The silicone rubber provides the elastic behaviour for the needed deformation of the columns and allows them to be bonded with the silicone top layer to form a monolithic part.

Each column has a diameter of 3 mm as shown in Figure 24 to reliably cover the 2 mm suction holes. The wall of the columns has the same thickness of 0.5 mm as the top layer and footprint. The pin dimensions were chosen by prototyping the self-regulating valves with different dimensions and testing the functionality in practice. This resulted in a pin diameter of 1 mm and a height of 1.5 mm, allowing them to extend 1 mm from the footprint for activation of the airflow in the air chamber. A pin with a larger height was much more prone to buckling, whereas a larger diameter increased the risk of contacting the sides of the suction holes, which hindered the functionality of the self-regulating valves.

4 PROTOTYPE

4.1 Material choice

The different layers of the ProSTATIC as briefly mentioned in Section 3.3 Final design of the ProSTATIC was made of silicone rubber. Silicone rubber is a well-known biocompatible material in the medical sector and used as material for prostatic dilators [103, 104]. The soft elastic nature of silicone rubber prevents high local peak forces on the prostate tissue during attachment, reducing the risk of high stresses occurring in the tissue [58], which is in line with Requirement 7. Furthermore, the elasticity of silicone rubber allows the footprint to adapt on different types of prostate surfaces. This is beneficial for forming an airtight seal to maintain the 50 kPa pressure inside of the air chamber as stated in Requirement 4. Additionally, silicone rubber has low permeability of both air and fluid, which is valuable for applications on a wet surfaces such as on prostate tissue [105]. Another advantage of using of silicone rubber is that it has a low acoustic impedance value of roughly 10×10^6 Rayleigh [105]. Acoustic impedance is a measure of the resistance a sound wave experiences when propagating through a material. A low impedance value means that ultrasound waves will not be hindered as much, which will not impact the imaging of the pelvic cavity when a transrectal ultrasound (TRUS) probe is used during brachytherapy.

The used silicone rubber was Smooth-SilTM 936 with shore hardness of 36A. Different types of silicone rubbers were tested varying between elastic modulus and shore hardness. High elastic silicone rubbers as Eco-flexTM 00-30 resulted in excessive buckling of the pins of the self-regulating valves. On the other hand, stiffer silicone rubbers as Smooth-SilTM 940 reduced the flexibility of the footprint. Eventually, Smooth-SilTM 936 was chosen as the best silicone rubber for the ProSTATIC, offering the wanted trade-off between structural stability and flexibility.

4.2 Manufacturing method: Mould casting

The used manufacturing method was casting of silicone rubber using moulds. Different mould designs were tested and eventually after multiple iterations the moulds shown in

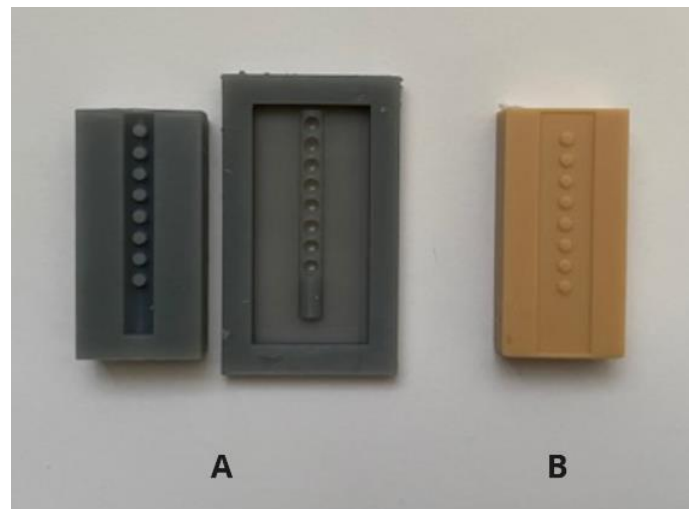


Figure 26: Image of the used moulds, where mould A is used for casting of the top and self-regulating valves and mould B for the footprint.

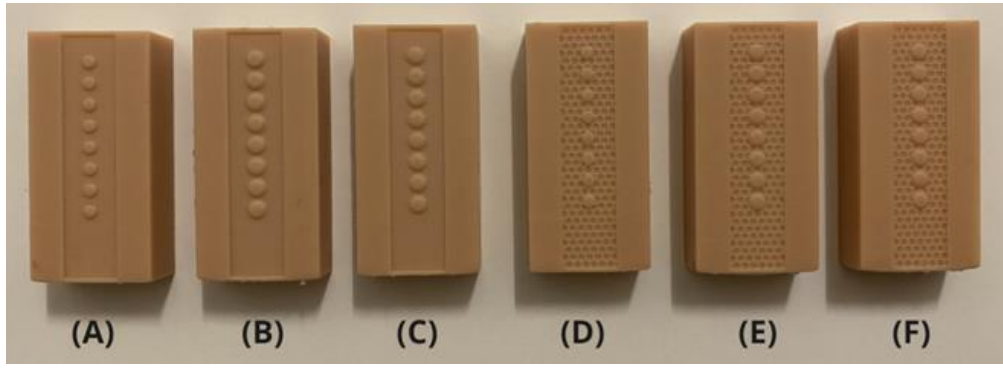


Figure 27: Image of the mould B types for the different footprint designs; (A) base footprint, (B) base footprint with enlarged suction holes, (C) base footprint with enlarged suction holes and radial ridges, (D) hexagon micro-patterned footprint, (E) hexagon micro-patterned footprint with enlarged suction holes, and (F) hexagon micro-patterned footprint with enlarged suction holes and radial ridges.

Figure 26 were seen as the best moulds for casting. The other mould designs can be seen in Appendix D. Two separate moulds were used: mould A for the top layer and self-regulating valves and mould B for the footprint. There were in total six mould B types as shown in Figure 27. These were based on the six different footprint designs as described in **Section 3.3 Final design of the ProSTATIC**. Mould A consists of two parts: the top and bottom part. The top part forms the general outline of the suction cup and the bottom part forms the hollow feature and self-regulating valves. The moulds were designed in CAD-software (Solidworks) and 3D-printed (Formlabs 3 printer). The two mould types were printed out of different materials. For mould B Model resin was used and for mould A Tough 1500 resin. The reason for this was that Tough 1500 resin is more pliable, which prevents chipping of the edges when the top part of mould A is clicked on and removed from the bottom part during casting.

The casting method was done via a stepwise procedure, where Figure 28 shows the used tools and resources. First, the silicone rubber mixture for the cast was prepared using a silicone rubber kit. Appendix E describes in detail on how the silicone rubber mixture was prepared. The required amount of silicone rubber was determined by calculating the weight of the ProSTATIC in CAD-software. A digital milligram scale was used to precisely weigh the needed amount of silicone rubber. The silicone rubber mixture was placed in a

cup and thoroughly mixed using a wooden stirrer for three minutes.

Before casting, the moulds were treated with Ease releaseTM spray for easy removal of the silicone rubber from the moulds after curing. The silicone mixture was poured onto one side of the mould and slightly pitched as demonstrated in Figure 28 to allow the mixture to flow through the mould. This technique limits the amount of air bubbles occurring in the mixture during casting. For mould A, the silicone mixture was cast into the bottom part and the top part was placed above it. For mould B, it was important to remove excess silicone by smoothing the surface of the mould out, otherwise it can result in a too thick footprint after curing. The silicone mixture in the moulds was let to be cured for 24 hours, according to the curing time of the silicone rubber. After curing, the silicone rubber was gently removed from the moulds. For mould A, the top part was removed and the silicone was gently pulled out of the bottom part. For mould B, the silicone was directly pulled out of the mould. Excess silicone was removed using a cutter knife. Figure 29 shows the two resulting parts after curing: the footprint and the top layer with the built-in self-regulating valves.

4.3 Assembly of the ProSTATIC

The monolithic part with the top layer and self-regulating valves and footprint were bonded together by utilising the same silicone rubber used for casting (Smooth-SilTM 936) as

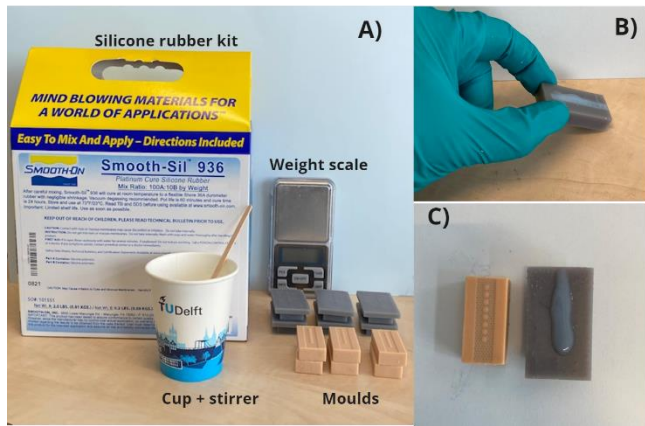


Figure 28: Images of A) the used resources to manufacture the prototypes, B) the pitching of the mould to allow the silicone rubber to flow through it, and C) the casted silicone rubber inside mould A and B ready to be cured.

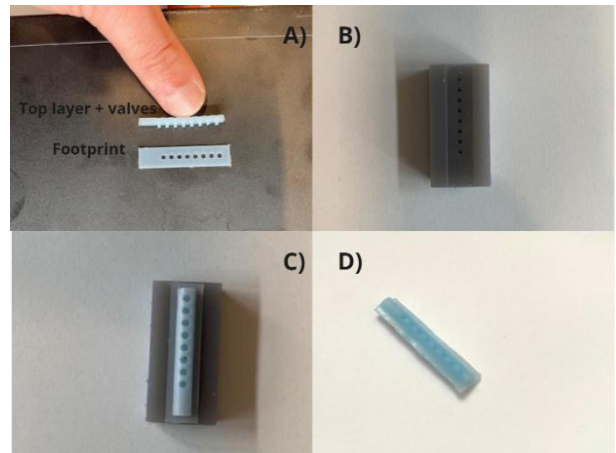


Figure 29: Images of A) the cured parts of the top layer with the self-regulating valves and the footprint, B) the plate used for assembly, C) the parts on the assembly plate, and D) the assembled version of the ProSTATIC.

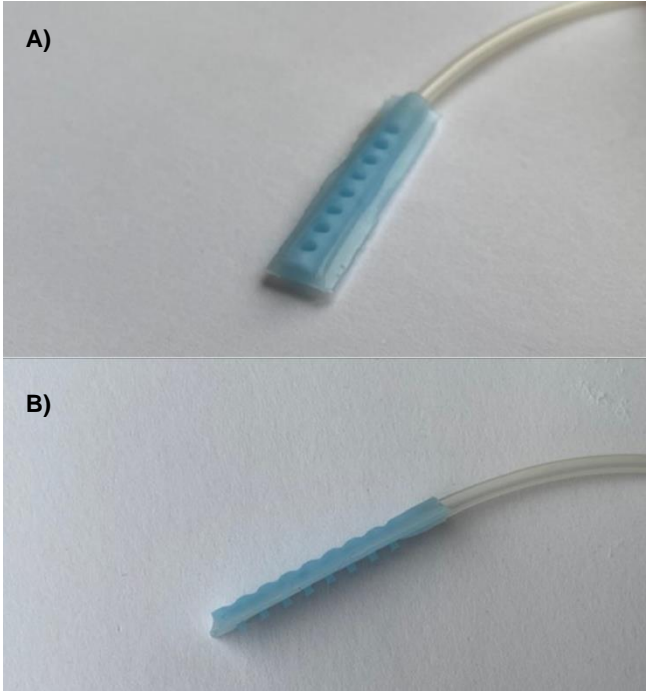


Figure 30: Images of the final prototype of the ProSTATIC connected to an air tube shown from A) the front and B) the side.

adhesive. Silicone rubber only adheres optimally with silicone based adhesives. Therefore, using silicone rubber as adhesive allowed to form a clean and airtight connection between the top and footprint. The assembly started by placing the footprint on an assembly as shown in Figure 29. The plate contained specially designed holes to fit the pins of the self-regulating valves in, so that the top layer could be placed straight on top of the footprint without tilting. The assembly plate was designed as a rectangular prism in CAD-software and was 3D-printed (Formlabs 3 printer). The dimensions of the plate can be seen in Appendix G.

Next, the silicone rubber adhesive was applied on the contact line between the top and footprint. The appliance was done by gravity-based dripping of the silicone rubber on the contact line; a thin stick was dipped in silicone rubber and moved over the contact line, while dripping the mixture till the contact line was fully covered. Thereafter, the silicone rubber was let to be cured for 24 hours. Figure 29 shows the assembled monolithic version of the ProSTATIC prototype and Figure 30 the final version with an air tube connected to the ProSTATIC. In total six suction cups were prototyped; one for every footprint design.

5 EXPERIMENTAL EVALUATION

5.1 Experiment I: Self-regulating valves

Experiment objective

The objective of Experiment I was to verify the functioning of the self-regulating valves on three types of prostate phantoms: (1) healthy tissue, (2) healthy-tumorous tissue, (3) full tumorous tissue.

Experiment variables

The working of the self-regulating valves was validated by measuring the development of the pressure difference ΔP

between the pressure inside of the ProSTATIC P and the atmospheric pressure P_{atm} in kPa as shown in Equation 5:

$$\Delta P = (P_{atm} - P) \quad (5)$$

In this experiment, the pressure difference in kPa was set as the dependent variable.

The experiment was performed on three types of prostate phantoms using (A) the base model of the ProSTATIC. These three phantoms differed from the percentage of nodules covering the surface and was therefore the independent variable. The elastic modulus of 68 kPa was the same for all the phantoms. The surface differed from (1) a surface with no nodules (healthy tissue), (2) a 50% covered surface (healthy-tumorous tissue), and (3) a 100% covered surface (full tumorous tissue). Nodules are lumps that occur on tissue surfaces due to a tumour [106]. A 4.2 mm diameter and 6.0 mm spacing between the nodules were taken based on the surface texture of a prostate with a tumour [107, 108].

The controlled variables were the actuation pressure of 50 kPa, the operation time of 48 seconds and the preload of 3 N on the ProSTATIC. The operation time was chosen based on the estimated insertion time of a brachytherapy needle [6, 109]. The value of the preload was simulated by the force exerted on a 300 cc tumorous prostate by a prostatic spacer [70].

Independent variables:

- Surface texture: (1) surface with no nodules (healthy tissue), (2) a 50% covered surface with nodules (healthy-tumorous tissue), and (3) a 100% covered surface with nodules (full tumorous tissue)

Dependent variables:

- Pressure difference between ProSTATIC and atmosphere in kPa

Controlled variables:

- ProSTATIC with (A) base footprint
- Preload 3 N
- Actuation pressure 50 kPa
- Operation time 48 seconds
- Elastic modulus phantoms 68 kPa

Experiment set-up

The experiment set-up of Experiment I is presented in Figure 31. The set-up consisted of a vacuum unit, a data acquisition unit, and a phantom platform.

Vacuum unit

The vacuum unit provided the desired pressure level of 50 kPa for the ProSTATIC. The vacuum unit consisted the vacuum tubing, a T-connector, syringe, and a syringe clamp. The ProSTATIC was connected to a 2.5 mm transparent rubber tube (SLNSIL-1.5x2.5 mm). This tube was connected to a larger 4 mm grey tube (FESTO PUN-4x0.75 mm) and fixed in a 4 mm T-connector (FESTO QST-4). The same grey

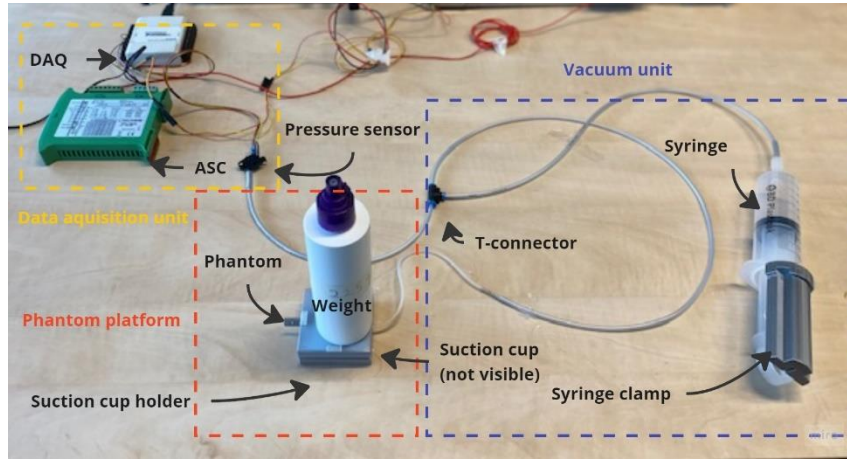


Figure 31: Image of the set-up of Experiment I consisting of the vacuum unit (purple), phantom platform (red), and data acquisition unit (yellow) with their corresponding components.

tube was used to connect the syringe with the T-connector, however the 4 mm grey tube could not directly fit on the tip of the 100 ml syringe, therefore a larger 6 mm tube (FESTO PUN-6x01.0 mm) was used as connection piece. The tubes were chosen based on their stiffness to prevent inward buckling when the vacuum was applied. The desired vacuum pressure of 50 kPa was maintained using a syringe clamp. The clamp was placed on the plunger of the syringe and pulled till the clamp was in-between the plunger tip and barrel. The clamp was custom designed for a 100 ml syringe and fabricated using a 3D-printer (Prusa i3 MK3S). The dimensions of the syringe clamp can be seen in Appendix G.

Phantom platform

The phantom platform consisted of the prostate phantom within a casing, a suction cup holder, fixating pins, and a weight. The three prostate phantoms were made using silicone rubber (Ecoflex™ 00-30) with an elastic modulus of roughly 68 kPa [110], which is similar to the elastic modulus of real prostate tissue 58.8 ± 8.2 kPa [111]. Silicone rubber is often used in literature as phantom for human tissue due to its small contracture over time [112]. Also, it does not require special storage conditions [112]. The three phantom types are shown in Figure 32. The phantoms were fabricated via mould casting. The design and dimensions of the used moulds can be consulted in Appendix G. These moulds were also the casing of the phantoms to hold them during the experiment. Furthermore, a suction cup holder was used to keep the ProSTATIC in place. The dimensions of the holder are shown in Appendix G. To place the prostate phantom straight on the suction cup, four fixating pins were used. These pins were inserted through specially designed holes in the phantom

casing and suction cup holder. The dimensions of these pins can be seen in Appendix G. A bottle containing 300 cc water was used as weight to simulate the 3.0 N preload on the ProSTATIC.

Data acquisition unit

The data acquisition unit consisted of a pressure sensor, an analogue signal conditioner (ASC), and a data acquisition card (DAQ). The pressure sensor (NXP, model MPX4115AP) was connected to a short 6 mm grey tube (FESTO PUN-6x01.0 mm), which was inserted over a smaller 4 mm tube (FESTO PUN-4x0.75 mm). The 4 mm tube was inserted in the T-connector together with the syringe and ProSTATIC. The pressure sensor was linked to an ASC (CPJ RAIL, SCAIME) and DAQ (NI USB-6008, National Instruments Corp.) sampled at 20 Hz. An ASC amplifies the electrical signal to a higher level and a DAQ transforms the analogue signal to a digital form that can be later processed in relevant data as force and pressure using computer software. The DAQ was connected to a laptop to transfer the digital data.

Experiment protocol

First, the self-regulating valves were tested on prostate phantom (1), then respectively on phantom (2), and (3). In total fifteen tests were performed, five for every phantom. Before starting with the experiment, the ProSTATIC was placed on the suction cup holder with the footprint facing upwards. Then, the phantom within the casing was placed on top of the ProSTATIC and the fixating pins were inserted. After the phantom was in place, the weight was put on top of the phantom. The ProSTATIC was now ready to be pressurised by pulling the syringe's plunger till the pressure of 50 kPa was reached. After the clamp was in place, the measurement was started.

5.2 Experiment II: Footprint grip

Experiment objective

The objective of Experiment II was to measure the maximum grip force of the ProSTATIC with the (A-F) six different footprints designed in Section 3.3 Final design of the ProSTATIC on a moving prostate phantom.

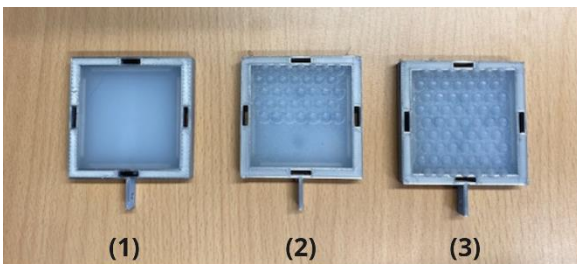


Figure 32: Image of the used prostate phantoms in Experiment I; (1) healthy tissue, (2) healthy-tumorous tissue, (3) full tumorous tissue.

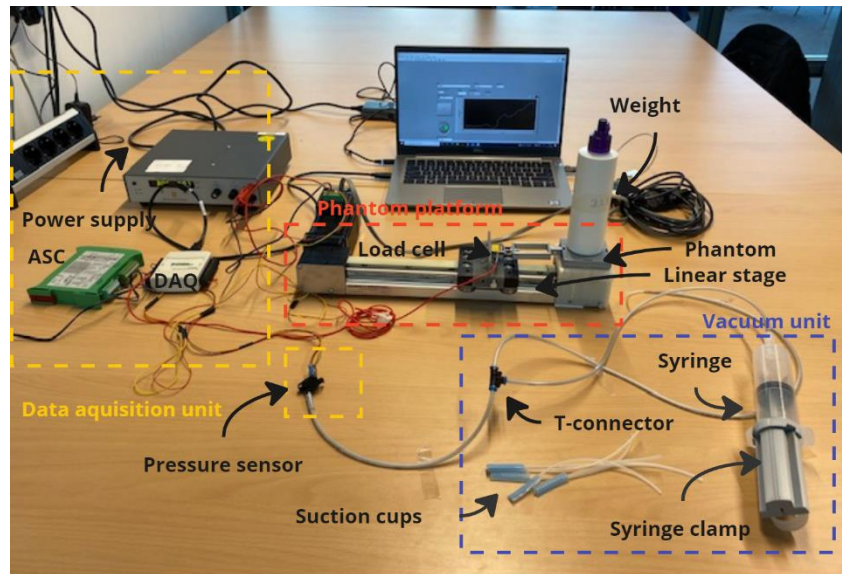


Figure 33: Image of the set-up of Experiment II consisting of the vacuum unit (purple), phantom platform (red), and data acquisition unit (yellow) with their corresponding components.

Experiment variables

The grip force was set as the independent variable of this experiment. The six different footprints were set as the dependent variable. The designs were as follows: (A) base footprint, (B) base footprint with enlarged suction holes, (C) base footprint with enlarged suction hole and radial ridges, (D) hexagon micro-patterned footprint, (E) hexagon micro-patterned footprint with enlarged suction holes, and (F) hexagon micro-patterned footprint with enlarged suction holes and radial ridges. The designs differed on three characteristics; surface pattern, suction hole size, and presence of the radial ridges. Also, the grip performance of the ProSTATIC was measured with and without vacuum.

The experiment was conducted on a smooth prostate phantom with an elastic modulus of 68 kPa ((1) healthy tissue phantom from Experiment I). It was found in literature that during brachytherapy the prostate is pushed with velocity of 0.4 mm/s over a 14 mm distance due to the insertion of the needle [17, 31]. For this experiment, the velocity of the stage was chosen to be 0.4 mm/s and the travel distance of maximal 28 mm was chosen to include the 14 mm prostate displacement. The ProSTATIC models were actuated with a 50 kPa pressure and the preload was set at 3 N.

Independent variables

- Six footprint designs: (A) base footprint, (B) base footprint with enlarged suction holes, (C) base footprint with enlarged suction holes and radial ridges, (D) hexagon micro-patterned footprint, (E) hexagon micro-patterned footprint with enlarged suction holes, and (F) hexagon micro-patterned footprint with enlarged suction holes and radial ridges
- Presence of vacuum

Dependent variables

- Grip force in N

Controlled variables

- Preload 3 N
- Linear stage speed 0.4 mm/s
- Travel distance 28 mm

- Elastic modulus phantom 68 kPa
- Actuation pressure 50 kPa

Experiment set-up

The experiment set-up of Experiment II is presented in Figure 33.

Vacuum unit

The same vacuum unit as described in Experiment I was used in this experiment as well.

Test platform

The test platform consisted of a horizontal linear translation stage (ALMOTION LT50-TR-G8). This stage provided the needed translation to mimic the prostate displacement as mentioned in the experiment variables. The stage was actuated using a built-in stepper motor to move it with a constant velocity of 0.4 mm/s over a 28 mm distance. The stage was powered by a power supply unit. The suction cup holder was fixated on the right side of the translation stage using a custom 3D-printed support (Ultimaker 3 printer). The support was fixated on the stage using M3x7 bolts and nuts. The dimensions of the support can be seen in Appendix G. Like in Experiment I, (1) the same healthy tissue phantom and weight were used.

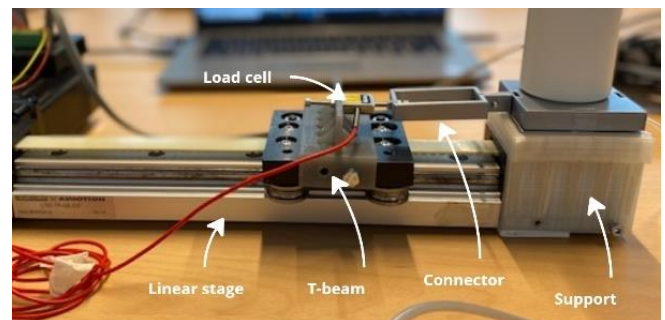


Figure 34: Image of the load cell connected to the horizontal linear stage using a T-beam and to the phantom casing with a connector piece.

Data acquisition unit

The data acquisition unit for Experiment II consisted of the same pressure sensor, ASC, and DAQ used in Experiment I and a load cell. The load cell (FUTEK, model LSB205) was used to measure the grip force of the ProSTATIC by moving the prostate phantom. The load cell was fixed on the moving stage using a custom 3D-printed T-beam and M5x7 bolts as shown in Figure 34. The T-beam was printed using a Formlabs resin printer (Form 3). The load cell was connected with the phantom casing using a 3D-printed rigid connection piece. The dimensions of the T-beam and connection piece are shown in Appendix G.

Experiment protocol

First, the models with the base footprint design (i.e., footprint designs (A)-(C)) were tested in alphabetical order. Thereafter, the other three models with the hexagon footprint design (i.e., footprint designs (D)-(F)) were tested in alphabetical order. Each grip force measurement for each footprint was repeated five times with and without vacuum, resulting in a total of 60 performed measurements.

Before starting the test, the set-up was prepared by (1) placing the suction cup holder in the support on the horizontal stage, (2) placing the ProSTATIC within the suction cup holder, (3) placing the phantom casing with the phantom on top of the ProSTATIC, and (4) fastening the casing with the load cell using the connection piece and a M4x7 bolt and nut. To mimic the wetness of real tissue, deionized water was injected on the phantom. Deionized water is often used as lubricant for tissue phantoms [57].

The suction cup holder was designed to maintain a gap between the suction cup holder and prostate phantom to prevent unwanted friction, which can lead to inaccurate grip performance measurements. Finally, the 300 cc water bottle was put on top.

Before starting the horizontal stage, the load cell was calibrated at the fixated location. The horizontal stage was actuated by a software called Q-programmer. Q-programmer is a computer program that allows the parameters as velocity and displacement to be set and operates the movement of the stage. The stage was set to have the same starting position for every measurement.

First, the measurements without vacuum were conducted for all footprints in alphabetical order, followed by the measurement with vacuum. Before starting the grip force measurements with vacuum, The syringe's plunger was pulled till a pressure of 50 kPa was reached and this pressure was maintained using the syringe clamp.

5.3 Experiment III: Prostate displacement

Experiment objective

The objective of Experiment III was to demonstrate the stabilisation capability of the ProSTATIC on a 3D-prostate phantom. The experiment was conducted using the best performing footprint from Experiment II. The simulated setting was a 3D-phantom of the pelvic cavity containing the models of the prostate, the surrounding tissue, and the rectum.

Experiment variables

Prostate displacement was the dependent variable of this experiment and was defined as the longitudinal (horizontal) distance in mm between the initial position and the displaced

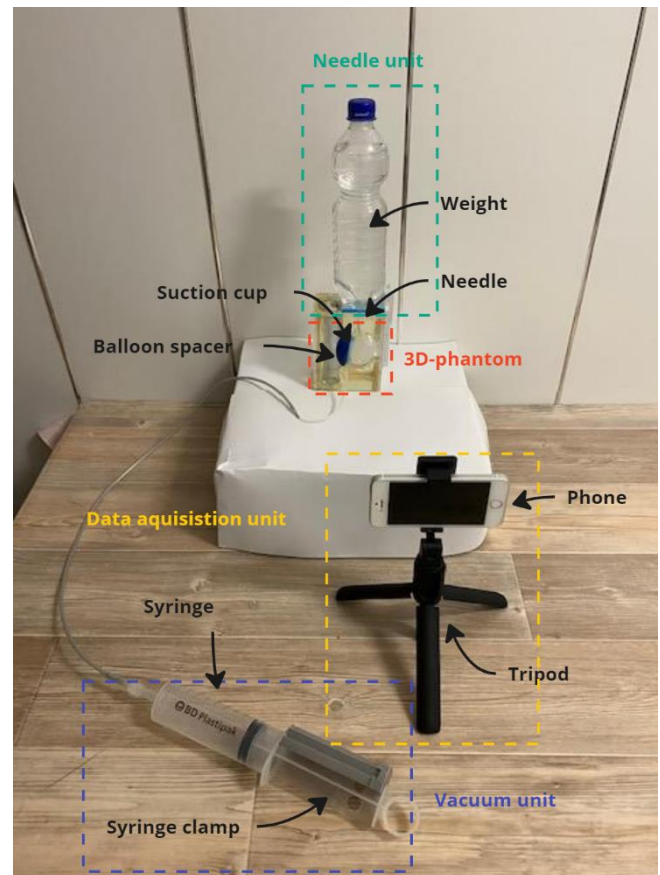


Figure 35: Image of the set-up of Experiment II consisting of the vacuum unit (purple), 3D-prostate phantom (red), and data acquisition unit (yellow) with their corresponding components.

position of the centroid of the prostate phantom. The independent variables were set as the presence of the ProSTATIC and vacuum. The pushing force on the prostate phantom was set at 5 N based on the average force exerted by a brachytherapy needle on a real prostate and the vacuum pressure was set at 50 kPa. The experiment was conducted using the best performing footprint from Experiment II. The measurements were conducted on a 3D-phantom of the pelvic cavity containing a spheroidal 50 x 45 x 40 mm prostate phantom with an elastic modulus of 68 kPa. The pushing force of 5 N was exerted using a 17 gauge steel rod resembling a brachytherapy needle and the preload was established by a 9 ml latex balloon resembling a prostatic spacer [113].

Independent variables

- Presence of the ProSTATIC
- Presence of vacuum

Dependent variables

- Longitudinal displacement of the prostate's centroid in mm

Controlled variables

- Pushing force 5 N
- Actuation pressure 50 kPa
- 3D-phantom of the pelvic cavity
- 17 gauge rod
- 9 ml balloon spacer
- ProSTATIC with the best performing footprint

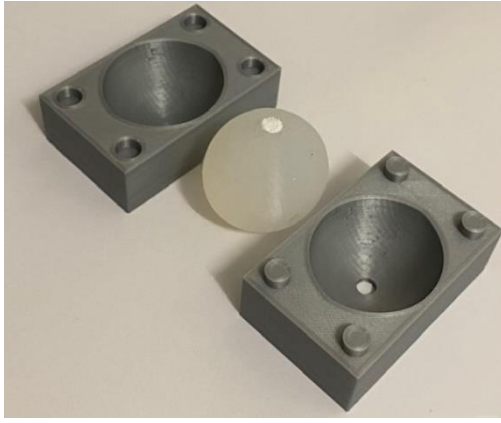


Figure 36: Image of the 3D-prostate phantom (middle) and the used mould.

Experiment set-up

The experiment set-up of Experiment III is presented in Figure 35.

Vacuum unit

The same vacuum unit used in Experiment I & II was utilised in this experiment as well.

3D -phantom

The 3D-phantom consisted of a prostate phantom, phantom of the surrounding tissue, phantom of the rectum, and a casing to place all the phantoms models in the desired configuration. The 3D-phantom was inspired by commercially available pelvic phantoms used for brachytherapy training [112, 114].

The 3D-prostate phantom as shown in Figure 36 was made out of silicone rubber with an elastic modulus of 68 kPa (Ecoflex™ 00-30) using mould casting. The mould was designed using a 40 x 45 x 50 mm prostate model in CAD-software and 3D-printed out of PLA (Ultimaker S5 printer). The mould dimensions are shown in Appendix G. The surrounding tissue phantom was made out of water-based gelatine. The gelatine formed 6% of the total weight to

resemble the stiffness of the surrounding tissue as fat and muscles [111]. Gelatine is a well-known substance to be used as tissue phantom due to its easy fabrication and tissue stiffness mimicry [112, 115]. In Appendix F the making of water-based gelatine is discussed. The rectum was simulated by a 115 mm long PVC-tube (25 x 3 mm). The PVC-tube was used to mimic the elastic nature of the rectum. The 3D-phantom casing was a 115 x 70 x 95 mm transparent box. One side of the casing was designed open to easily insert the prostate phantom and balloon spacer. Furthermore, the casing consisted of a 31 mm hole on both sides to connect the PVC-tube and a 2 mm hole to insert the needle during the experiment. The casing was an assembly of five panels, that seemingly fitted in each other via shape fitting. The panels were fixed together with kit (Pattex contact tix-gel) to create a leak free casing. These panels were designed using CAD-software (Solidworks) and fabricated out of 3 mm thick PMMA using laser cutting. The dimensions of the panels are presented in Appendix G.

Real prostatic balloon spacers used in brachytherapy were not commercially available and therefore the spacer for the experiment was replicated by a water balloon filled with 9 cc saline water [113].

The 3D-phantom itself was assembled by first fastening the PVC-tube in the casing using kit as shown in Figure 37. After that, the casing was filled with gelatine of the surrounding tissue. Filling was done stepwise, to correct align the prostate phantom with the rectum. First, the casing was filled till a 25 mm layer of gelatine was formed (see Figure 37). The casing was then placed in a refrigerator for 12 hours at 4 degrees Celsius. After the layer of gelatine solidified, the prostate phantom was placed on top, slightly above the rectum (see Figure 37). The prostate was kept in place via tape. After the prostate was in place, the casing was fully filled with gelatine. It was important to prevent the gelatine going in-between the rectum and the prostate phantom to keep space for the insertion of the ProSTATIC and balloon spacer later on. Therefore a thin foil was placed in-between the rectum and prostate phantom, which was later removed after the gelatine was fully solidified. Figure 37 shows the assembled 3D-pelvic phantom including the prostate phantom and rectum.

For this experiment the 3D-pelvic phantom was placed on its back, with the opening of the rectum facing upwards. This configuration allows to easily create the 5 N pushing force via gravitational force using a weight as will be discussed in the following section.

Needle unit

The needle unit consisted of a needle and a weight. For the needle a 17 gauge steel rod was used. The 5 N pushing force

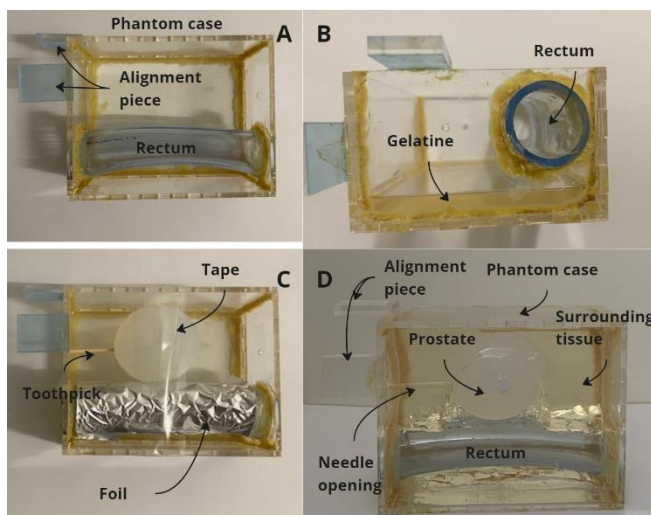


Figure 37: Images of the assembly of the 3D-pelvic phantom: A) the fastening of the rectum (PVC-tube) and alignment pieces, B) the filling of the 3D-phantom casing with 6% gelatine, C) the placement of the prostate phantom on the gelatine layer, and (D) the assembled version of the 3D- pelvic phantom with the components.

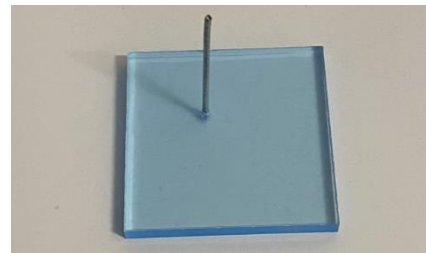


Figure 38: Image of the 17 gauge rod connected to a PMMA slab to resemble a brachytherapy needle.

was created by placing a 500 cc bottle on top of the needle. The needle was fixed to a slab as shown in Figure 38, allowing the bottle to be put on top of the needle without falling. The slab was aligned with two vertical pieces placed on two sides of the 3D-phantom to keep the needle straight during insertion.

Data acquisition unit

To measure the displacement of the prostate, millimetre graph paper was used. The measuring paper was adhered at the backside of the phantom casing. The centroid of the prostate phantom was marked with a white dot to easily measure the distance between the initial and displaced position. The displacement was captured using a telephone camera (12 Megapixel TrueDepth camera, iPhone 11) placed in a tripod (Maxxter).

Experiment protocol

Before starting the measurements, the 3D-phantom casing was placed vertically. Then the prostatic balloon spacer was placed between the rectum and prostate phantom, followed by the 17 gauge needle in the corresponding hole in the casing. The camera was placed straight in front of the prostate phantom and a measurement was conducted by placing the weight on top of the needle. First the measurement of the displacement without the ProSTATIC was performed, followed by the ProSTATIC in place with no vacuum, and lastly the ProSTATIC actuated with vacuum. Each measurement was repeated five times, resulting in total of 15 measurements.

5.4 Data analysis

The results of Experiment I and II were obtained via a computer software called LabVIEW 2018. The results were processed in Microsoft Excel. For Experiment I, the pressure difference graphs were plotted and compared between the three phantoms. Pressure difference graphs present the difference between the measured pressure in the ProSTATIC and the atmospheric in kPa over time. It allows for a clear visualisation of potential air leaks. For Experiment II, the development of the grip force in Newton and corresponding pressure difference graphs in kPa were plotted over a displacement. This allowed to see a potential relation between the grip force and pressure. Furthermore, the maximum grip force for every footprint design was presented. Also, the friction coefficient of the footprints were determined to see if the hexagon micro-pattern had an effect on the friction coefficient. The grip force and friction coefficients data were also analysed using student t-tests to identify if the differences in results were significant between the different footprints. The statistical significance value was set at a value of 0.05. If the t-tests yielded a lower value, it would mean that the differences were indeed significant i.e., the suction hole size and/or surface patterning had an effect on the grip force.

The results of the Experiment III were acquired via videos made by a telephone camera. The displacements were visually obtained by reading the longitudinal displacement of the prostate phantom's centroid via measurement paper. The measured displacements in millimetres were then processed in Microsoft excel. The displacements results were also analysed using t-tests with a significance value of 0.05, to

check if the differences between the results of the displacement were significant and therefore conclude if the ProSTATIC had effect on the prostate displacement.

6 EXPERIMENTAL RESULTS

6.1 Experiment I: Self-regulating valves

In an ideal situation, where no air leaks occur, the pressure difference between the ProSTATIC and atmosphere remains constant at 50 kPa over time on all types of prostate surfaces, indicating that the self-regulating valves work optimally. Experiment I showed via pressure difference graphs that the self-regulating valves work well on (1) healthy prostate tissue, but not on (2) healthy-tumorous tissue, and (3) full

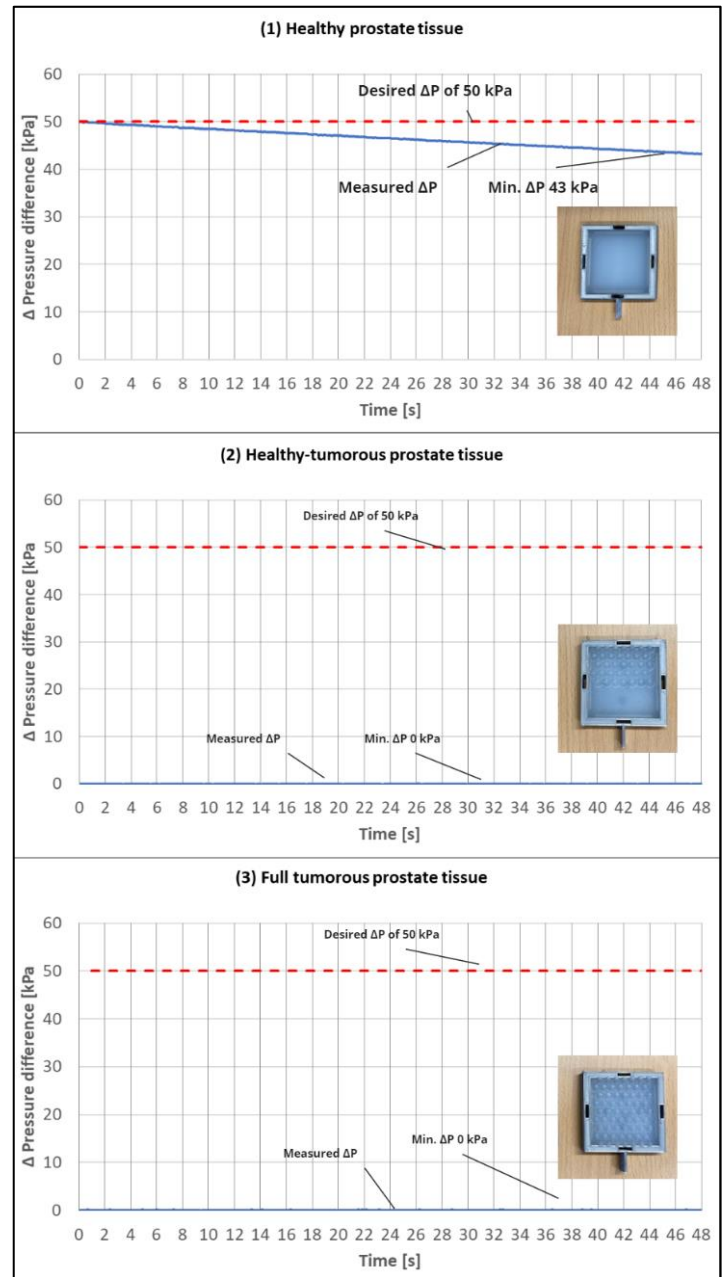


Figure 39: Graphs of the pressure difference between the ProSTATIC and atmosphere on (1) healthy, (2) healthy-tumorous, and (3) full tumorous prostate tissue phantoms. The desired pressure difference of 50 kPa is also shown (red line).

tumorous tissue (see Figure 39). When attached to (1) healthy tissue, the graph shows that the pressure inside the ProSTATIC is approximately constant at the beginning, but slowly increases at the end of the time period resulting in a pressure difference of roughly 43 kPa. This means that the measured pressure difference deviates with 7 kPa from the ideal situation when applied on (1) healthy tissue, indicating that there is a slight air leak. For the other prostate phantoms (2 & 3) the pressure difference between the ProSTATIC and the atmosphere was 0 kPa over the entire time period, indicating that there was a potential air leak somewhere within the ProSTATIC from the start of the measurement. The pressure difference graphs for all the measurements performed in this experiment can be found in Appendix H.

6.2 Experiment II: Footprint grip

Figure 40 shows the grip performance of the different footprint designs when a 50 kPa vacuum is applied. Beforehand, it was hypothesised that the hexagon micro-pattern (i.e., footprint designs (D)-(F)) would increase the grip force due to having a higher friction coefficient. However, Experiment II showed that (C) the base footprint with enlarged suction holes and radial ridges had the highest maximum grip force of 5.3 ± 0.14 N and was the only footprint design reaching the 5.0 N grip force mark needed for prostate stabilisation as stated in Requirement 1. While it can be seen that the other footprint designs (i.e., footprint designs (A), (B), (D)-(F)) generated a lower grip force than 5.0 N, especially the hexagon micro-patterned footprints (i.e., footprint designs (D)-(F)) having surprisingly the lowest grip performance. However, this result did not mean that the micro-pattern failed to increase the friction coefficient as stated beforehand. Therefore, to validate this assumption, the friction coefficient of each footprint was determined via Equation 6 [116],

$$F_G = \mu * F_p \quad (6)$$

$$\mu = \frac{F_G}{F_p} \quad (7)$$

where μ is the friction coefficient, F_G is the measured maximum grip force in N, and F_p is the preload of 3 N. The results in Figure 41 show that the footprints with the hexagon

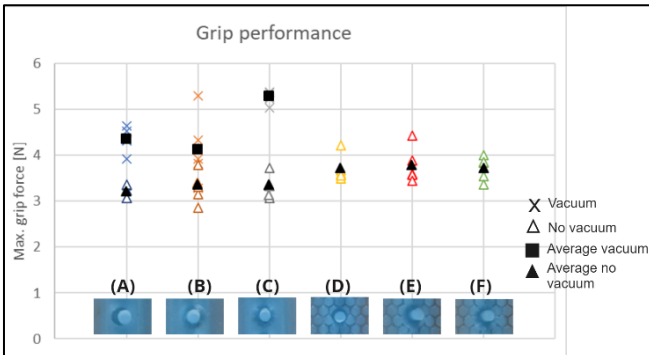


Figure 40: Results of the maximum grip force of the ProSTATIC with the six different footprint designs (A-F) with vacuum (presented in a X-shape) and without vacuum (presented in a Δ-shape) for all measurements. The average maximum grip forces are marked with a blacked out shape.

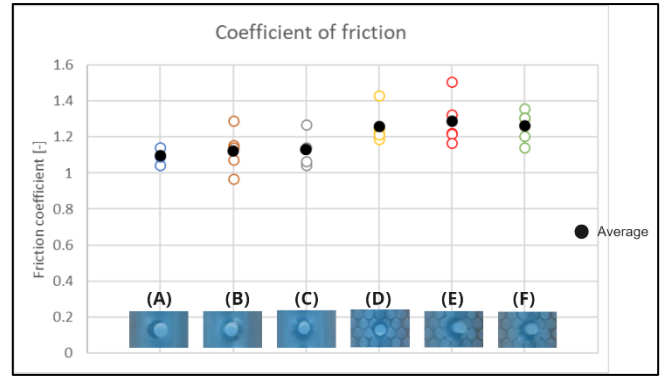


Figure 41: Results of the friction coefficient of the six footprint designs (A-F) for all measurements. The average friction coefficients are marked with a blacked out circle.

micro-pattern (i.e., footprint designs (D)-(F)) had a higher friction coefficient than their counterparts (i.e., footprint designs (A)-(C)), indicating that the hexagon micro-pattern indeed increased the friction coefficient. By virtue of these results, only (C) the base footprint containing enlarged suction holes and radial ridges was used in Experiment III to demonstrate its effect on prostate displacement.

The data were assumed to be normally distributed based on two normality tests done for data with small sample sizes (number of experiment repetitions is five or lower). Appendix K contains the performed normality tests. A t-test ($t(8)=0.61$, $p=0.56$) showed that there was no significant difference between grip performance (A) the base footprint and (B) base footprint with enlarged suction holes. However, for (C) the footprint with enlarged suction holes and radial ridges there was a significant difference in grip performance. This indicates that radial ridges are indeed beneficial in

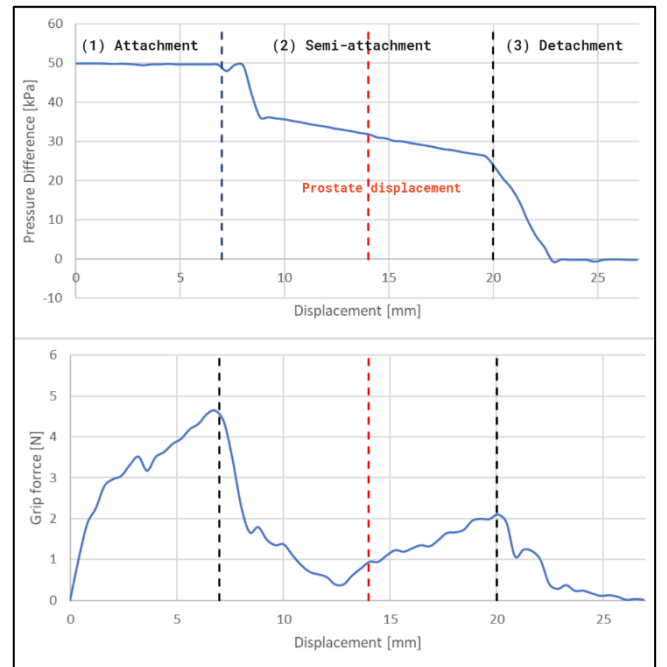


Figure 42: Graphs of the grip force and pressure development of the ProSTATIC over the displacement. The average prostate displacement is marked (red line). The graphs show the main phases of attachment; (1) attachment, (2) semi-attachment, and (3) detachment.

maintaining the effective suction area by preventing the tissue to be pushed within the holes.

Additionally, the grip performance of the ProSTATIC with the different footprints without vacuum, i.e., in their passive states, was tested as shown in Figure 40. The results showed that even without vacuum the ProSTATIC models generated a noticeable grip force. The footprints with the hexagon micro-pattern (i.e., footprint designs (D)-(F)) had relatively the highest grip forces in their passive states. A t-test between footprint design (A) and (D) showed that the difference in results was significant ($t(8)=3.4$, $p=0.0093$). This result indicates that an addition of a hexagon micro-pattern on the footprint indeed increases the grip force by increasing the friction coefficient, as beforehand discussed.

Furthermore, graphs of the development of the grip force and the pressure difference over the displacement were plotted as can be seen in Figure 42. The grip force and pressure graphs are presented under each other to see the correlation between the pressure difference and the grip force. Furthermore, for each footprint design, a graph of the development of the grip force and the pressure difference over the displacement were plotted as can be seen in Figure 42. The grip force and pressure graphs are presented under each other to see the correlation between the pressure difference and grip force.

The graphs also contain a visual indicator at 14 mm, which resembles the average displacement of the prostate during brachytherapy. The graphs show that there were three main phases of attachment on the tissue by the ProSTATIC: (1) attachment, (2) semi-attachment, and (3) detachment of the ProSTATIC. In phase (1), the footprint is fully attached to the tissue creating the highest grip force and maintaining the vacuum pressure of 50 kPa. In phase (2), some suction holes detach from the tissue due to movement of the phantom, resulting in some vacuum loss and therefore a decrease in grip force. The self-regulating valves stabilise the vacuum inside of the ProSTATIC by covering the detached suction holes. In phase (3), the remaining suction holes detach from the tissue, losing the vacuum pressure and therefore nullifying the grip force. The grip and pressure difference graphs for all the footprints can be found in Appendix I.

6.3 Experiment III: Prostate displacement

In Experiment III, the ProSTATIC with (3) the base footprint with enlarged suction holes and radial ridges demonstrated its stabilisation capability. Figure 43 clarifies the different components of the 3D-pelvic phantom. The results in Figure 44 visualise the displacement (A) without the ProSTATIC, (B) with the ProSTATIC without vacuum applied, and (C) with the ProSTATIC attached to the prostate phantom with vacuum applied. The results showed that without the ProSTATIC the centroid of the prostate was averagedly displaced 4.8 ± 0.84 mm in longitudinal direction. With the ProSTATIC attached to the prostate the displacement was limited to 1.3 ± 0.57 mm. This result showed that the ProSTATIC reduced prostate displacement by 75%. Also, the ProSTATIC without vacuum showed that the displacement was reduced to 3.0 ± 0.71 mm. This is a reduction of 38%, indicating that even without vacuum the ProSTATIC can contribute to prostate stabilisation. A t-test showed that the difference in results between using the ProSTATIC and not

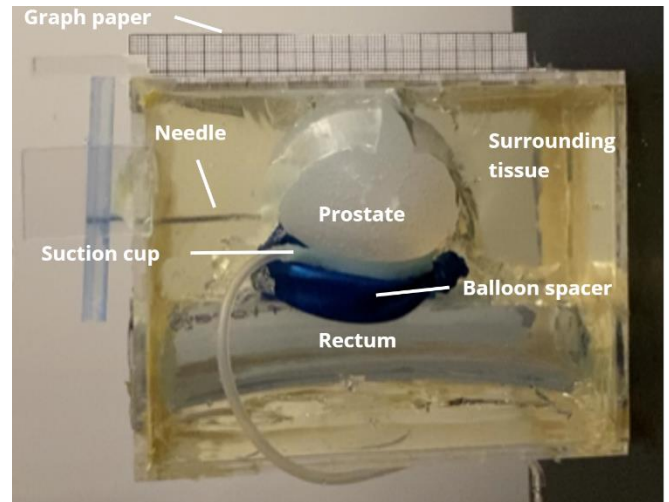


Figure 43: Close-up image of the used 3D-phantom for the pelvic cavity and the corresponding components.

using it was significant ($t(8)=7.95$, $p=0.0001$). The same yielded for the results of using vacuum and not using vacuum ($t(8)=4.4$, $p=0.0022$). The data were assumed to be normally distributed based on two normality tests conducted for data with small sample sizes (number of experiment repetitions is five or lower).

7 DISCUSSION

7.1 Main findings & interpretation

Prototype

In this study, a methodical and iterative design approach was used to design a stabilisation instrument for the prostate gland during brachytherapy. This resulted in a prototype of a novel modular suction cup with independent functioning suction holes referred to as the ProSTATIC. The ProSTATIC utilises the principle of suction to generate a grip force to counter the pushing force of a needle on the prostate gland. The ProSTATIC was designed as a structure of layers with their own functionality; (1) the top, (2) the footprint, and (3) the self-regulating valves. A prototype of the ProSTATIC was monolithically fabricated out of silicone rubber (Smooth-SilTM 936) using mould casting. The prototype was used in experiments to evaluate the functionality and performance of the ProSTATIC.

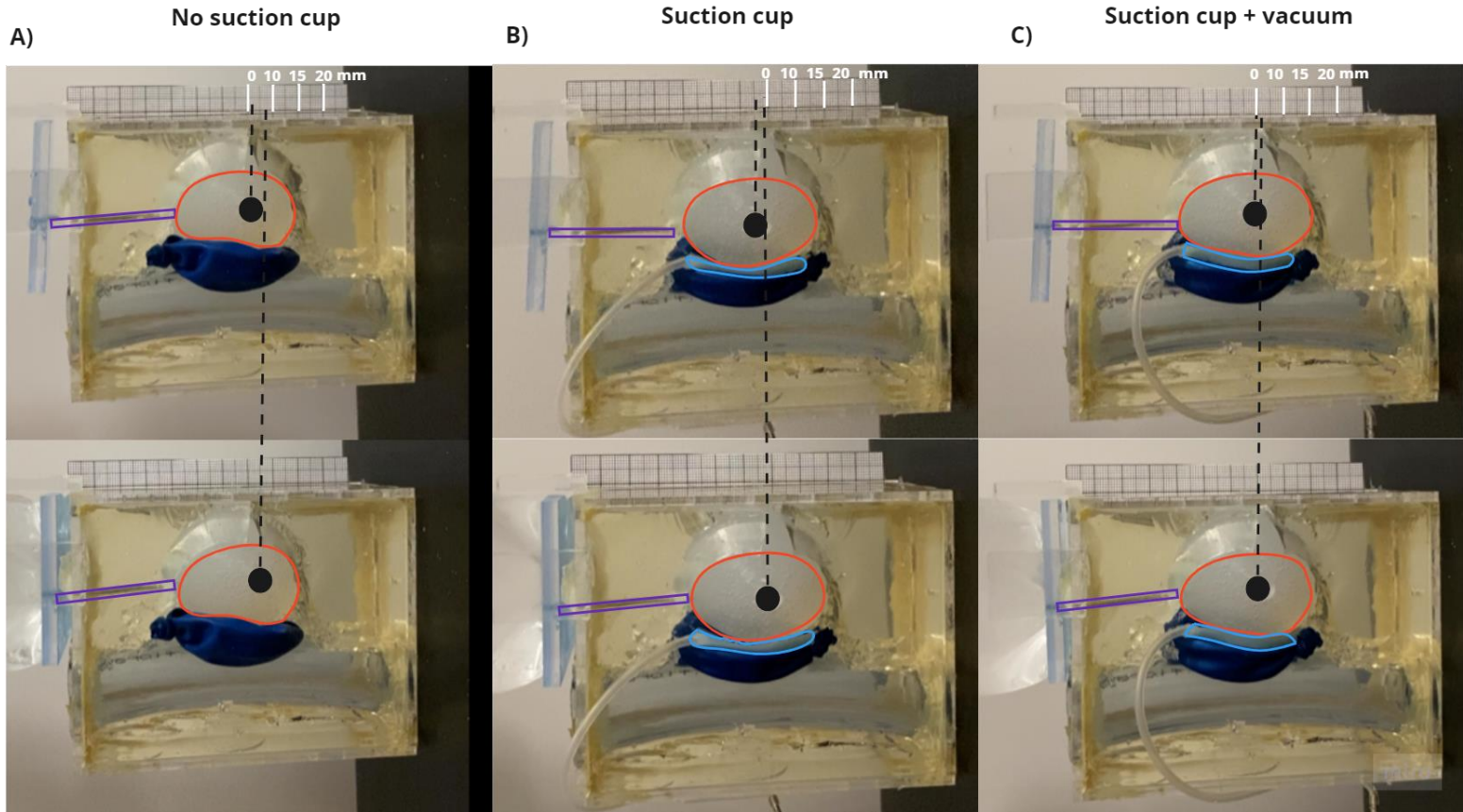


Figure 44: Photographic results of the longitudinal prostate displacement A) without the ProSTATIC suction cup, B) with the ProSTATIC without vacuum, and C) The ProSTATIC actuated with vacuum. Colour indications were added to see the displacement of the middle point (black dot) more easily and distinguish the prostate (orange), the ProSTATIC (blue), and the needle (purple) from the surrounding tissue.

Functioning of self-regulating valves

Experiment I showed that the self-regulating valves of the ProSTATIC only work well on the phantom concerning (1) healthy prostate tissue, but not on (2) healthy- tumorous, and (3) full tumorous tissue. On (1) healthy tissue phantom, the pressure difference between the ProSTATIC and the atmosphere was slightly reduced over time to a value of roughly 43 kPa. This shows that there was a pressure loss of 7 kPa from the initial pressure difference of 50 kPa. Boyle's law states that the pressure is inversely proportional to the volume of the gas i.e., if the volume increases, the pressure will decrease as shown in Figure 45 [117]. Applying this law to the pressure inside the ProSTATIC, we can say that initially the extracted air volume from the ProSTATIC suction cup was relatively larger, resulting in lower a

Boyle's law

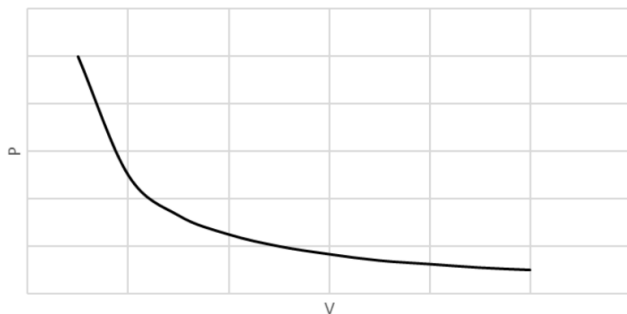


Figure 45: Visual representation of Boyle's law; the pressure is inversely proportional to the volume of the gas, where the vertical axis represents the pressure and the horizontal axis the volume.

pressure. However, over time if an air leak is present, the extracted air volume within the syringe will reduce, resulting in a decrease in the pressure difference. This corresponds with the results from Experiment I, where a decrease in the pressure difference is seen. The cause of the pressure loss may not per se be the result of a failure of the self-regulating valves. Rather, it could be a result of not forming an optimal seal of the footprint with the phantom tissue, leading to an air leak(s) at the edges of the footprint. Also, the pressure loss could be due to extrinsic errors such as the tubing and syringe not being fully airtight, resulting in occurrences of small air leaks.

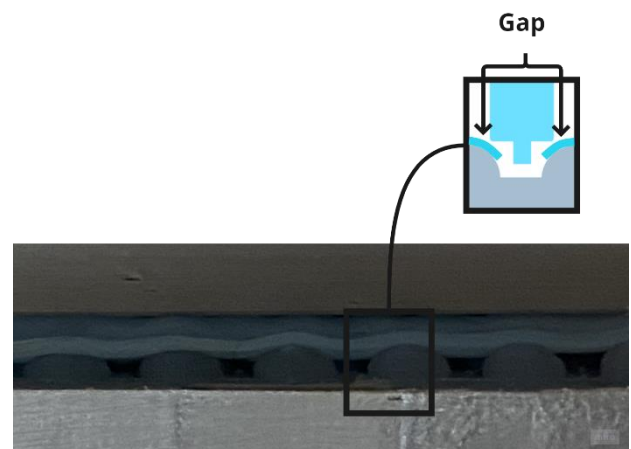


Figure 46: Image of the deformation of the interface between the footprint and nodules during preload resulting in air gaps between the self-regulating valves and footprint.

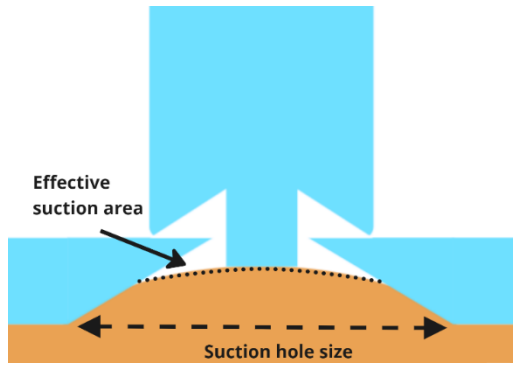


Figure 47: Schematic image of a tissue being pushed within the truncated holes, reducing the effective area of suction.

For both the (2 & 3) healthy-tumorous tissue and full tumorous tissue phantoms the pressure difference was 0 kPa at the start of the measurements. When closely inspecting the interface of the nodules and footprint during the experiment, it can be seen that some suction holes were deformed in shape. The deformation was most likely caused by the nodules pressing against the area around the suction holes during preloading of the ProSTATIC as schematically visualised in Figure 46. As a result, the self-regulating valves could not properly cover the deformed holes, resulting in air gaps between self-regulating valves and footprint.

Grip performance

In Experiment II the results indicated that ProSTATIC with (C) the base footprint with enlarged suction holes and radial ridges had the highest maximum grip force of 5.3 ± 0.14 N on prostate phantom. Meaning that this was the only footprint design that met Requirement 1: providing at least a grip force of 5 N to stabilise the prostate during brachytherapy. The (1) base footprint and (2) footprint with enlarged suction holes had roughly the same grip performance; 4.4 ± 0.28 N and 4.1 ± 0.75 N respectively. This could be explained by the fact that in a truncated suction hole tissue can be pushed deeper as shown in Figure 47, resulting in a much lower effective area of suction. The added radial ridges inside the suction holes seemed to have significant effect on maintaining the effective area of suction and therefore having a relatively larger grip performance than without.

The hexagon micro-patterned footprints (i.e., footprint designs (D)-(F)) had surprisingly the lowest grip performance. Beforehand, it was hypothesised that the hexagon micro-pattern would increase the grip force due to having a higher friction coefficient. However, the pressure difference graphs of these footprints (see Appendix I) showed that no vacuum was established at all, resulting in zero suction force generation. This result could be explained by the fact that no airtight seal was formed between the phantom and the footprint due to the presence of the channels between the hexagon pillars, which expanded to edges of the footprint. However, this result did not mean that the micro-pattern failed to increase the friction coefficient. Rather, the determined friction coefficients of the footprints showed that the footprints with the hexagon micro-pattern (i.e., footprint designs (D)-(F)) had higher friction coefficients compared to their base model counterparts (i.e., footprint designs (A)-(C)). It is perhaps surprising to remark that the friction coefficients were all higher than 1, but this is normal for silicone rubber,

especially on applications on other rubber substrates such as the used silicone rubber phantom in Experiment II [118, 119].

Prostate stabilisation

The ProSTATIC with (C) the base footprint design of enlarged suction holes and radial ridges demonstrated in Experiment III that the longitudinal prostate displacement was averagely reduced from 4.8 ± 0.84 mm to 1.3 ± 0.57 mm. This is a reduction of 75%. Not having a 100% reduction value could be explained due to the stretching of the elastic ProSTATIC in shear direction, which might lead to slipping of the footprint from the prostate phantom. The results indicate that the ProSTATIC indeed could stabilise the prostate during brachytherapy. Furthermore, the ProSTATIC also demonstrated that without vacuum it can still reduce prostate displacement from 4.8 ± 0.57 mm to 3.0 ± 0.71 mm, indicating that it still can contribute to prostate stabilisation due to the micro-gripping capability of the pins of the self-regulating valves and the high friction coefficient value of silicone rubber.

Requirements check

A checklist of the design requirements as stated in **Section 3.1 Design requirements** is shown in Table 1, which describes if these requirements are fulfilled by the prototype of the ProSTATIC.

Table 1: Checklist of the design requirements, where Y stands for fulfilled, Y* partially fulfilled, and N not fulfilled.

Requirements		
Functionality	Fulfilled (Y/Y*/N)	Explanation
1. Grip force 5 N	Y*	Only the ProSTATIC with (C) the base footprint with enlarged suction holes and radial ridges was able to generate a grip force of at least 5 N.
2. Limit prostate displacement	Y	The ProSTATIC demonstrated in Experiment III that it can limit the displacement by 75%.
3. Transperineally insertion 90 mm	Y	The ProSTATIC can be guided via the opening in the perineum and placed in the rectoprostatic space.
4. Seal generation & pressure maintenance 50 kPa	Y*	The ProSTATIC was only able to form a seal with (3) the healthy prostate phantom.
5. Manual operation	Y	The ProSTATIC was able to be manually inserted and pressurised without any assistance.
6. Compatible with needles and spacer	Y	The ProSTATIC did not hinder the functionality of the needles and spacer.
7. Damage control	Y	The used silicone rubber and 50 kPa vacuum pressure did not damage the tissue phantoms.
Dimensions		
8. Fit in 5 mm incision	Y	The shape and elasticity of the ProSTATIC allows fitting in the incision.
9. Fit in rectoprostatic space 43 x 30 x 11 mm	Y	The ProSTATIC is smaller than the rectoprostatic space.

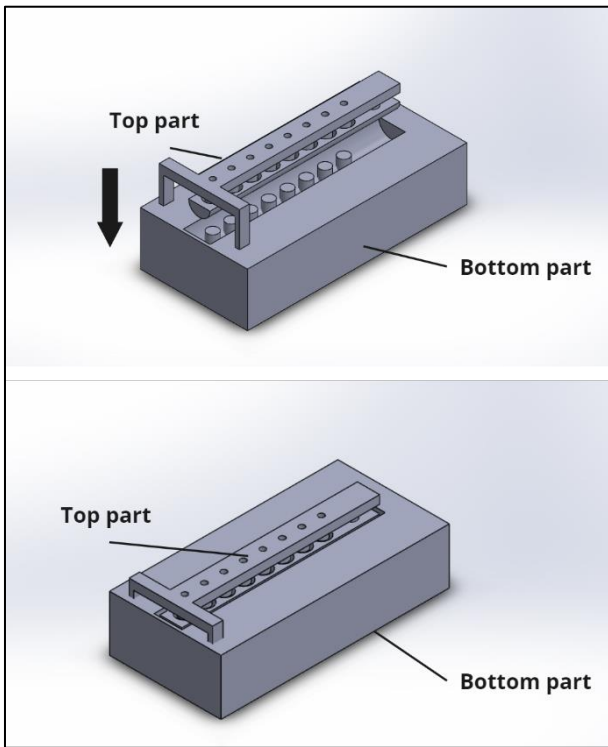


Figure 48: Illustration of a single mould consisting of a top and bottom part to manufacture the ProSTATIC without assembly. The top part is clicked on top of the bottom part.

7.2 Limitations & recommendations

The used silicone rubber for the prototype (Smooth-SilTM 936) has a curing time of 24 hours, leading to an inefficient manufacturing process [110]. The process could be made more efficient by designing a new mould where the assembly of the ProSTATIC layers is not needed. A proposal of such a mould is shown in Figure 48. It consists of two parts; a top part for the self-regulating valves and the bottom part for the top layer and footprint. The use of a single mould removes the need of assembly of the footprint and top layer, reducing the manufacturing time by 24 hours. However, the downside of using a single mould is the increased complexity, especially on such small scale. Another option can be to treat the silicone rubber mixture with heat to reduce the curing time or even use a different silicone rubber with a lower curing time.

For the fabrication of the hexagon micro-pattern, a 3D-printer of the brand Formlabs (Form 3) was used. However, due to the printer resolution the exact dimensions of the hexagon pillars, as presented in literature, could not be applied. As a result, the dimensions were scaled to the minimum print size of the printer. The minimum print size was obtained by conducting a print test of different-sized hexagon shapes on a cube as shown in Figure 49 and analysing at which dimensions the hexagon shape was still recognizable. The upscaling of the hexagon pillar dimensions and therefore the channels between the pillars could have affected the seal-forming capability of the hexagon micro-patterned footprints. For future prototyping, a fabrication method that can create a mould with the correct hexagon pillar dimensions is recommended. An example of such a fabrication method is SU8 photolithography. This method allows creating of micro-patterns in a material by exposing

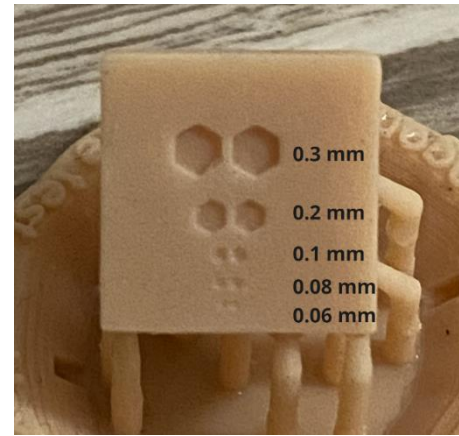


Figure 49: Image of a test of the print resolution of the Formlabs Form 3 printer to analyse at which dimensions the hexagon shapes are still recognizable. Hexagons smaller than 0.2 mm show detail loss.

UV-light through a micro-structured mask on a photoresist-coated silicone substrate, leaving a latent pattern in the substrate that can be used as a mould to create the micro-pattern [120].

Prostate phantoms

The experiments of this study were conducted on phantoms that mimicked the prostate. In practice the prostate differs in characteristics for each man, resulting in some limitations of our phantoms. One of these limitations was that the focus was on prostate surface texture and not on stiffness. As a result, only the elastic modulus of normal prostate tissue 58.8 ± 8.2 kPa was comprised for all the phantoms using silicone rubber with an elastic modulus of 68 kPa [111]. However, the presence of a tumour cells can result in different elastic moduli; for benign prostate tissue 54.47 ± 25.04 kPa and malignant prostate tissue 95.52 ± 39.65 kPa [121].

Another limitation was that the surface texture used for tumour tissue in Experiment I was a pattern created based on the average nodule size and shape of malignant prostate tissue. This resulted in a phantom with a homogeneous and isotropic surface texture, whereas in real life prostate tissue is anisotropic and heterogeneous [122].

Therefore, for future testing the usage of more fidelity phantoms is recommended. Real prostate tissue is ideal, however the accessibility of using real human tissue is limited due to ethical regulations and standards by the EU Tissue Directive [123]. The same yields for the usage of animal tissue. An alternative and more accessible method can be creating a custom mould from 3D-scans (via MRI or CT) of a real prostate, capturing the anisotropic and heterogeneous characteristics [124].

Experiments

One of the main limitations was the small sample size of the conducted measurements, which consisted of five repetitions per experiment. A larger sample size gives more precision of the results and the power to conclude from these results by using statistical analysis. Choosing the correct statistical analysis method depends on whether the data were seen as normally distributed or not. Normality tests are used to give evidence if the data are normally distributed. For the results in Experiment I & II, we used two normality tests;

Kolmogorov-Smirnov & Shapiro-Wilk tests. These tests require only five or lower values to check for normality[125]. The results showed that the data in both experiments can be assumed as normally distributed, except for the (D) hexagon micro-patterned footprint. However, we still choose to approach it as a normal distribution due to other data passing the tests. For future testing, it is recommended to increase the sample size if possible.

Also, it could be interesting to test the grip performance by varying the pressure inside of the ProSTATIC, to see the relationship between the grip force and pressure difference. Furthermore, the grip performance on non-flexible materials such as glass could also be tested to get more insight into the grip capability outside of tissue manipulation. Additionally, measuring the grip performance of different configurations of the ProSTATIC by placing it transversal (rotating it 90 degrees) or opposite longitudinal (rotating in 180 degrees) and using multiple suction cups could also be insightful.

Furthermore, a practical limitation in Experiment II was the difficulty of placing and balancing the weight, without letting the tissue phantom contact the surface of the suction cup holder. If not correctly placed, the phantom tilts and touches the suction cup holder causing unwanted friction, which can lead to incorrect measurements of the grip performance. For future measurements, an easier weight loading method could be used for example by placing two ProSTATIC suction cups next to each other instead of one in the middle. When using this method the preload weight needs to be doubled and the results give the grip performance of two suction cups.

In Experiment III, the 6% gelatine was used as a tissue-mimicking phantom for the surrounding tissue, as it is cheap, easy to use, and the stiffness can be controlled by changing the gelatine concentration. However, in between the measurements it was noticed that the gelatine started to rupture as shown in Figure 50, which was caused by high stresses occurring in the gelatine due to the force of the needle. For future testing, a more durable material such as silicone rubber or multiple gelatine phantoms should be used. Also, Experiment III only included the measurements of the longitudinal displacement of the prostate. In future experiments, the displacements in sagittal and frontal directions and the rotational displacements in the three planes

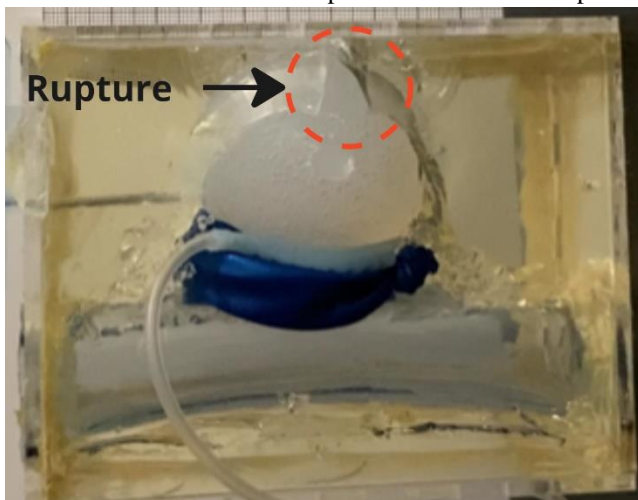


Figure 50: Image of the occurrence of a rupture caused by stresses in the gelatine phantom due to the force of the needle on the prostate phantom.

should be included to acquire the overall stabilisation performance of the ProSTATIC.

7.3 Future work

Footprint optimisation

One of the future focus points should be finding the optimised footprint flexibility to reduce the deformation of the suction holes, which hinder the functionality of the self-regulating valves. Finite element modelling (FEM) could be used to find the optimal elastic modulus of the footprint by simulating the stresses and deformations of the footprint in shear and normal direction or making the stiffness of the footprint variable by adding a layer-jamming mechanism. A layer-jamming mechanism consists of a stack of multiple layers of flexible material [86]. When these layers are pressed against each other, they will reduce the sliding action between the layers by increasing the friction, resulting in an increased stiffness. For the ProSTATIC this layer-jamming mechanism can be implemented in the air chamber. The applied vacuum will compress these layers and create a higher stiffness of the footprint during operation. This allows the footprint to be flexible for surface adaptability and become stiff during stabilisation.

Furthermore, the micro-pattern on the footprint could be optimised as well. The current hexagon micro-pattern hinders the sealing capability of the suction cup due to the presence of channels at the edges of the footprint. This could be improved by not letting the pattern expand to the footprint edges, by determining the distance between the pattern boundary and edges, where the air leaks are minimal. Another option can be downscaling the micro-pattern and therefore also the channels between the hexagon pillars till the air leakages are minimised. Also, research in different micro-patterns could lead to a more beneficial micro-pattern for the ProSTATIC.

Integrated preload mechanism

The preload is a perpendicular force applied on the ProSTATIC to press it against the prostate to establish a needed seal for suction. In this study, the preload was generated via a prostatic spacer used during brachytherapy. However, this made the usage of the ProSTATIC dependent on the presence of the spacer. Therefore, for future iterations an integrated preload mechanism for the ProSTATIC should be researched on. A proposal of such a mechanism can be adding a balloon feature on top of the ProSTATIC as an additional layer as shown in Figure 51. When inserting the ProSTATIC in the retroprostatic space, the balloon is empty, however when in place the balloon is inflated with air (or a

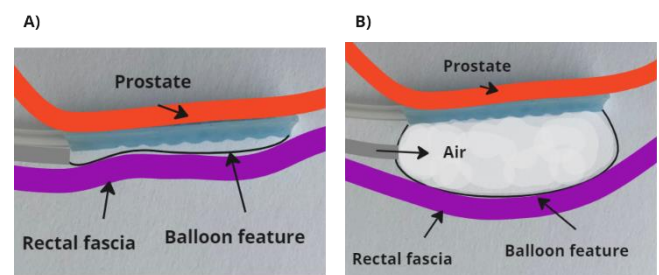


Figure 51: Illustration of an integrated preload mechanism in the form of a balloon feature on the ProSTATIC. The balloon is A) deflated when inserted through the perineum and B) inflated with air when in place.

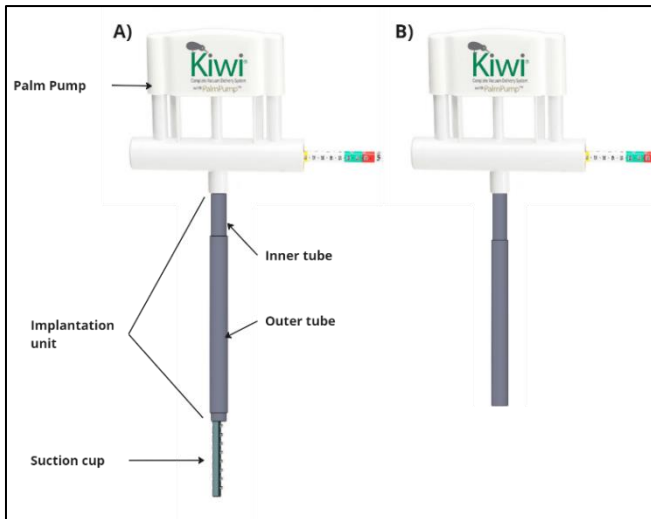


Figure 52: Illustration of the ProSTATIC with the Palm Pump™ and the concentric tubes implantation unit during A) operation mode where the ProSTATIC is exposed and B) passive mode where the ProSTATIC is covered by the concentric tubes. The image of the Palm Pump™ was adapted [126].

saline solution), increasing the volume of the balloon and therefore pressing the ProSTATIC against the prostate. For the inflation of the balloon a separate vacuum pump can be used or a one-way valve can be integrated in the balloon. The integrated balloon can also function as a spacer between the rectal fascia and prostate, removing the need of a separate spacer.

Clinical usage

Adding a vacuum system and implantation unit to the ProSTATIC can give an impression of the operation during an actual brachytherapy session. Vacuum generators are generally present within the operation rooms, making the usage simple as just connecting the ProSTATIC with tubing. The benefit of using a vacuum generator is maintaining the vacuum pressure via a continuous outflow of air from the ProSTATIC, compensating for the potential vacuum losses during the intervention. However, the continuous airflow can affect the pressure within the pelvic cavity. Therefore, a safer alternative can be using a manual vacuum pump such as the Palm Pump™, which is a manual operable device used as a vacuum pump for foetal delivery systems like the Kiwi Omni cup™ to assist in childbirth [126].

For a safe insertion of the ProSTATIC, an implantation unit can be used. An example of such a unit is a concentric configuration of two biocompatible tubes, i.e., an inner and outer tube. The ProSTATIC is connected to the inner tube and placed in the outer tube, which will be inserted through an incision in the perineum. When reaching the retroprosthetic space, the ProSTATIC becomes exposed by pulling the outer tube backwards, while holding the inner tube stable. If the ProSTATIC is not needed anymore, the outer tube can be pushed over the ProSTATIC again and pulled out of the body. Additionally, medical lube or talc powder can be used to reduce the friction between the tubes and the ProSTATIC. An visual impression of the ProSTATIC with the Palm Pump™ and implantation unit is presented in Figure 52.

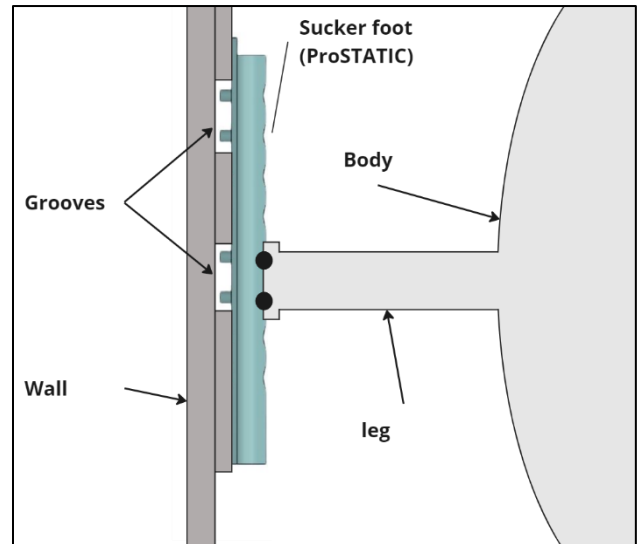


Figure 53: Illustration of the application of the ProSTATIC as a sucker foot for a rescue robot. The image shows the interaction of the sucker foot consisting of the ProSTATIC with a vertical wall with grooves and ridges during climbing. The sucker foot is connected to the body of the robot via a leg.

Application fields

The ProSTATIC can be applied for different surgical interventions besides brachytherapy that also utilise needles such as focal laser ablation, cryotherapy, and needle biopsies [21, 127, 128].

Additionally, the suction cup can be applied on different slippery organs and structures e.g., liver, kidney, and arteries that need volumetric stabilisation. The ProSTATIC can also be favourable to replacing currently used surgical tools. For example, the epicardium of a beating heart needs to be stabilised to perform safe coronary artery bypass surgeries [77]. This is currently done by using the Octopus heart stabiliser as mentioned in **Section 2.4 State of the art: the Octopus heart stabiliser™**, which is a suction cup with multiple suction holes connected to a single air chamber. However, this suction cup is prone to attachment failures when a single suction hole fails to make a sealed contact with the epicardium [63]. The ProSTATIC however could provide more reliability due to the presence of the self-regulating valves reducing the risk of attachment failures, making the surgery more time efficient and safer.

The ProSTATIC can also be used as a surgical gripper for tissue manipulation as lifting or holding. Currently used grippers often utilise macro teeth jaws to pinch the delicate tissue in between. However, this results in high stresses occurring in the tissue, which can lead to tissue trauma [57, 58].

Besides the medical scene, the ProSTATIC can be applied in other industries as well. An application can be to utilise it as a robotic gripper to gently grip and place fragile microchips in hardware or even for packaging delicate consumer meat.

Another interesting application as visualised in Figure 53, is using the ProSTATIC as foot for the locomotion unit of a rescue robot as one proposed by Hirose *et al.* [102]. This robot can be used for dangerous operations involving irregular and wet surfaces e.g., rescuing a person from a high building during rain by climbing the wet walls. The flexibility

of the ProSTATIC allows for adapting to uneven grooves of the building and the self-regulating valves prevent attachment failures of the robot when making contact with a cracked wall surface.

Symbiosis with other techniques

In this study, we focussed on designing an instrument to deal with global prostate displacement, to eventually reduce target deviation errors within the prostate. However, targeting errors caused by the needle as described in **Section 1.2 Target deviation error** also include other error sources such as needle bending and prostate deformation. These sources are thoroughly studied in literature, resulting in solutions in the form of needle steering, symmetric needle tip designs, and new insertion techniques such as spinning and high-speed insertion. For future research, it could be interesting to combine these methods with the ProSTATIC to design a new instrument that could fully deal with target deviation errors.

8 CONCLUSION

In this study, we designed and evaluated a novel instrument that can stabilise the prostate during brachytherapy by limiting the experienced displacement by the needles. The stabilisation instrument is a slender suction cup that can be transperineally inserted via a 5 mm incision, to attach on the prostate surface within the rectoprostatic space. The suction cup is referred as the ProSTATIC and has a modular multi-holed design consisting of three structural layers with their own functionality; (1) the top layer to maintain the pressure inside of the ProSTATIC and provide for the structural stability, (2) the footprint to adapt and form a closed seal with the prostate surface, and (3) the self-regulating valves to increase the attachment reliability on irregular surface textures. For the footprint, we assessed different micro-patterns and suction hole sizes to increase the overall grip force. The monolithic prototype of the ProSTATIC was fabricated out of biocompatible and ultrasound-compatible silicone rubber using mould casting. The experimental evaluation using silicone rubber based prostate phantoms showed that the ProSTATIC with the base footprint design with the enlarged suction holes and radial ridges was able to generate a maximum grip force of 5.3 ± 0.14 N, which was larger than the 5 N required for prostate stabilisation and demonstrated that prostate displacement was reduced by 75% during needle insertion. The prototype proposed in this study forms an initial breakthrough in safe and reliable volumetric stabilisation of the prostate gland during brachytherapy.

9 REFERENCES

- Xia, S.-J., D. Cui, and Q. Jiang, *An overview of prostate diseases and their characteristics specific to Asian men*. Asian Journal of Andrology, 2012. **14**(3): p. 458-464.
- Sung, H., et al., *Global Cancer Statistics 2020: GLOBOCAN Estimates of Incidence and Mortality Worldwide for 36 Cancers in 185 Countries*. CA: A Cancer Journal for Clinicians, 2021. **71**(3): p. 209-249.
- Marieb, E.N. and K. Hoehn, *Human Anatomy & Physiology, Global Edition*. Vol. Tenth edition. Global edition. 2015, Harlow: Pearson.
- The Prostate Gland - Structure - Vasculature - Lymph - TeachMeAnatomy*.
- Nag, S., P.S. Fernandes, and R. Bahnson, *Transperineal image-guided permanent brachytherapy for localized cancer of the prostate*. Urologic Oncology: Seminars and Original Investigations, 1998. **4**(6): p. 191-202.
- Brachytherapy - Mayo Clinic*.
- Prostatectomy - an overview | ScienceDirect Topics*.
- External beam radiation therapy for prostate cancer - Horwitz - 2000 - CA: A Cancer Journal for Clinicians - Wiley Online Library*.
- Putora, P.M., et al., *Erectile function following brachytherapy, external beam radiotherapy, or radical prostatectomy in prostate cancer patients*. Strahlentherapie und Onkologie, 2016. **192**(3): p. 182-189.
- Zhang, P., et al., *Radical prostatectomy versus brachytherapy for clinically localized prostate cancer on oncological and functional outcomes: a meta-analysis*. Translational Andrology and Urology, 2020. **9**(2): p. 332-343.
- Shariat, S.F. and C.G. Roehrborn, *Using Biopsy to Detect Prostate Cancer*. Reviews in Urology, 2008. **10**(4): p. 262-280.
- The Needles*. TheFreeDictionary.com.
- Podder, T., et al., *A method to minimize puncturing force and organ deformation*. 2006.
- Cui, F., et al., *PREDICTION OF PROSTATE MOTION AND DEFORMATION USING FEM MODELING FOR BETTER BIOPSY ACCURACY*. p. 11.
- Li, A.D.R., et al., *Mosquito proboscis-inspired needle insertion to reduce tissue deformation and organ displacement*. Scientific Reports, 2020. **10**(1): p. 12248.
- Hungr, N., et al., *A 3-D Ultrasound Robotic Prostate Brachytherapy System With Prostate Motion Tracking*. Robotics, IEEE Transactions on, 2012. **28**: p. 1382-1397.
- Podder, T.K., et al. *Evaluation of robotic needle insertion in conjunction with in vivo manual insertion in the operating room*. in *ROMAN 2005. IEEE International Workshop on Robot and Human Interactive Communication*, 2005. 2005.
- Taschereau, R., et al., *Seed misplacement and stabilizing needles in transperineal permanent prostate implants*. Radiotherapy and Oncology, 2000. **55**(1): p. 59-63.
- Seifabadi, R., et al., *Accuracy Study of a Robotic System for MRI-guided Prostate Needle Placement*. The international journal of medical robotics + computer assisted surgery : MRCAS, 2013. **9**(3): p. 305-316.
- Stone, N.N., et al., *Prostate gland motion and deformation caused by needle placement during brachytherapy*. Brachytherapy, 2002. **1**(3): p. 154-160.
- Li, A.D.R., et al., *Needle deflection and tissue sampling length in needle biopsy*. Journal of the Mechanical Behavior of Biomedical Materials, 2020. **104**: p. 103632.

22. Riviere, C.N., R.S. Rader, and P.K. Khosla. *Characteristics of hand motion of eye surgeons*. in *19th Annual International Conference of the IEEE Engineering in Medicine and Biology Society. 'Magnificent Milestones and Emerging Opportunities in Medical Engineering'*. 1997. IEEE.
23. De Silva, T., et al., *Quantification of prostate deformation due to needle insertion during TRUS-guided biopsy: comparison of hand-held and mechanically stabilized systems*. *Medical Physics*, 2011. **38**(3): p. 1718-1731.
24. Malone, S., et al., *Respiratory-induced prostate motion: quantification and characterization*. *International Journal of Radiation Oncology*Biophysics*, 2000. **48**(1): p. 105-109.
25. Scott, O., P. Osmotherly, and P. Chiarelli, *Assessment of pelvic floor muscle contraction ability in healthy males following brief verbal instruction*. *Australian and New Zealand Continence Journal*, 2013. **19**: p. 12-17.
26. Keus, F., et al., *Evidence at a glance: error matrix approach for over-viewing available evidence*. *BMC Medical Research Methodology*, 2010. **10**(1): p. 90.
27. Seifabadi, R., et al., *Robotic system for MRI-guided prostate biopsy: feasibility of teleoperated needle insertion and ex vivo phantom study*. *International Journal of Computer Assisted Radiology and Surgery*, 2012. **7**(2): p. 181-190.
28. Xu, H., et al. *MRI-Guided Robotic Prostate Biopsy: A Clinical Accuracy Validation*. 2010. Springer.
29. Waldman, S.A. and A. Terzic, *Healthcare Evolves From Reactive to Proactive*. *Clinical pharmacology and therapeutics*, 2019. **105**(1): p. 10-13.
30. Gurjar, O.P., R. Arya, and H. Goyal, *A study on prostate movement and dosimetric variation because of bladder and rectum volumes changes during the course of image-guided radiotherapy in prostate cancer*. *Prostate International*, 2020. **8**(2): p. 91-97.
31. Podder, T., et al., *Methods for prostate stabilization during transperineal LDR brachytherapy*. *Physics in Medicine and Biology*, 2008. **53**(6): p. 1563-1579.
32. Goksel, O., S.E. Salcudean, and S.P. Dimaio, *3D simulation of needle-tissue interaction with application to prostate brachytherapy*. *Computer Aided Surgery*, 2006. **11**(6): p. 279-288.
33. Lagerburg, V., et al., *Measurement of prostate rotation during insertion of needles for brachytherapy*. *Radiotherapy and Oncology*, 2005. **77**(3): p. 318-323.
34. Zhang, M., et al., *Quantitative Characterization of Viscoelastic Properties of Human Prostate Correlated with Histology*. *Ultrasound in Medicine & Biology*, 2008. **34**(7): p. 1033-1042.
35. Alterovitz, R., et al., *Simulating needle insertion and radioactive seed implantation for prostate brachytherapy*. *Studies in health technology and informatics*, 2003. **94**: p. 19-25.
36. Li, A.D.R., et al., *Multi-Bevel Needle Design Enabling Accurate Insertion in Biopsy for Cancer Diagnosis*. *IEEE Transactions on Biomedical Engineering*, 2021. **68**(5): p. 1477-1486.
37. Sakes, A., D. Dodou, and P. Breedveld, *Buckling prevention strategies in nature as inspiration for improving percutaneous instruments: a review*. 2016. **11**(2): p. 021001.
38. Phee, L., et al. *Ultrasound Guided Robotic System for Transperineal Biopsy of the Prostate*. in *Proceedings of the 2005 IEEE International Conference on Robotics and Automation*. 2005.
39. Misra, S., et al. *Observations and models for needle-tissue interactions*. in *2009 IEEE International Conference on Robotics and Automation*. 2009.
40. Chevie, J., et al., *Flexible Needle Steering in Moving Biological Tissue With Motion Compensation Using Ultrasound and Force Feedback*. *IEEE Robotics and Automation Letters*, 2018. **3**(3): p. 2338-2345.
41. Abolhassani, N., R. Patel, and F. Ayazi. *Effects of Different Insertion Methods on Reducing Needle Deflection*. in *2007 29th Annual International Conference of the IEEE Engineering in Medicine and Biology Society*. 2007.
42. Patriciu, A., et al., *Automatic Brachytherapy Seed Placement Under MRI Guidance*. *IEEE transactions on bio-medical engineering*, 2007. **54**(8): p. 1499-1506.
43. Mahvash, M. and P.E. Dupont, *Fast Needle Insertion to Minimize Tissue Deformation and Damage*. *IEEE International Conference on Robotics and Automation : ICRA : [proceedings]* *IEEE International Conference on Robotics and Automation*, 2009. **2009**: p. 3097-3102.
44. Lagerburg, V., et al., *A new robotic needle insertion method to minimise attendant prostate motion*. *Radiotherapy and Oncology*, 2006. **80**(1): p. 73-77.
45. Dattoli, M. and K. Waller, *A simple method to stabilize the prostate during transperineal prostate brachytherapy*. *International Journal of Radiation Oncology*Biophysics*, 1997. **38**(2): p. 341-342.
46. Sherman, J., et al. *Efficacy of Prostate Stabilizing Techniques during Brachytherapy Procedure*. in *2006 International Conference of the IEEE Engineering in Medicine and Biology Society*. 2006.
47. Hungr, N., et al., *A 3D Ultrasound Robotic Prostate Brachytherapy System with Prostate Motion Tracking*. *IEEE Transactions on Robotics*, 2012. **28**(6): p. 1382-1397.
48. Westendorp, H., et al., *Edema and Seed Displacements Affect Intraoperative Permanent Prostate Brachytherapy Dosimetry*. *International Journal of Radiation Oncology, Biology, Physics*, 2016. **96**(1): p. 197-205.
49. Singh, O. and S.R. Bolla, *Anatomy, Abdomen and Pelvis, Prostate*, in *StatPearls*. 2022, StatPearls Publishing: Treasure Island (FL).
50. Jahangiri, A. *Rectovesical pouch | Radiology Reference Article | Radiopaedia.org*. *Radiopaedia*.
51. Pinkawa, M., *Current role of spacers for prostate cancer radiotherapy*. *World Journal of Clinical Oncology*, 2015. **6**(6): p. 189-193.

52. Premier Medical Group Announces Use of SpaceOAR® Hydrogel for Prostate Cancer Radiation Therapy, in Premier Medical Group. 2018.
53. Vanneste, B., et al., *Implantation of a biodegradable rectum balloon implant: Tips, Tricks and Pitfalls*. International braz j urol : official journal of the Brazilian Society of Urology, 2017. **43**.
54. Sawayanagi, S., et al., *Injection of hydrogel spacer increased maximal intrafractional prostate motion in anterior and superior directions during volumetric modulated arc therapy-stereotactic body radiation therapy for prostate cancer*. Radiation Oncology, 2022. **17**(1): p. 41.
55. Wang, L., et al., *Mechanics of Crater-Enabled Soft Dry Adhesives: A Review*. Frontiers in Mechanical Engineering, 2020. **6**: p. 601510.
56. *BID 2018-2019_13_Bioclamping_Biological Grasping_handouts - ME41095 Bio Inspired Design (2018/19 Q1)*.
57. Chen, H., et al., *Bioinspired Surface for Surgical Graspers Based on the Strong Wet Friction of Tree Frog Toe Pads*. ACS Applied Materials & Interfaces, 2015. **7**(25): p. 13987-13995.
58. van Assenbergh, P., et al., *Implementation of anisotropic soft pads in a surgical gripper for secure and gentle grip on vulnerable tissues*. Proceedings of the Institution of Mechanical Engineers, Part H: Journal of Engineering in Medicine, 2021. **235**(3): p. 255-263.
59. Langowski, J.K.A., et al., *Tree frog attachment: mechanisms, challenges, and perspectives*. Frontiers in Zoology, 2018. **15**: p. 32.
60. Stark, A.Y., T.W. Sullivan, and P.H. Niewiarowski, *The effect of surface water and wetting on gecko adhesion*. Journal of Experimental Biology, 2012. **215**(17): p. 3080-3086.
61. Louagie, Y., et al., *Beating Heart Surgery using the Octopus™ Tissue Stabilizers : Initial Experience including Triple Vessel Disease and high-risk Patients*. Acta Chirurgica Belgica, 2001. **101**(3): p. 130-134.
62. Kiaii, B., et al., *Chapter 6 - Hybrid Coronary Revascularization*, in *Atlas of Cardiac Surgical Techniques (Second Edition)*, F.W. Sellke and M. Ruel, Editors. 2019, Elsevier. p. 83-102.
63. Singh, S.K., et al., *Making octopus tissue stabilizer more effective—a valuable technique*. Indian Journal of Thoracic and Cardiovascular Surgery, 2013. **29**(1): p. 52-54.
64. Max, Z., *Suction cup*. 1936, Zaiger Max.
65. White, F.M., *Fluid Mechanics*. 2016: McGraw-Hill Education.
66. Borgnakke and Sonntag, *Fundamentals of Thermodynamics*. 8 ed. 2013: Don Fowley.
67. Singh, A. and T. Aung, *Effect of barometric pressure on sea level variations in the Pacific region*. The South Pacific Journal of Natural Science, 2005. **23**.
68. Sandoval, J., et al., *Combining Suction and Friction to Stabilize a Soft Gripper to Shear and Normal Forces, for Manipulation of Soft Objects in Wet Environments*. IEEE Robotics and Automation Letters, 2022. **7**: p. 1-1.
69. Mantriota, G., *Optimal grasp of vacuum grippers with multiple suction cups*. Mechanism and Machine Theory, 2007. **42**(1): p. 18-33.
70. Zell, M.A., et al., *Holmium laser enucleation of the prostate for very large benign prostatic hyperplasia (≥ 200 cc)*. World Journal of Urology, 2021. **39**(1): p. 129-134.
71. Lorenz, B., et al., *Static or breakloose friction for lubricated contacts: The role of surface roughness and dewetting*. Journal of physics. Condensed matter : an Institute of Physics journal, 2013. **25**: p. 445013.
72. van Assenbergh, P., et al., *Pull-off and friction forces of micropatterned elastomers on soft substrates: the effects of pattern length scale and stiffness*. Beilstein Journal of Nanotechnology, 2019. **10**: p. 79-94.
73. Beckert, M., B. Flammang, and J. Nadler, *A Model of Interfacial Permeability for Soft Seals in Marine-Organism, Suction-Based Adhesion*. MRS Advances, 2016. **-1**: p. 1-13.
74. Xiang, J., et al., *Transperineal versus transrectal prostate biopsy in the diagnosis of prostate cancer: a systematic review and meta-analysis*. World Journal of Surgical Oncology, 2019. **17**(1): p. 31.
75. Borst, C., et al., *Coronary artery bypass grafting without cardiopulmonary bypass and without interruption of native coronary flow using a novel anastomosis site restraining device ("Octopus")*. Journal of the American College of Cardiology, 1996. **27**(6): p. 1356-1364.
76. Ammannaya, G.K.K., et al., *Effect of octopus tissue stabilizer on cardiac output during off-pump coronary artery bypass graft surgery*. Kardiochirurgia i Torakochirurgia Polska = Polish Journal of Cardio-Thoracic Surgery, 2019. **16**(2): p. 69-73.
77. Jansen, E.L., et al., *Off-pump coronary bypass grafting: how to use the octopus tissue stabilizer*. The Annals of Thoracic Surgery, 1998. **66**(2): p. 576-579.
78. Ali, A., et al., *Stabilizing interventional instruments in the cardiovascular system: A classification of mechanisms*. Medical Engineering & Physics, 2021. **89**: p. 22-32.
79. Williams, J., et al., *Hyaluronic acid rectal spacer in EBRT: Usability, safety and symmetry related to user experience*. Journal of Medical Imaging and Radiation Sciences, 2022. **53**(4): p. 640-647.
80. Tuncel, A., et al., *Does disposable needle guide minimize infectious complications after transrectal prostate needle biopsy?* Urology, 2008. **71**(6): p. 1024-1027; discussion 1027-1028.
81. *ISO 17664:2004(en), Sterilization of medical devices — Information to be provided by the manufacturer for the processing of resterilizable medical devices*.
82. Malchesky, P.S., et al., *Reprocessing of reusable medical devices*. ASAIO journal (American Society

- for Artificial Internal Organs: 1992), 1995. **41**(2): p. 146-151.
83. ASTM F2119 - 07 en.
84. Committee, F., *Practice for Marking Medical Devices and Other Items for Safety in the Magnetic Resonance Environment*. ASTM International.
85. NEN Connect - IEC 60601-2-37:2007+A1:2015 en.
86. Bamotra, A., et al., *Layer-Jamming Suction Grippers With Variable Stiffness*. Journal of Mechanisms and Robotics, 2019. **11**(3).
87. Song, S., et al., *Adaptive Self-Sealing Suction-Based Soft Robotic Gripper*. Advanced Science, 2021. **8**(17): p. 2100641.
88. Feder, J., *The Perimeter-Area Relation*, in *Fractals*, J. Feder, Editor. 1988, Springer US: Boston, MA. p. 200-211.
89. Baik, S., et al., *Capillarity-Enhanced Organ-Attachable Adhesive with Highly Drainable Wrinkled Octopus-Inspired Architectures*. ACS Applied Materials & Interfaces, 2019. **11**(29): p. 25674-25681.
90. Kennedy, E.B.L., et al., *Octopus arms exhibit exceptional flexibility*. Scientific Reports, 2020. **10**(1): p. 20872.
91. *What Are the Suction Cups on an Octopus Called?* Sciencing.
92. Kier, W. and A. Smith, *The Structure and Adhesive Mechanism of Octopus Suckers*. Integrative and comparative biology, 2002. **42**: p. 1146-53.
93. Tramacere, F., et al., *Octopus-like suction cups: From natural to artificial solutions*. Bioinspiration & biomimetics, 2015. **10**: p. 035004.
94. Andriot, M., et al., *Silicones in Industrial Applications*. Inorganic Polymers, 2009.
95. Bont, M., C. Barry, and S. Johnston, *A review of liquid silicone rubber injection molding: Process variables and process modeling*. Polymer Engineering & Science, 2021. **61**.
96. Mitterberger, M., et al., *Ultrasound of the prostate*. Cancer Imaging, 2010. **10**(1): p. 40-48.
97. Zhakypov, Z., et al., *An Origami-Inspired Reconfigurable Suction Gripper for Picking Objects With Variable Shape and Size*. IEEE Robotics and Automation Letters, 2018. **PP**: p. 1-1.
98. Sareh, S., et al., *Anchoring like octopus: biologically inspired soft artificial sucker*. Journal of The Royal Society Interface, 2017. **14**(135): p. 20170395.
99. Shiratori, T., et al. *Hexagonal Microstructure Bioinspired by the Toe Pad of a Tree Frog For Increasing Adhesive Force in Shear Direction*. in *2022 IEEE 35th International Conference on Micro Electro Mechanical Systems Conference (MEMS)*. 2022.
100. Li, M., et al., *Pillar versus dimple patterned surfaces for wettability and adhesion with varying scales*. Journal of The Royal Society Interface, 2018. **15**(148): p. 20180681.
101. Lee, S.H., et al., *Passive air leakage detection mechanism for enhanced vacuum suction actuator efficiency*. Microsystem Technologies, 2022. **28**(10): p. 2353-2359.
102. Hirose, S., A. Nagakubo, and R. Toyama. *Machine that can walk and climb on floors, walls and ceilings*. in *Fifth International Conference on Advanced Robotics 'Robots in Unstructured Environments*. 1991.
103. Gauhar, V., et al., *Catheter-Associated Urinary Infections and Consequences of Using Coated versus Non-Coated Urethral Catheters—Outcomes of a Systematic Review and Meta-Analysis of Randomized Trials*. Journal of Clinical Medicine, 2022. **11**(15): p. 4463.
104. Bianchi, A., S.W. Leslie, and G.T. Chesnut, *Difficult Foley Catheterization*, in *StatPearls*. 2022, StatPearls Publishing: Treasure Island (FL).
105. Zhang, H. and A. Cloud, *The Permeability Characteristics of Silicone Rubber*. 2006.
106. Leslie, S.W., et al., *Prostate Cancer*, in *StatPearls*. 2022, StatPearls Publishing: Treasure Island (FL).
107. Eichelberger, L.E., et al., *Maximum tumor diameter is an independent predictor of prostate-specific antigen recurrence in prostate cancer*. Modern Pathology, 2005. **18**(7): p. 886-890.
108. Swanson, G.P., et al., *Pathological Characteristics of Low Risk Prostate Cancer Based on Totally Embedded Prostatectomy Specimens*. The Prostate, 2015. **75**(4): p. 424-429.
109. Chicheł, A., M. Kanikowski, and J. Skowronek, *Vital role of volume and number of needles in HDR brachytherapy (HDR-BT) of prostate cancer*. Journal of Contemporary Brachytherapy, 2009. **1**(3): p. 145-150.
110. *Material Specification Charts*. Smooth-On, Inc.
111. Shaaer, A., et al., *Multipurpose ultrasound-based prostate phantom for use in interstitial brachytherapy*. Brachytherapy, 2021. **20**(6): p. 1139-1145.
112. Chiu, T., et al., *Low-cost 3D print-based phantom fabrication to facilitate interstitial prostate brachytherapy training program*. Brachytherapy, 2020. **19**(6): p. 800-811.
113. Levy, Y., et al., *Biodegradable inflatable balloon for reducing radiation adverse effects in prostate cancer*. Journal of Biomedical Materials Research Part B: Applied Biomaterials, 2009. **91B**(2): p. 855-867.
114. *Tissue Equivalent Ultrasound Prostate Phantom > Ultrasound Phantoms > Nuclemed*.
115. Scali, M., P. Breedveld, and D. Dodou, *Experimental evaluation of a self-propelling bio-inspired needle in single- and multi-layered phantoms*. Scientific Reports, 2019. **9**: p. 19988.
116. Hibbeler, R.C., *Statics*. 13 ed. 2012, Singapore: Pearson.
117. West, J.B., *The original presentation of Boyle's law*. Journal of Applied Physiology, 1999. **87**(4): p. 1543-1545.
118. *Coefficient of Friction Equation and Table Chart*.
119. Parekh, J., et al., *In vitro investigation of friction at the interface between bone and a surgical instrument*. Proceedings of the Institution of Mechanical Engineers, Part H: Journal of Engineering in Medicine, 2013. **227**(6): p. 712-718.

120. Campo, A.d. and C. Greiner, *SU-8: a photoresist for high-aspect-ratio and 3D submicron lithography*. Journal of Micromechanics and Microengineering, 2007. **17**(6): p. R81.
121. Ji, Y., et al., *Stiffness of prostate gland measured by transrectal real-time shear wave elastography for detection of prostate cancer: a feasibility study*. The British Journal of Radiology, 2019. **92**(1097): p. 20180970.
122. Nilsson, M., et al., *Mapping prostatic microscopic anisotropy using linear and spherical b-tensor encoding: A preliminary study*. Magnetic resonance in medicine, 2021. **86**(4): p. 2025-2033.
123. Hartshorne, G.M., *Challenges of the EU 'tissues and cells' directive*. Reproductive BioMedicine Online, 2005. **11**(4): p. 404-407.
124. Sandgren, K., et al., *Registration of histopathology to magnetic resonance imaging of prostate cancer*. Physics and Imaging in Radiation Oncology, 2021. **18**: p. 19-25.
125. Zylstra, R.R., *NORMALITY TESTS FOR SMALL SAMPLE SIZES*. Quality Engineering, 1994. **7**(1): p. 45-58.
126. Siggelkow, W., et al., *Comparison of Obstetric Efficacy and Safety of the Kiwi OmniCup with Conventional Vacuum Extraction*. Geburtshilfe und Frauenheilkunde, 2014. **74**(2): p. 146-151.
127. Cytron, S., et al., *Cryoablation of the prostate: technical recommendations*. Prostate Cancer and Prostatic Diseases, 2009. **12**(4): p. 339-346.
128. Lee, T., et al., *Focal Laser Ablation for Localized Prostate Cancer: Principles, Clinical Trials, and Our Initial Experience*. Reviews in Urology, 2014. **16**(2): p. 55-66.
129. *BID 2018-2019_13_Bioclamping_Biological Grasping - ME41095 Bio Inspired Design (2018/19 Q1)*.

APPENDICES

A. Clamping methods

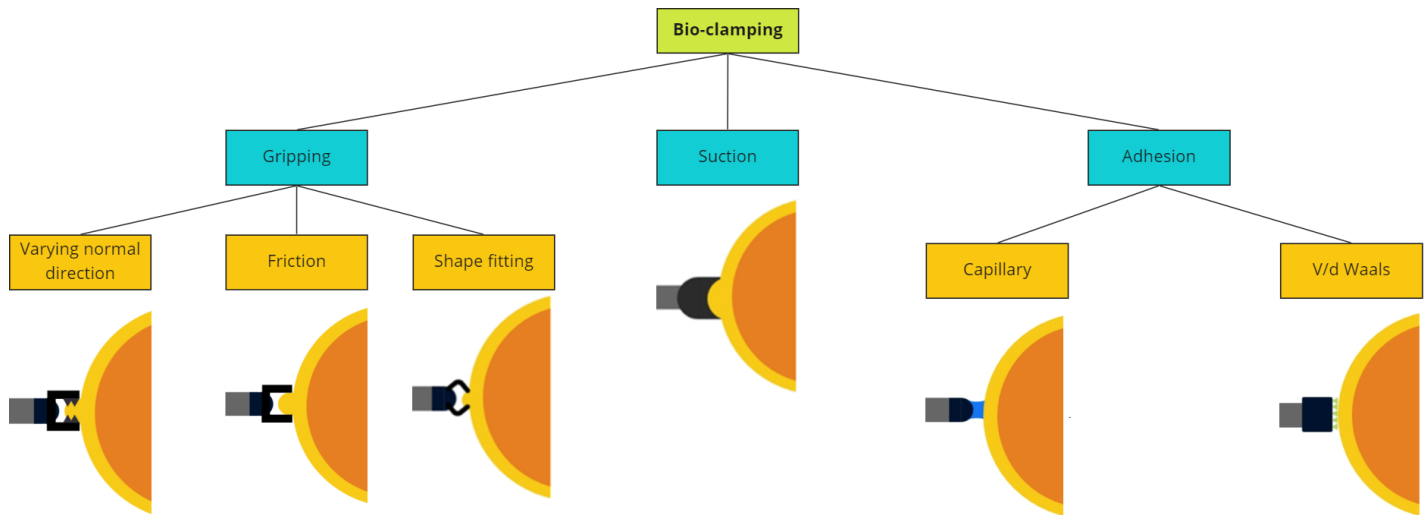


Figure 54: Categorised overview of the clamping methods found in nature.

Gripping

Varying normal direction

By varying the direction of the normal forces on an object, grip can be achieved [129]. Often, graspers with rugged surfaces are used to establish the varying direction of the normal forces. Also, the use of these rugged graspers can increase the contact surface with the object, creating a larger area for friction.

Friction

Friction based gripping makes use of normal forces exerted on an object by two opposite graspers, to create a friction force in opposite direction of the load [129]. The friction force can be increased by increasing the normal forces and/or the friction coefficient between the graspers and the object.

Shape fitting

Shape fitting creates grip by shaping around an object using its graspers [78, 129]. The graspers contact the object and exert normal forces in opposite direction of the load. The role of friction is reduced within this clamping method.

Suction

Suction uses pressure differences between an object and its surroundings to create suction force on the object in opposite direction of the load [68]. Suction uses suction cups to establish a lower pressure within these cups compared to the pressure of the atmosphere, generating vacuum.

Adhesion

Capillary adhesion

Capillary adhesion makes use of a liquid bridge between the surface of an object and the instrument to create adhesive forces [59]. These adhesive forces will act as tension forces when the object is pushed away by a load. On fully wetted surfaces the capillary adhesive bond reduces due to incapability of forming a liquid bridge [59]. In nature, capillary adhesion is a well-known mechanism mainly used by tree frogs to adhere on surfaces [59].

Van der Waals adhesion

Van der Waals adhesion is an intermolecular attraction between the molecules of an object and instrument, generating an adhesive contact force. Van der Waals adhesion is weakened on rougher and wetted objects due to a reduced effective contact area[55]. Van der Waals adhesion is a well-known mechanism used in nature by geckos to climb on dry walls [60].

B. Micro-patterns research



Figure 55: The common three types of micro-patterns used on graspers to grip soft elastic substrates.

Types

There are mainly three types of micro-patterns used on graspers to grip soft elastic substrates as tissue as shown in Figure 55: flat, pillars, and dimples [100]. A flat pattern is referred a smooth surface, which is the most simple design. A micro-pattern with pillars contain protrusions at the grasper surface. Dimples are holes within a surface. When a dimple-patterned surface is pushed against a tissue, the tissue will fill the holes and grip will be secured. In literature these patterns are widely tested on tissue like substrates to measure their effect on friction force [57, 72, 100]. The results showed that a micro-pattern containing pillars has the highest friction coefficient on tissue. The reasoning behind is that the channels between the pillars allow for drainage of the moist, creating a more dry contact area with the tissue. Additionally, the drained moist in the channels can generate capillary adhesion resulting in a stronger grip [100]. A dimpled-pattern stores the moist within the holes, however in contrast with channels of the pillars, the dimples are enclosed meaning that they will act as a reservoir rather than a drainage mechanism. This can lead to a lubricate effect on the tissue. The same yields for a flat surface, where the moist cannot be drained and acts as a lubricate.

Pillar shapes

Different pillar types can be used as micro-pattern for grippers as shown in Figure 56. Each pillar type can be separated based on their base shape. Based on these shape differences each pillar type can have varying friction performances on tissue. On slippery tissue the hexagon pillars have shown to have the highest friction coefficient [57].The hexagon shape allows to have the most channels on the surface due to number of sides, resulting in more moist being drained by these channels and therefore forming a much dryer contact area with the tissue.






Surface pattern	Description
	1 mm tooth
	Hexagonal pillar
	Rhomboid pillar
	Triangular pillar
	Quadrangular pillar

Figure 56: The different types of pillar shapes.

C. Self-regulating valves mechanisms

Airflow regulation valves

In the literature, there are some examples of self-regulating valves mechanism applied on suction based systems. One of them is the airflow based valve-regulating mechanism discussed by Hirose *et al.* [102]. (see Figure 57). This valves mechanism is applied on a sucker based foot of a robot designed to climb vertical surfaces. Each sucker foot consists of separated suction holes, which are controlled by regulation valves. The regulations valves are located in the air chamber above the suction holes and are connected to spring-elements. In passive state the regulations valves are kept open by the spring-elements. When a vacuum is applied on the suckers, air will flow through the suction holes. The suction holes that did not form a seal with the surface will experience a stronger air flow, which will overcome the spring-element and close the corresponding suction hole.

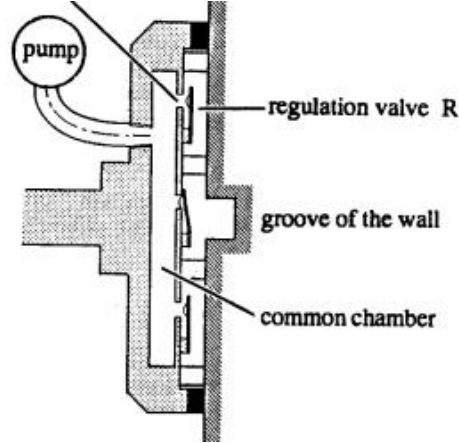


Figure 57: The mechanism of the airflow regulation valves presented by Hirose *et al.* [102].

Spring-based valves mechanism

Another regulating valve mechanism is the spring-based valves mechanism proposed by Lee *et al.* [101] as shown in Figure 58. The mechanism consists of pistons connected to springs inside of cylindrical suction holes. In passive state, the springs press the pistons against an opening in the cylinders, which is referred as an O-ring. If the tip of the cylinder makes contact with a surface, the spring inside the cylinder compresses, removing the piston from the O-ring. This opens an air passage and creates a vacuum inside the cylinder.

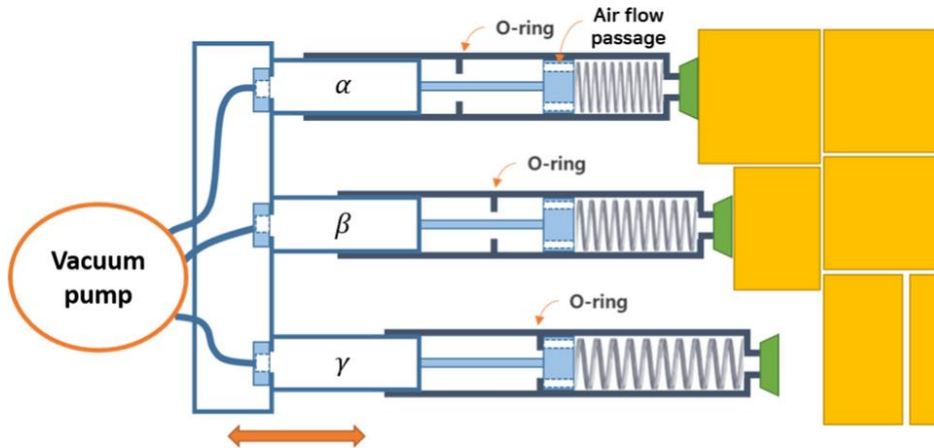


Figure 58: The spring-based valves mechanism presented by Lee *et al.* [101].

D. Mould iterations

#1 Mould with fitting pins- PLA printer

Parts

- Base mould for half-cylindrical shape, columns, wall spikes, fitting holes, leakage channels, and vertical holes
- Top mould for tubing, columns, and pins
- Open footprint mould with extending cylindrical pins

Encountered issues

- Fitting holes and shafts have too small fitting tolerance; printer not accurate enough; too much time lost in sanding; one pin broke off during the process
- Pins of the self-regulating valves did not form; assumed that silicone rubber flows away from the sides
- Patterned holes at the top part of arched contour; assumed to be caused by vertical holes
- Footprint too thick; extended pins on the mould prevent to remove excess silicone
- Lots of air bubbles with in suction cup

Improvement points

- New safer fitting mechanism
- Removal vertical air holes from base mould
- Cylindrical pins on base mould same height as footprint thickness

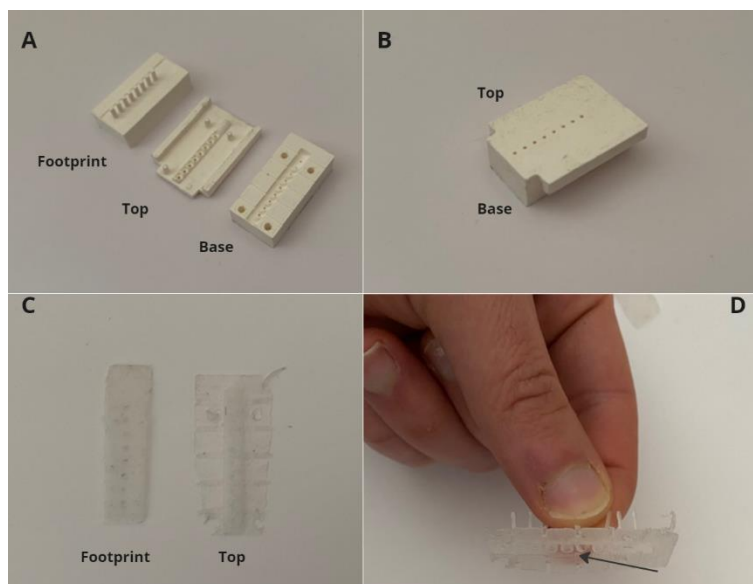


Figure 59: Images of the (A) the moulds, (B) assembly of the top and base part, (C) the cured footprint and top layer with the self-regulating valves, and (D) not forming of the pins.

#2 Mould with lit mechanism – PLA printer

Parts

- Base mould for half-cylindrical shape, columns spikes, and leakage channels
- Top mould for tubing, columns, and pins
- Open footprint mould with pins based on the footprint thickness

Encountered issues

- Still sanding needed of base mould to fit with top mould
- Still pins not forming; assumed that silicone drained away in the leaking channels due to gravity

Improvement points

- More accurate printing

- Removal of leakage channels from base mould
- Addition of leakage channels on top mould

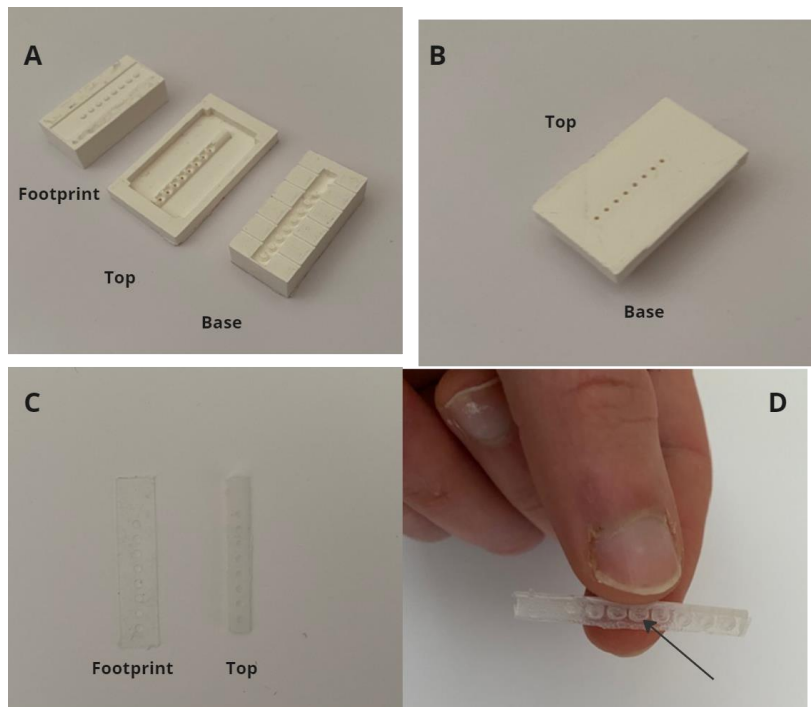


Figure 60: Images of the (A) the moulds, (B) assembly of the top and base part, (C) the cured footprint and top layer with the self-regulating valves, and (D) not forming of the pins.

#3 Mould with leaking channels on top- Resin printer

Parts

- Base mould for half-cylindrical shape, columns, and pins
- Top mould for tubing, columns, pins, and leakage channels
- Open footprint mould with pins based on the footprint thickness

Encountered issues

- Still sanding needed of the base mould to fit with top part
- Pins in top mould do not connect with column of base mould; silicone does not flow from the top to base mould; leakage channels to slim and wide.
- Printing material too brittle; chips away during assembling of mould

Improvement points

- Re-checking dimensions of the mould
- Removing drainage channels at the top mould
- Greater fitting tolerances
- More durable printing material for base mould

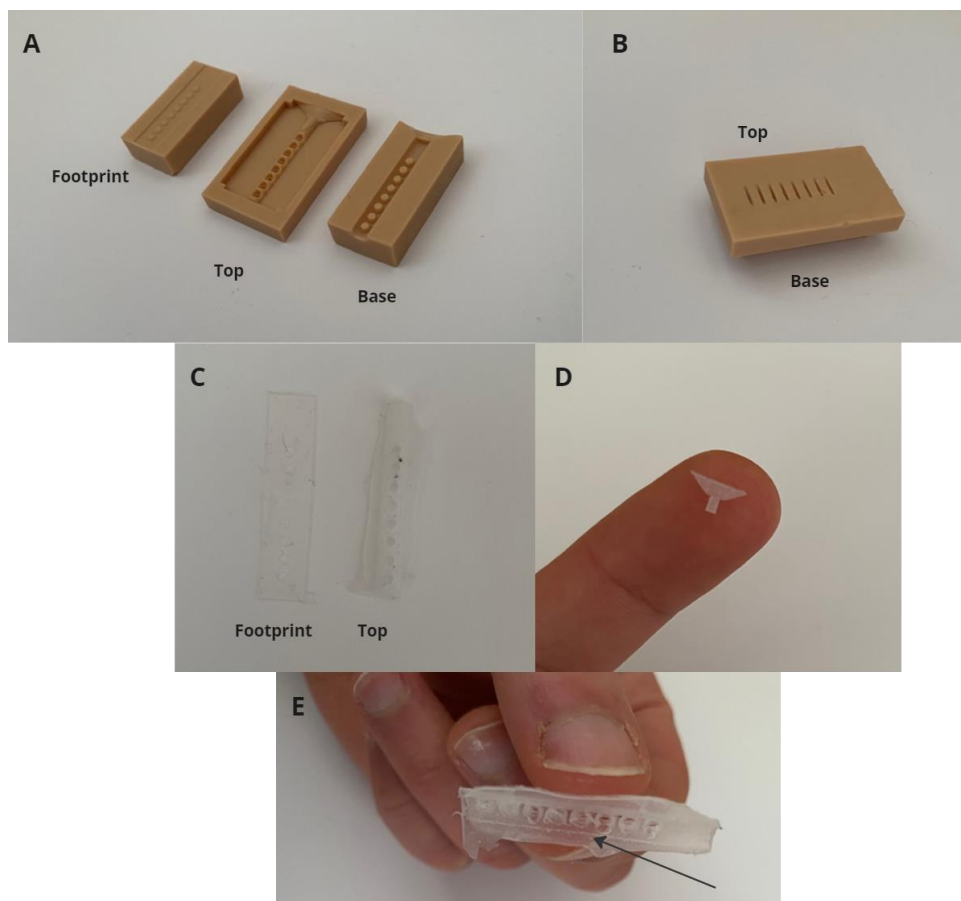


Figure 61: Images of the (A) the moulds, (B) assembly of the top and base part, (C) the cured footprint and top layer with the self-regulating valves, (D) the pins getting stuck in the leakage channels, and (E) not forming of the pins.

E. Working with silicone rubber

Preparing silicone rubber

Silicone rubber is a mixture of two substances as shown in Figure 62, known as substance A and B. Substance A is the base silicone and substance B is the curing agent. Depending on the type of silicone rubber, every silicone rubber has a pre-given mixture ratio in weight or volume. An incorrect mixture ratio can result in silicone rubber with incorrect mechanical properties. A digital scale is used to measure the weight of both substances accurately. Furthermore, both substances are needed to be kept at room temperature to prevent changes in mechanical properties. After the correct amount of each substance is measured, they can be poured together into a cup. The two substances are mixed for couple a minutes to achieve an uniform mixture. When mixing is done, it is important to check for air entrapped within in the form of air bubbles. Entrapped air can alter the properties of the end product. It is recommended for silicone rubber with a viscosity of higher than 15000 cps at room temperature to degas it using a degassing system. Finally, it is important to know the pot life of the silicone rubber. The pot life gives the time limit of how long the mixture can be kept in the cup without curing. Therefore it is important to cast the mixture and degas it within this time limit. After the degassing the mixture is ready to be applied based on the used casting method. Additionally, a release agent can be used before casting to make it easier to remove the silicone from the cast after curing, which is especially helpful for complex designs with small features.

Post-processing silicone rubber

After the silicone has cured, it can be gently removed from the cast using a pincer. The benefit of silicone rubber is that it has good release properties. Furthermore, possible excess silicone rubber at the sides can be removed by cutting it off and small tears can be repaired using silicone glue.

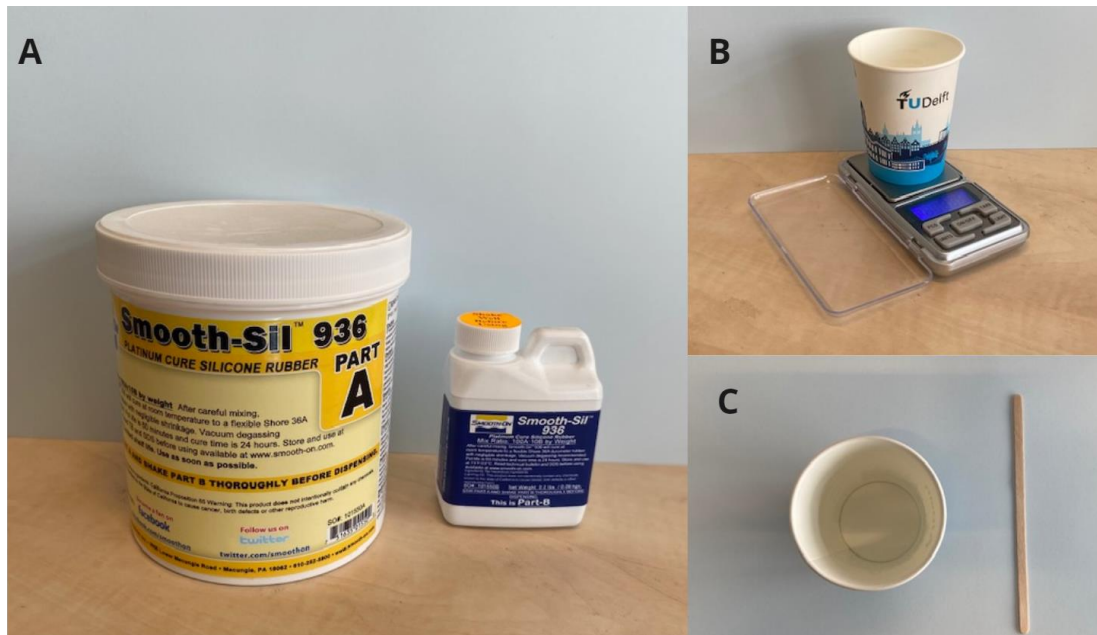


Figure 62: Images of (A) the two substances (A&B) needed for preparation of the silicone rubber mixture, (B) the accurate weighing of the substances using a digital scale, and (C) mixing of the two substances using a cup and stirrer.

F. Guidelines for making gelatine phantoms

Resources (see Figure 63)

- Gelatine powder
- Scale
- Measuring cup
- Stirrer

Instructions

The following steps are based on the instructions given by Scali *et al.* [115] on how to make a tissue phantom from gelatine. First, weigh the amount of needed gelatine using a scale. If you want to make a gelatine-based tissue phantom, a certain weight percentage (% wt) of gelatine powder for the gelatine mixture can be used to mimic the stiffness. Next, mix the gelatine within the amount of boiled water for the desired % wt using a measuring cup. Stir the mixture thoroughly using a stirrer. Make sure that all gelatine powder is well dissolved in the warm water. Keep mixing until no bubbles of gelatine are seen. Also, make sure that there are no air bubbles in the mixture, and let the mixture stand for a few minutes. Additionally, remove generated foam from the top. When there are no air bubbles left in the gelatine mixture, it can be poured into a desired container or cast to achieve a certain shape for the gelatine. The gelatine needs to be poured carefully so that no air bubbles form in the mixture. If there are air bubbles in the mixture, pop them using a needle. Let the gelatine mixture set in a refrigerator for roughly twelve hours at four degrees Celsius. When the gelatine mixture is solidified, it can be used as a phantom.

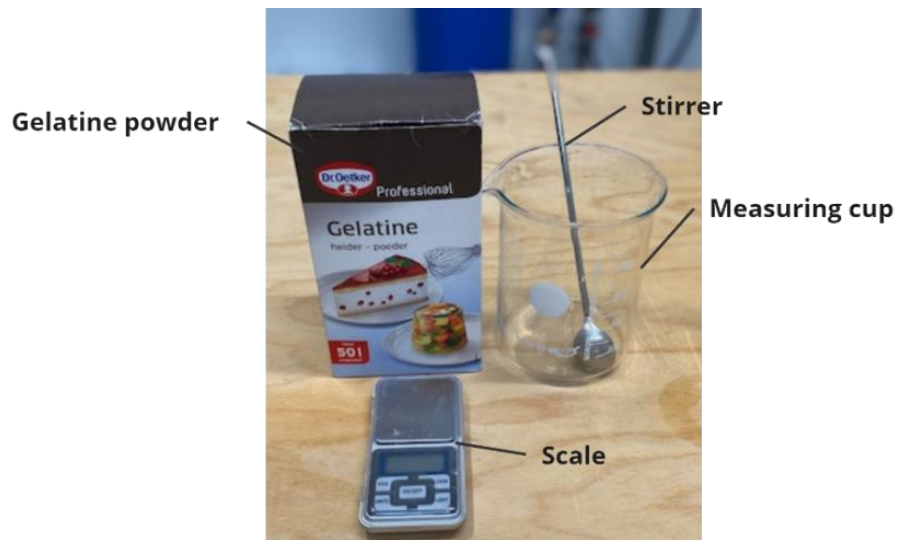
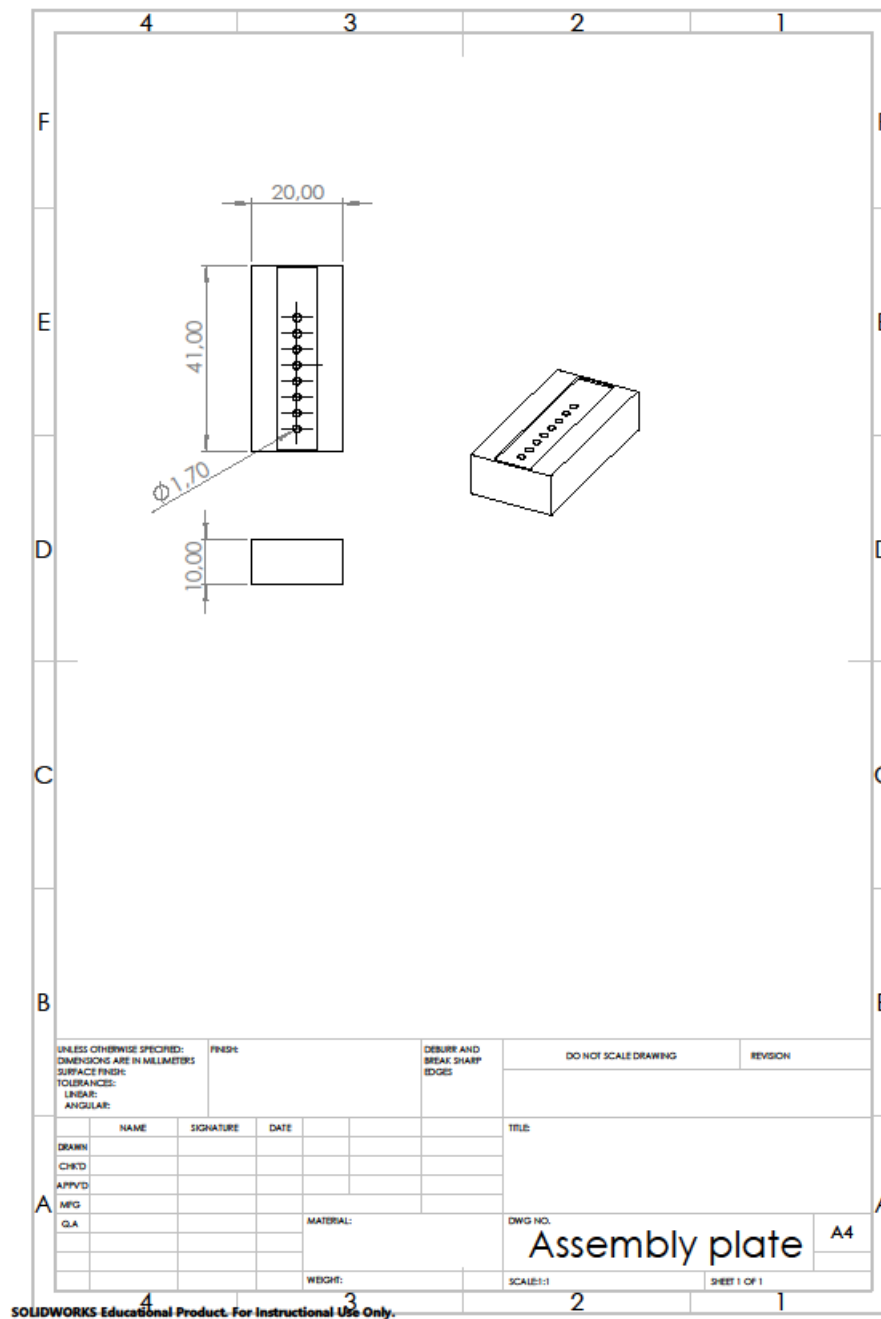
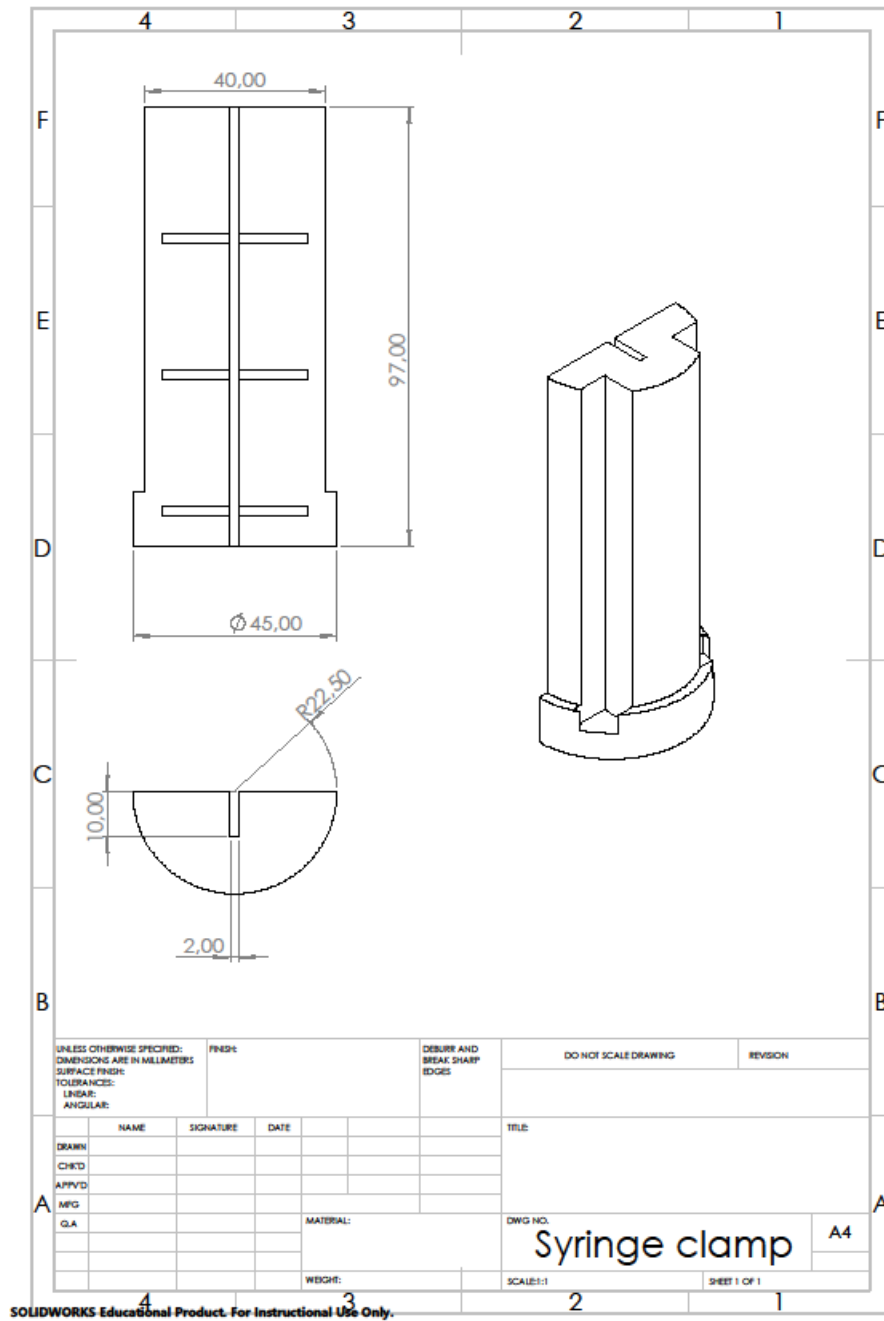


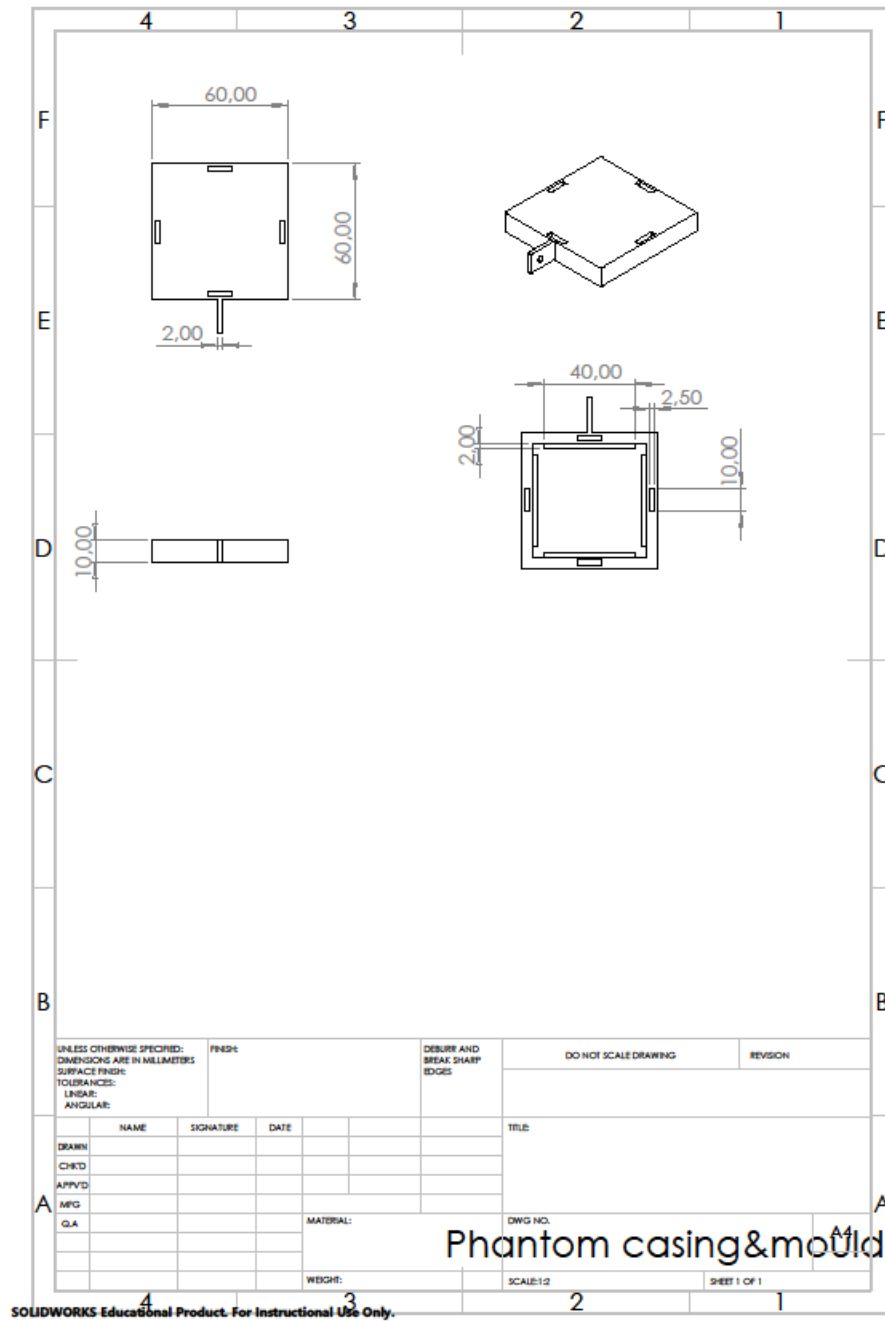
Figure 63: The needed resources for making gelatine; gelatine powder, scale, a measuring cup, and a stirrer.

G. Technical drawings

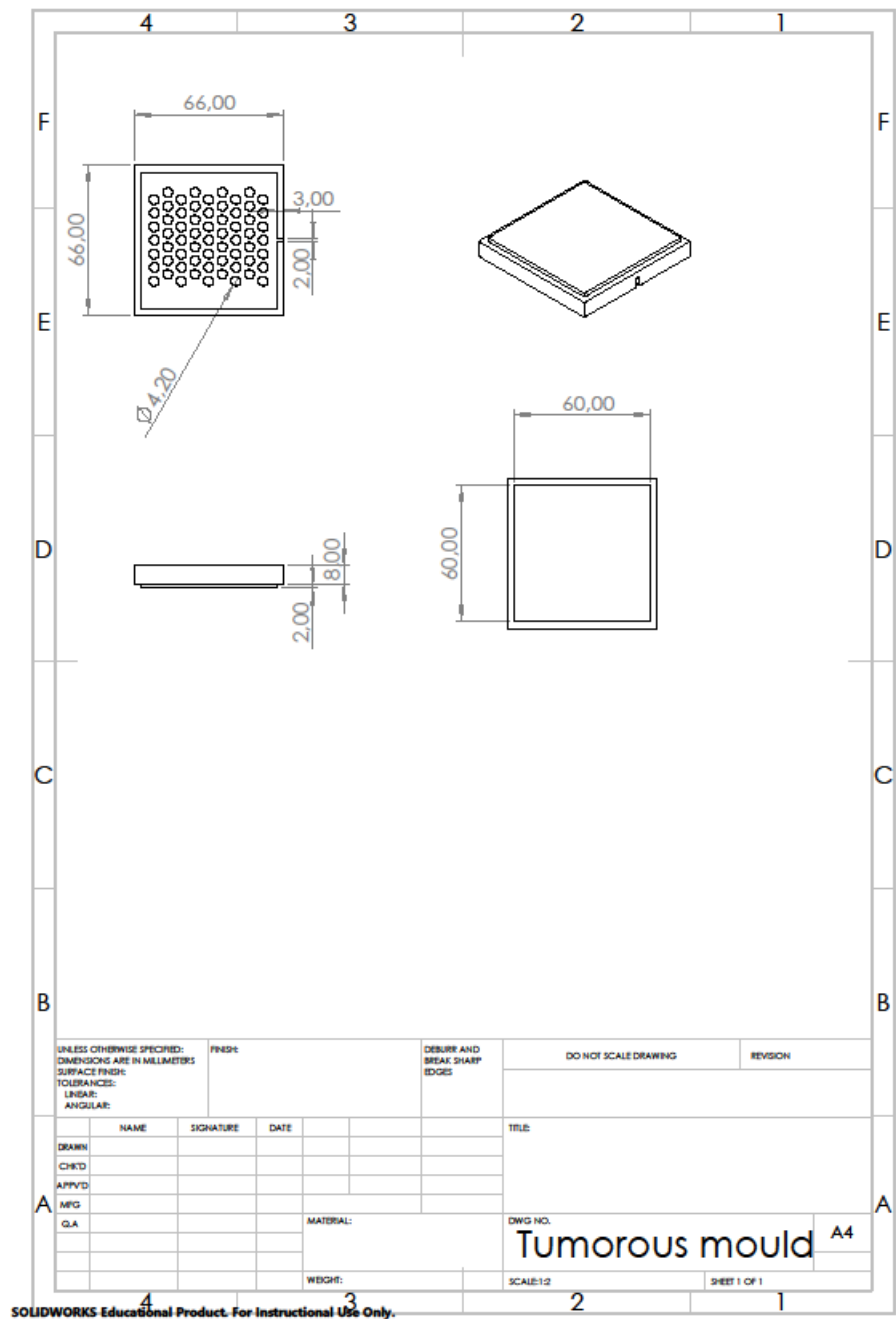




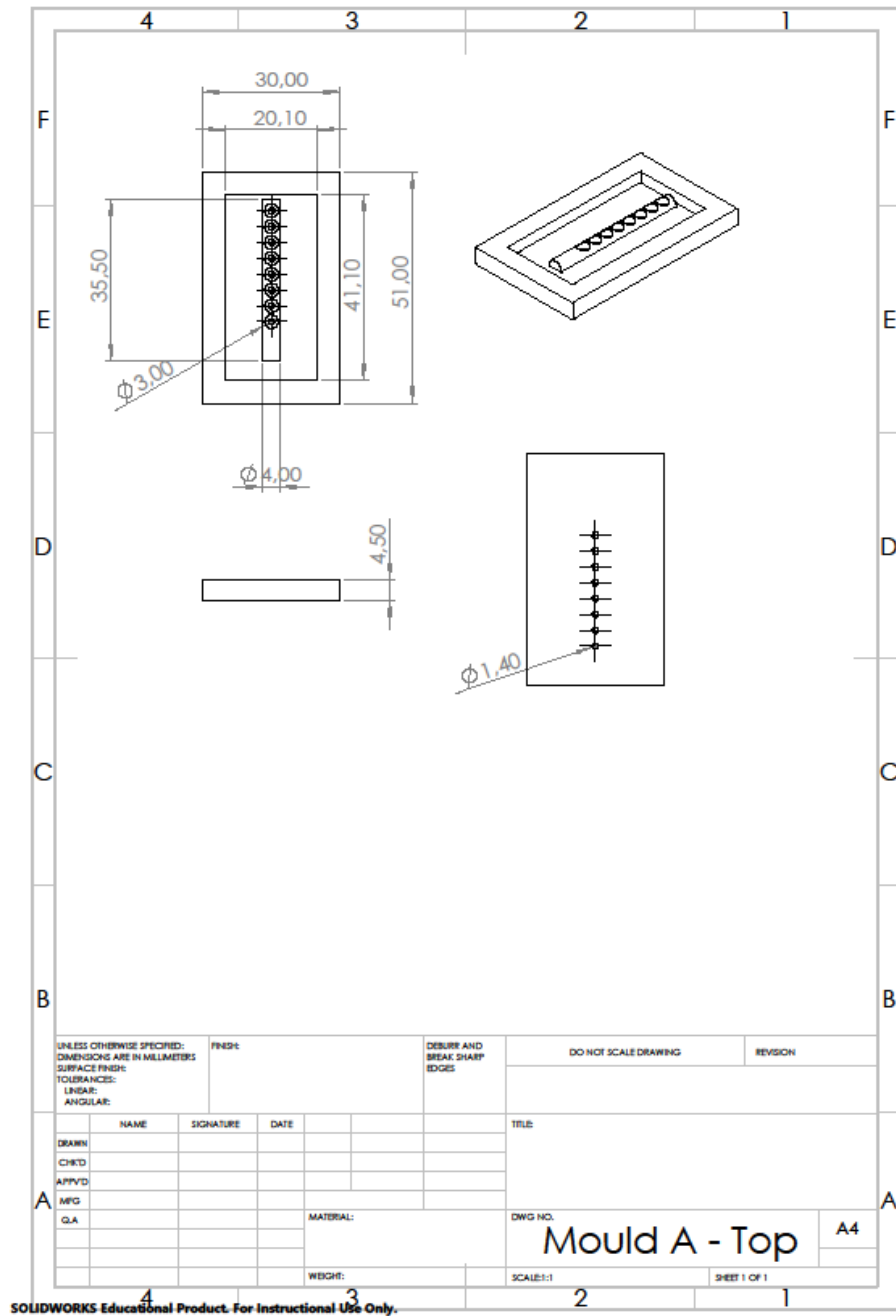
SOLIDWORKS Educational Product. For Instructional Use Only.

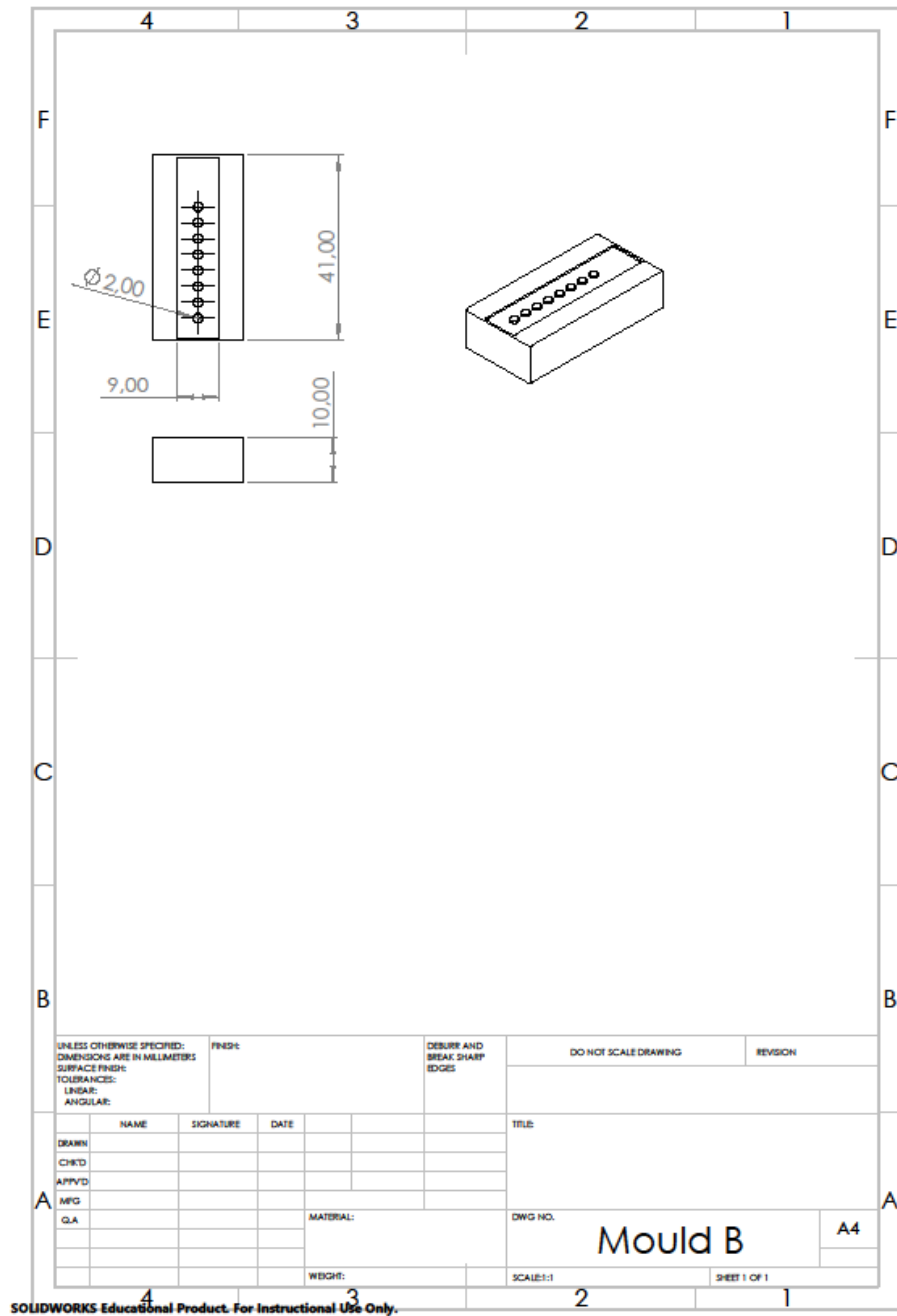


SOLIDWORKS Educational Product. For Instructional Use Only.

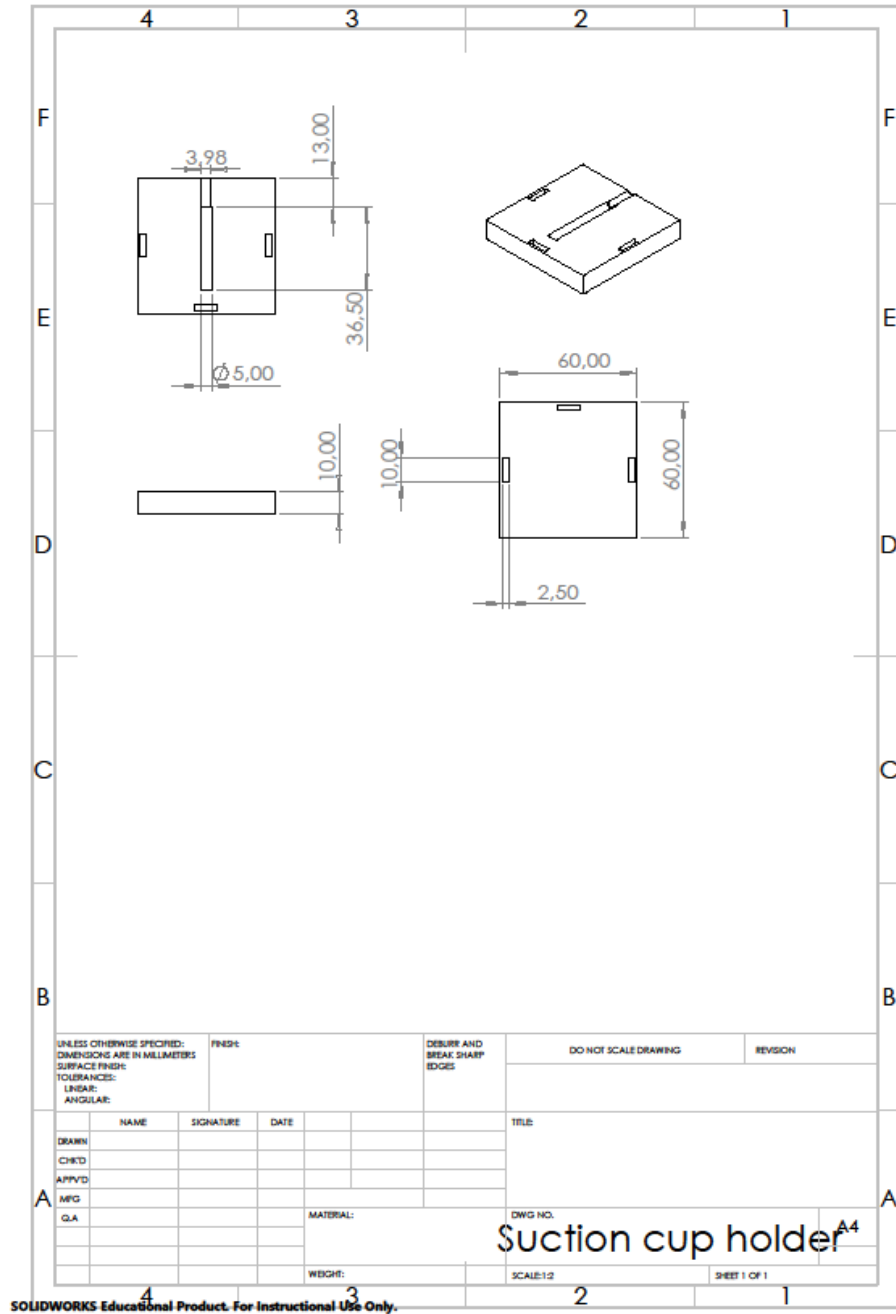


SOLIDWORKS Educational Product. For Instructional Use Only.

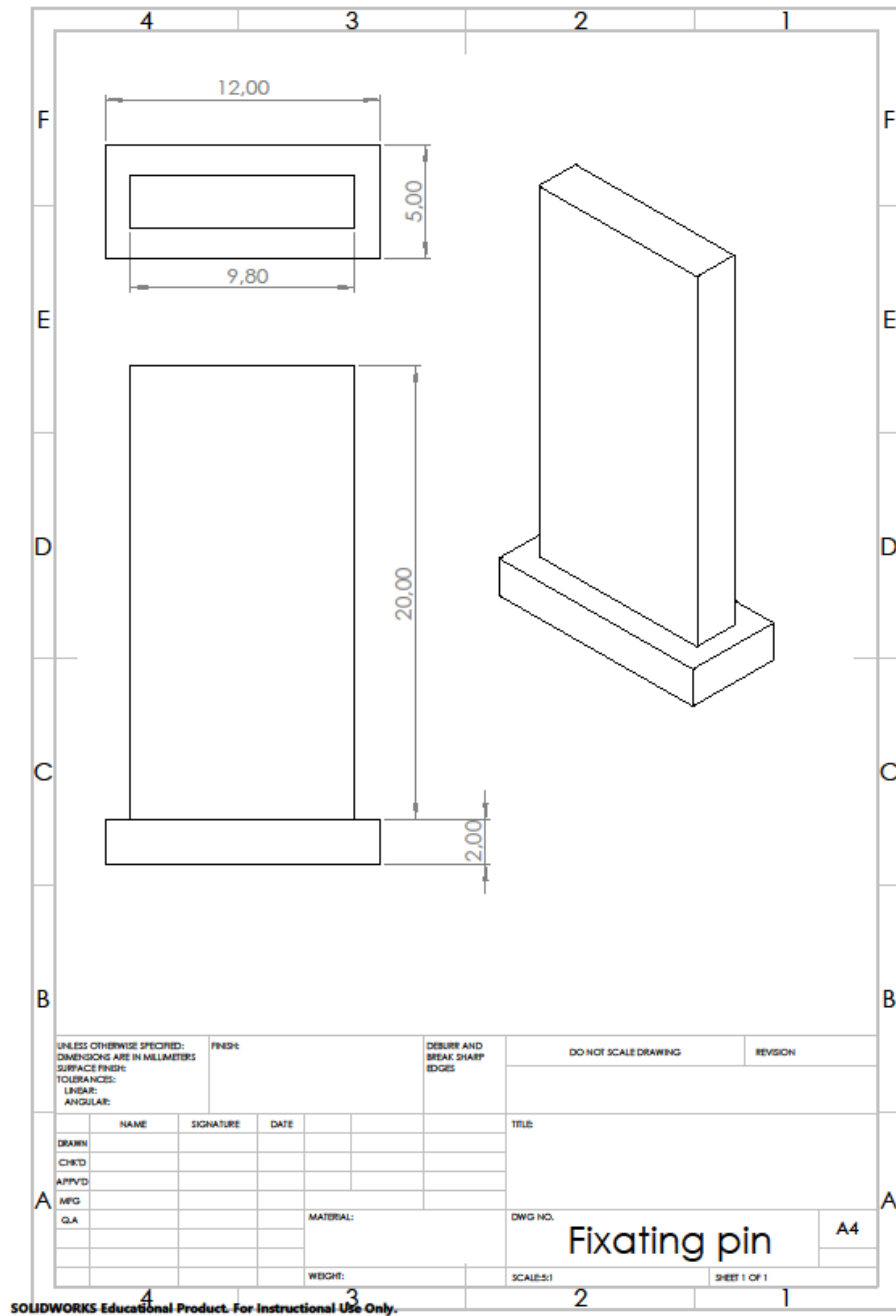




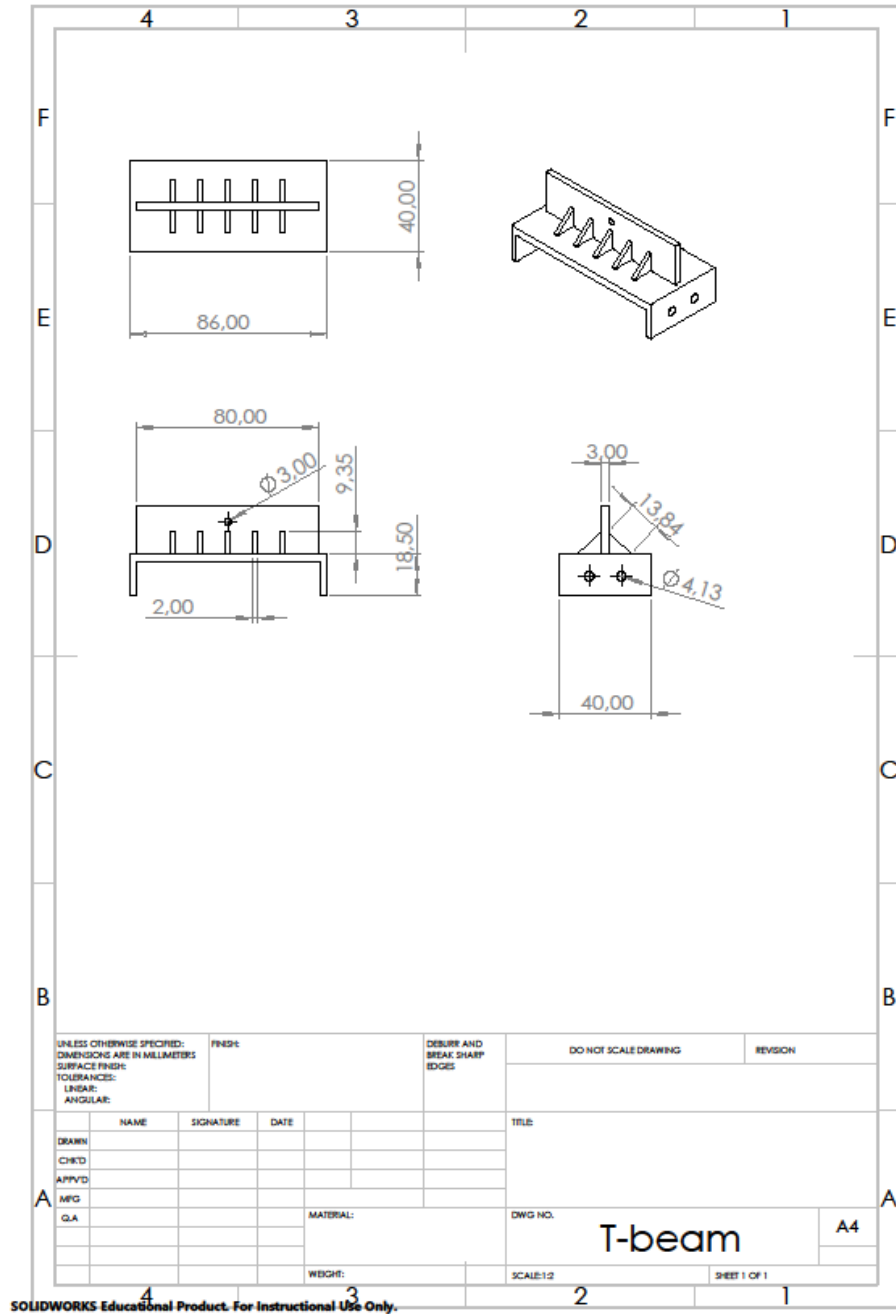
SOLIDWORKS Educational Product. For Instructional Use Only.



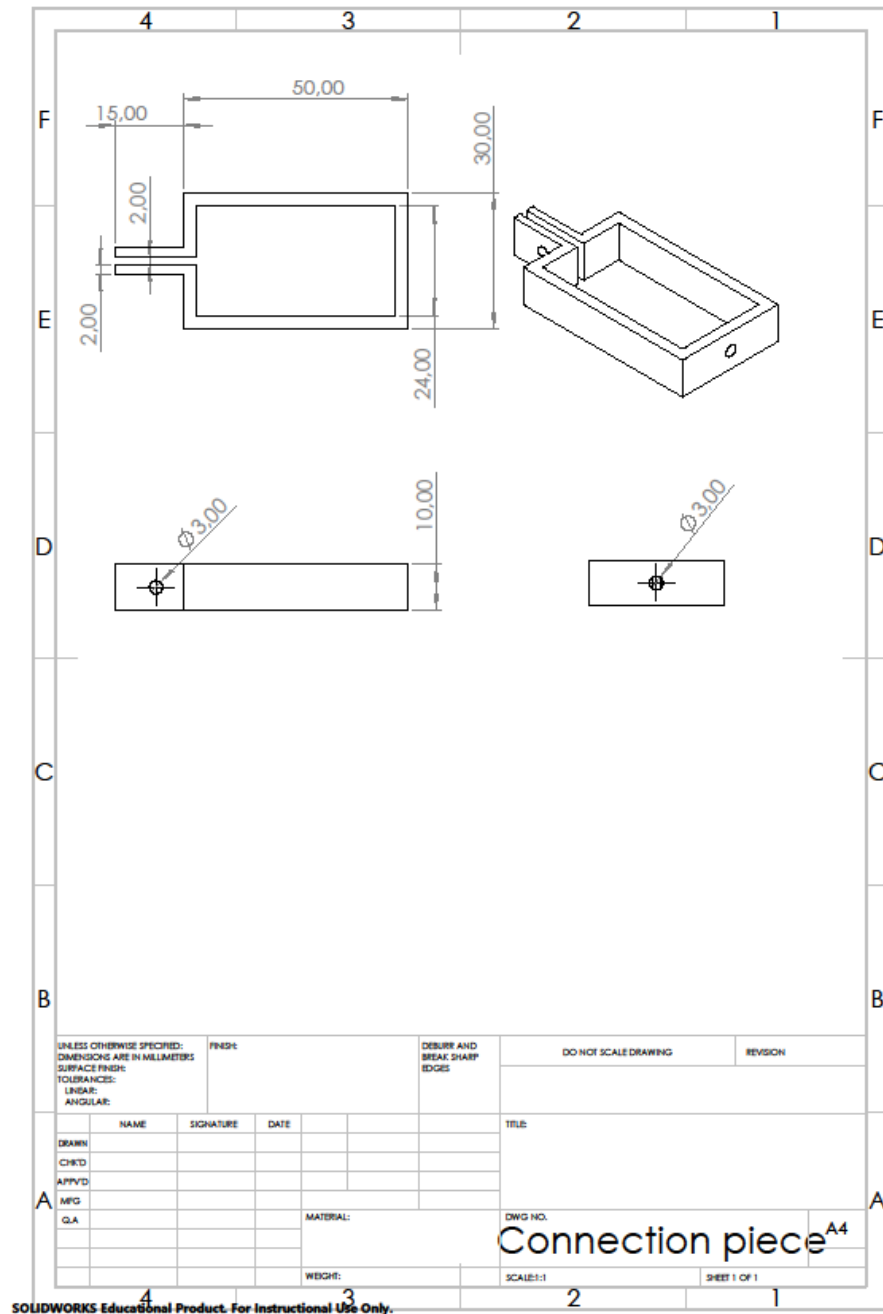
SOLIDWORKS Educational Product. For Instructional Use Only.



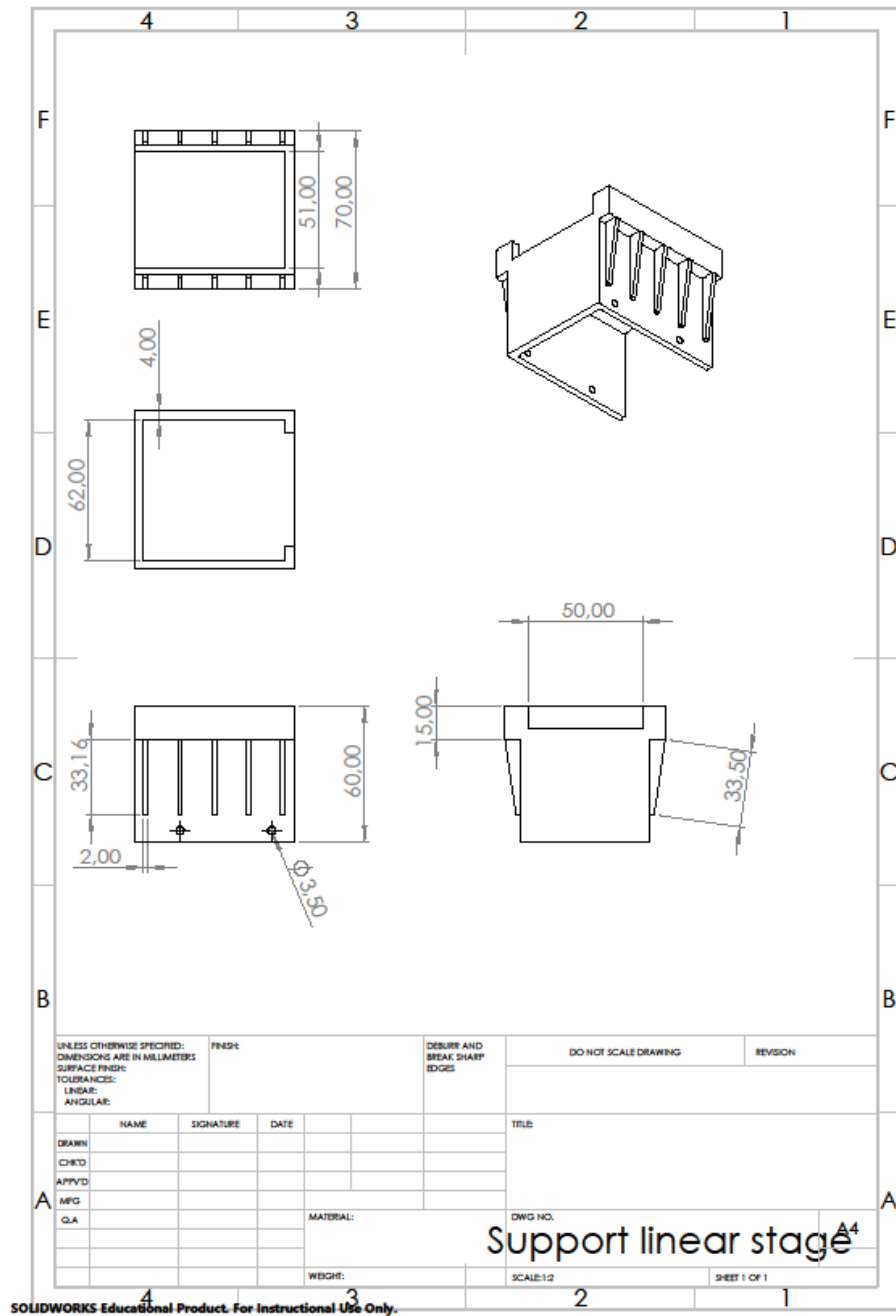
SOLIDWORKS Educational Product. For Instructional Use Only.



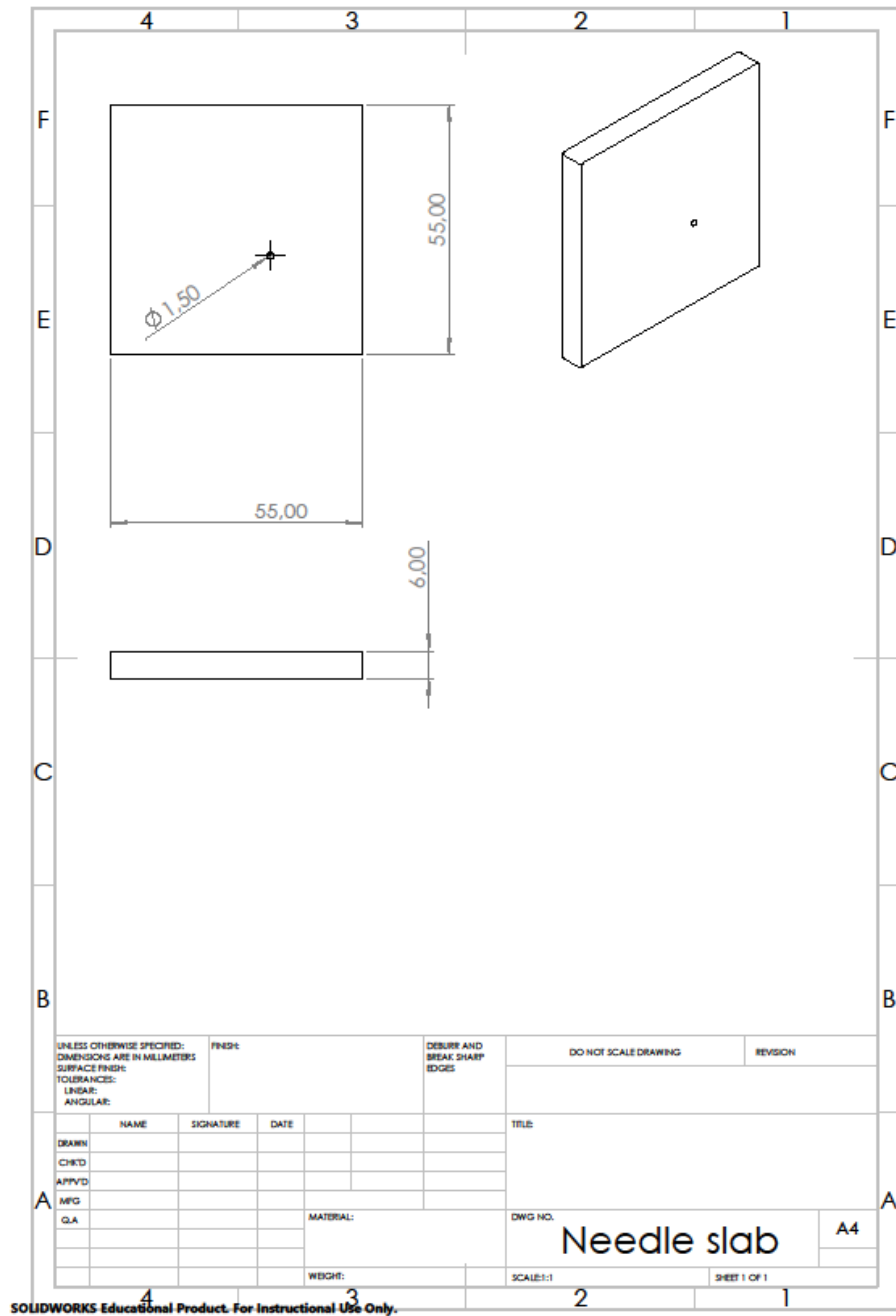
SOLIDWORKS Educational Product. For Instructional Use Only.



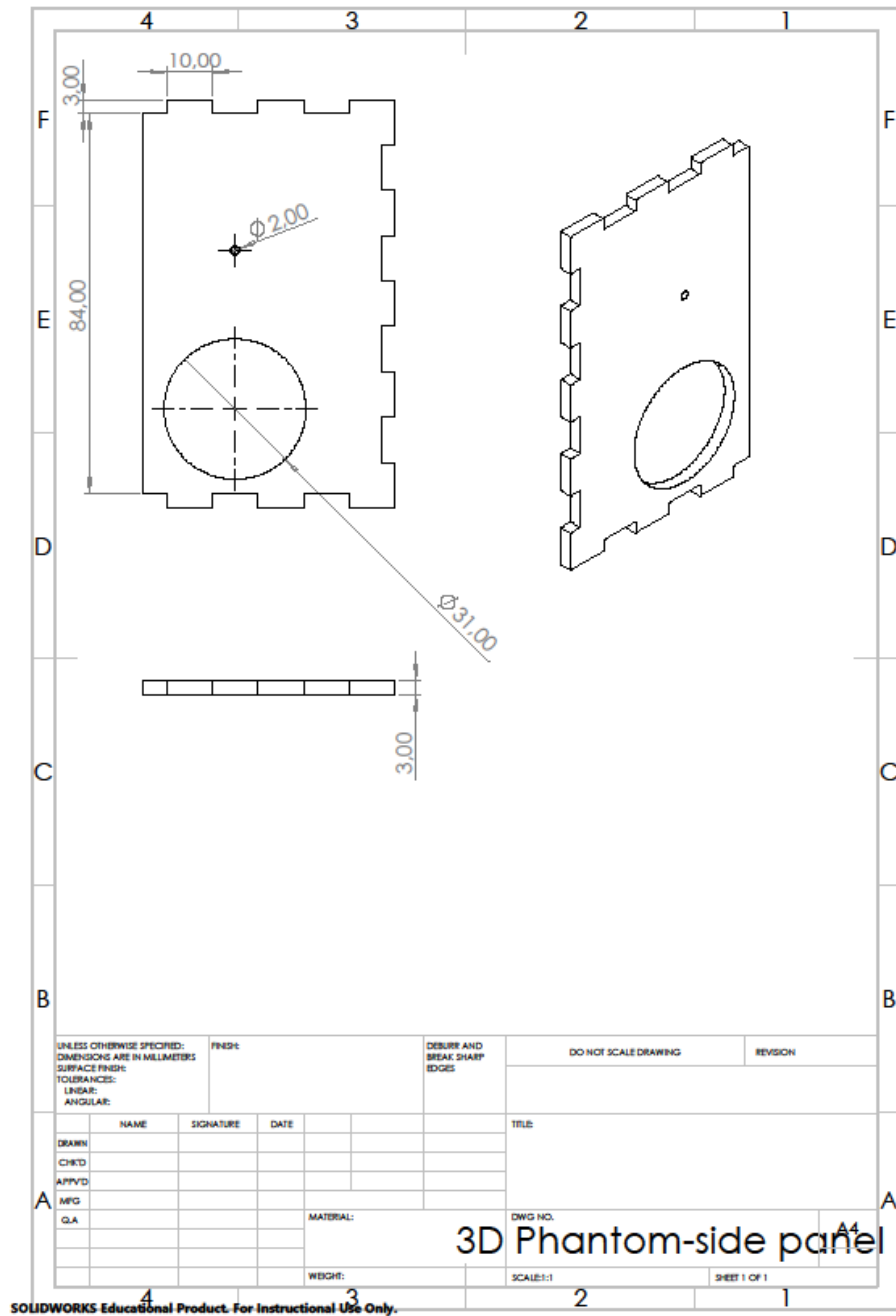
SOLIDWORKS Educational Product. For Instructional Use Only.



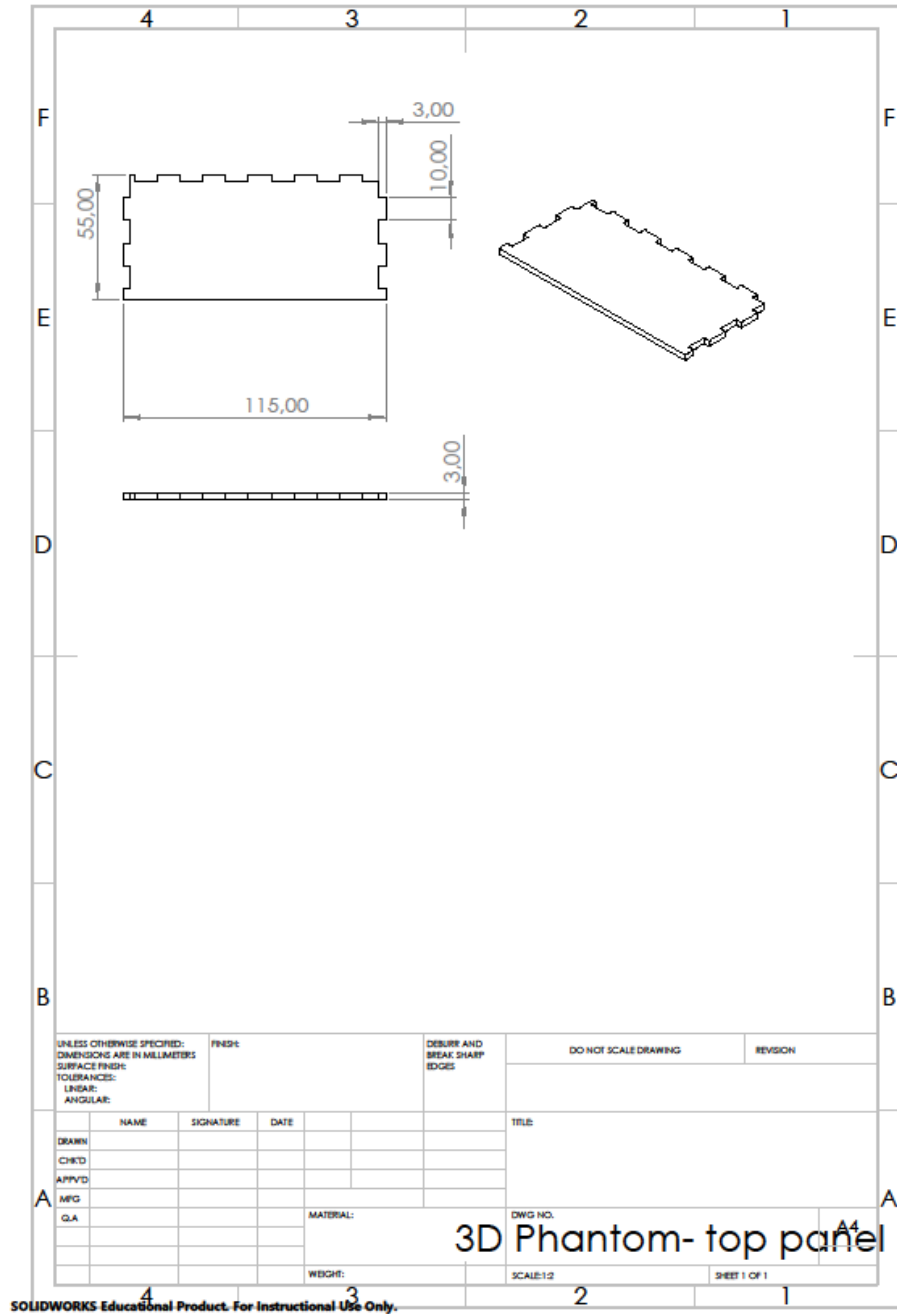
SOLIDWORKS Educational Product. For Instructional Use Only.



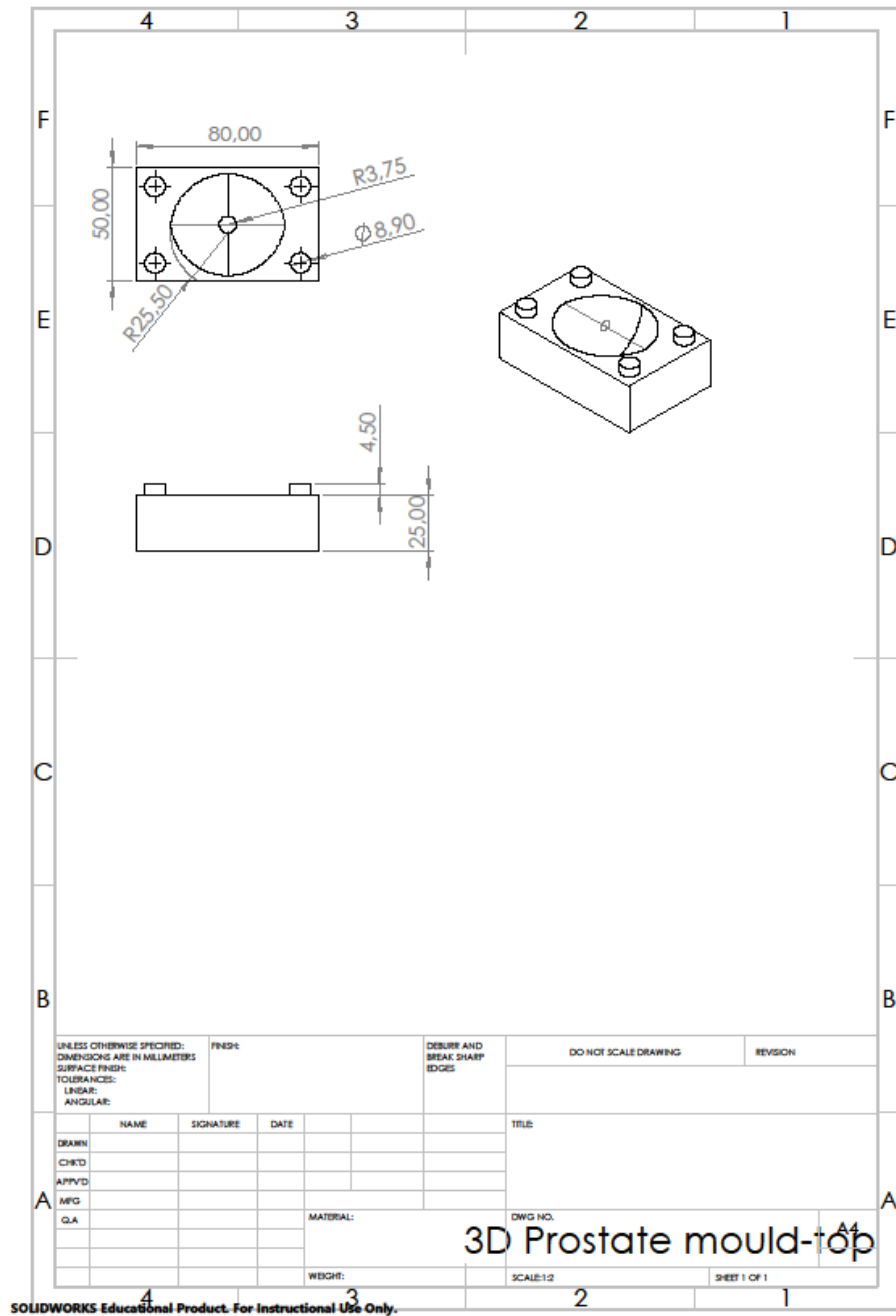
SOLIDWORKS Educational Product. For Instructional Use Only.



SOLIDWORKS Educational Product. For Instructional Use Only.

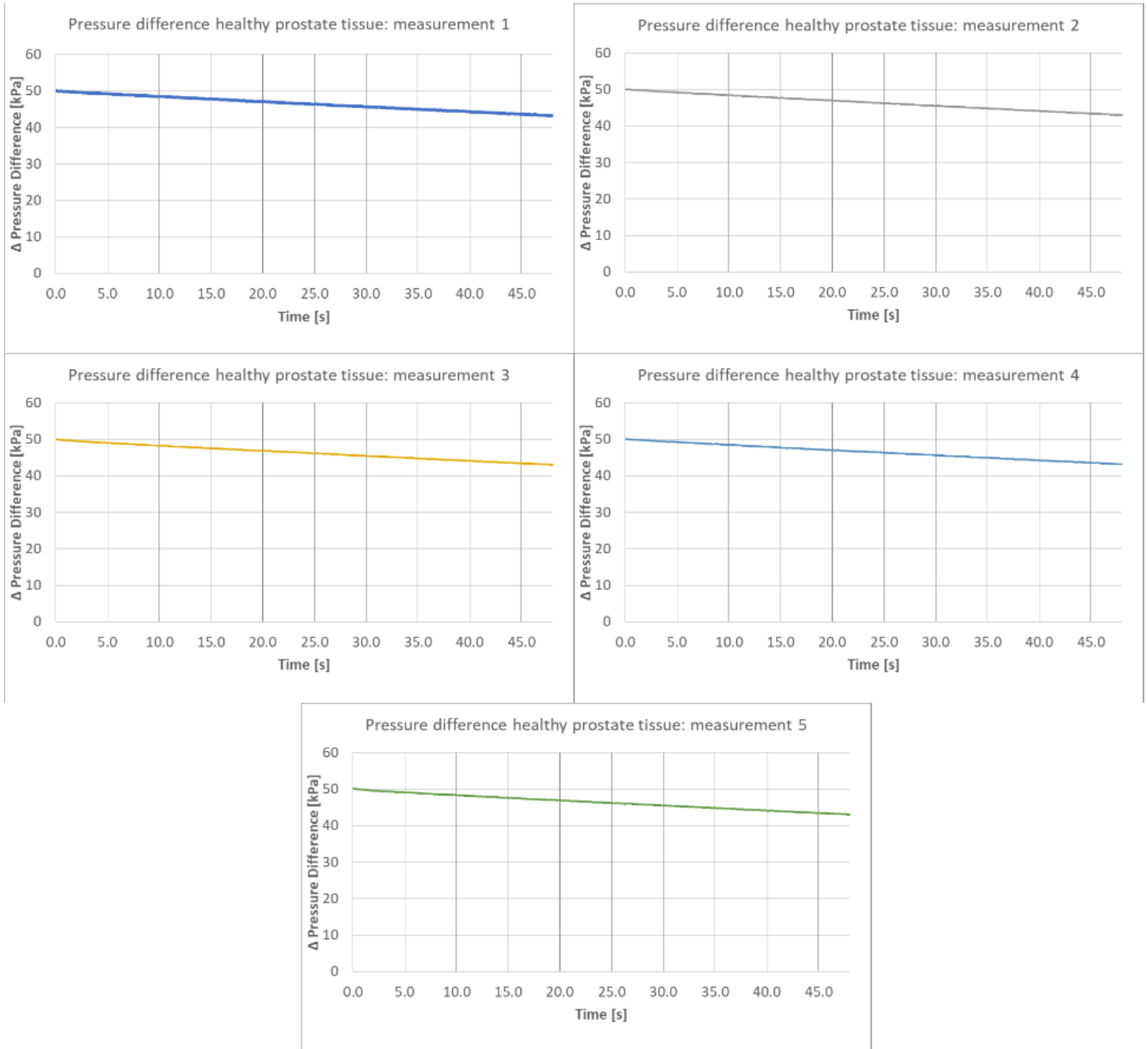


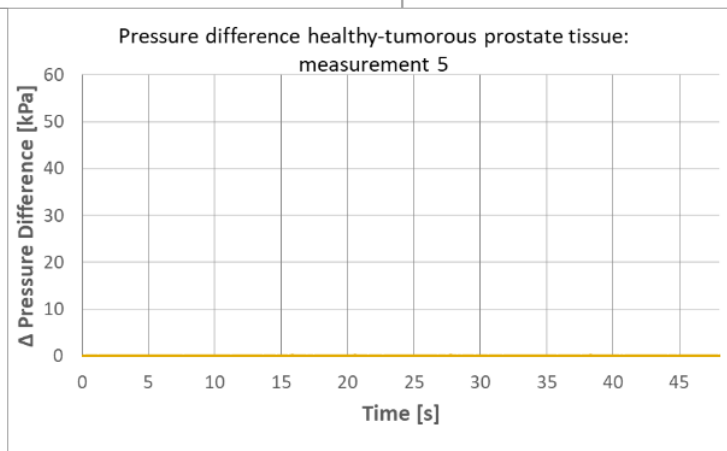
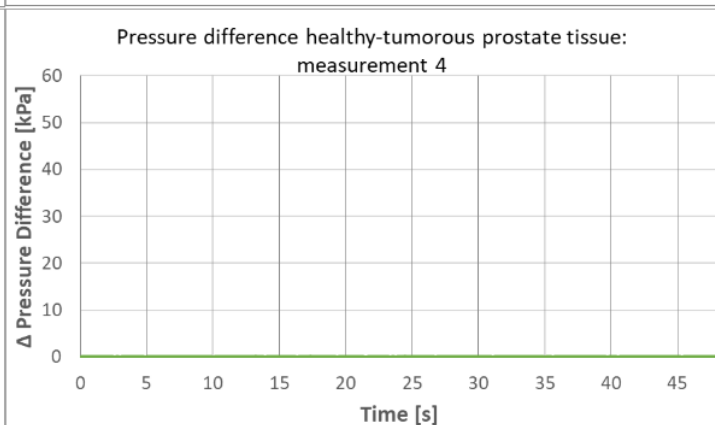
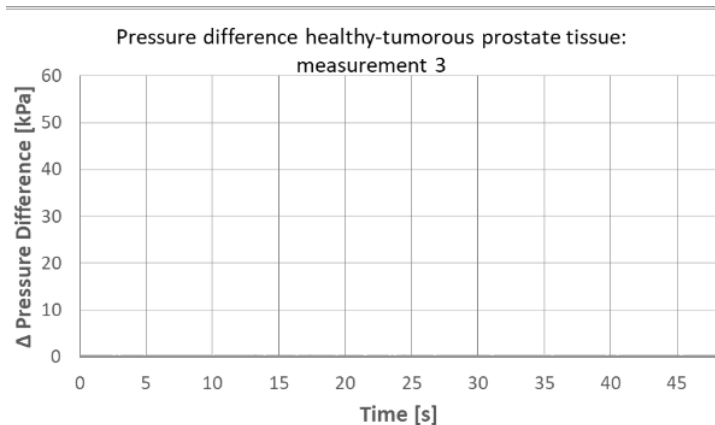
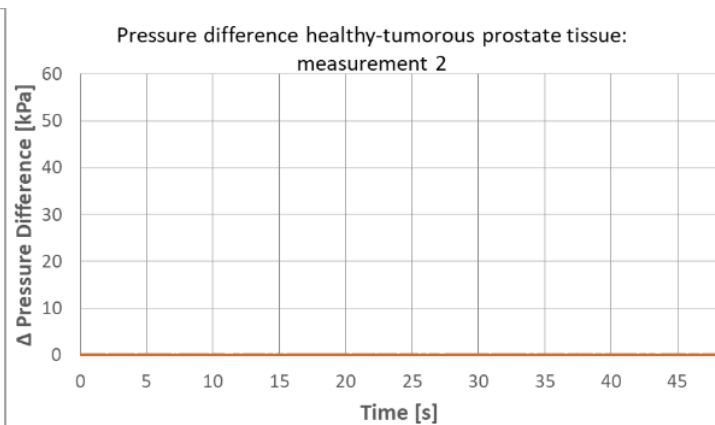
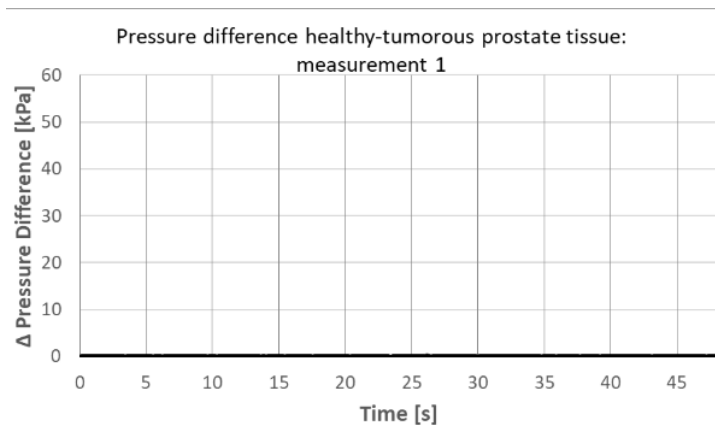
SOLIDWORKS Educational Product. For Instructional Use Only.

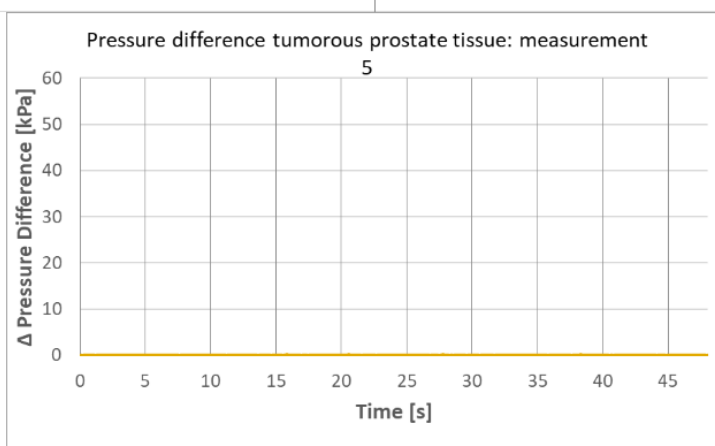
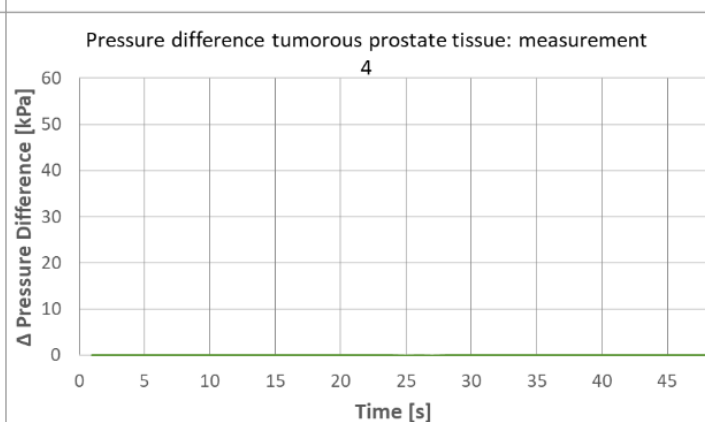
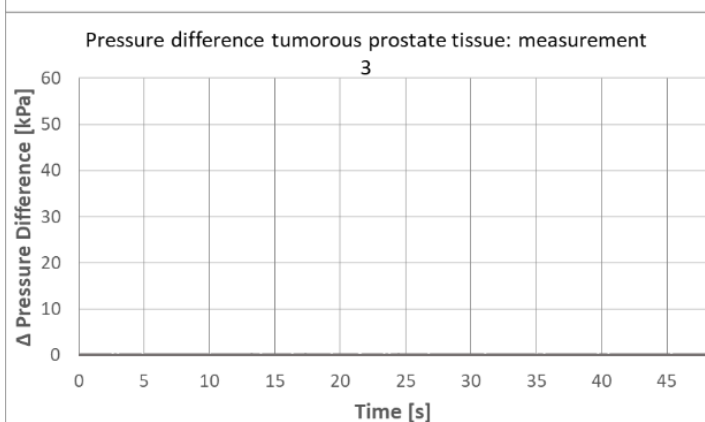
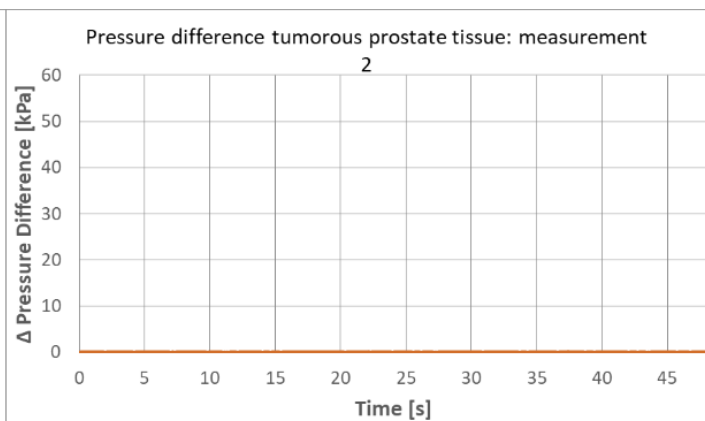
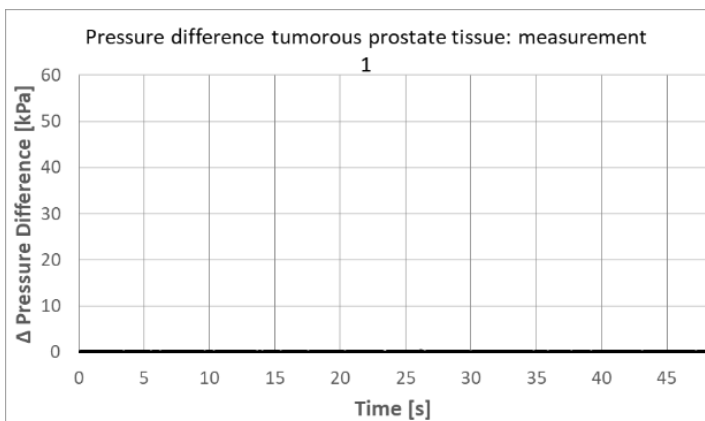


SOLIDWORKS Educational Product. For Instructional Use Only.

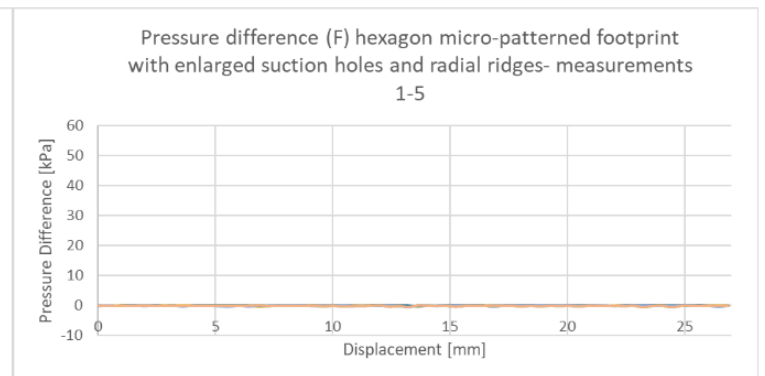
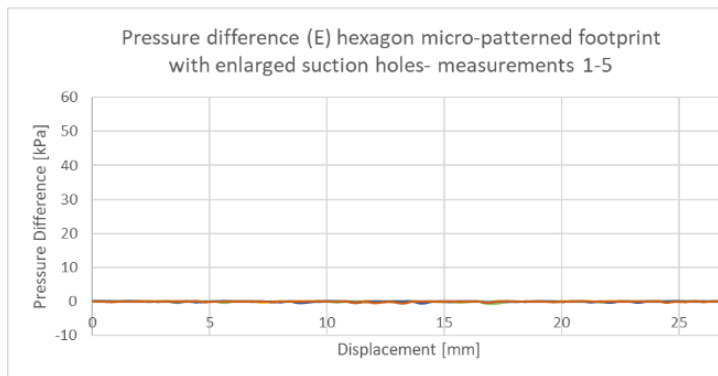
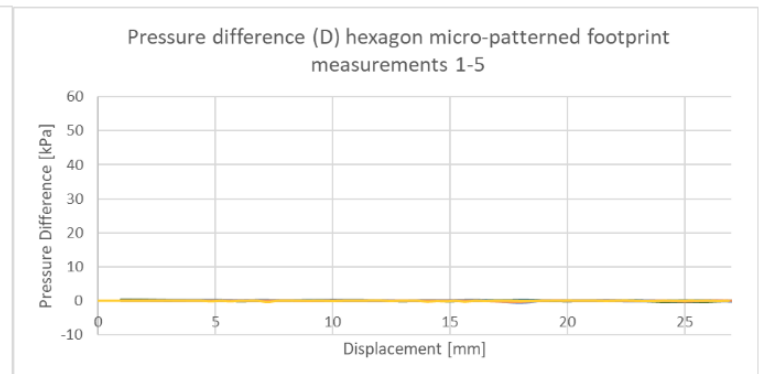
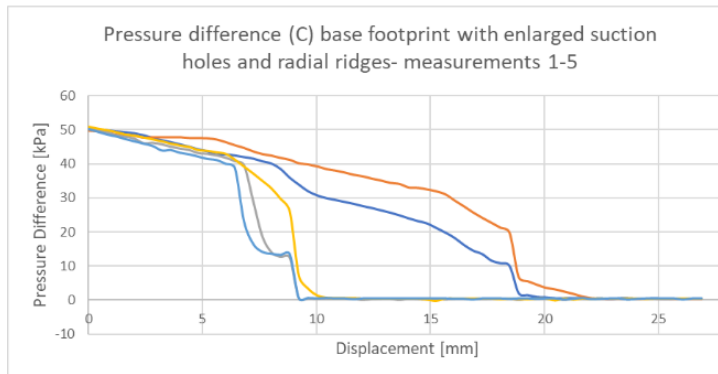
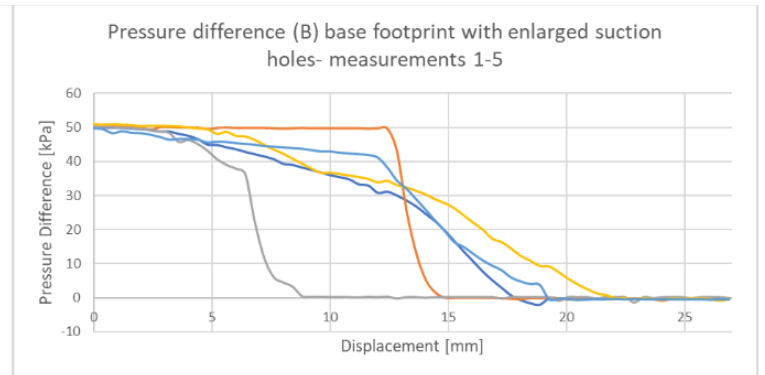
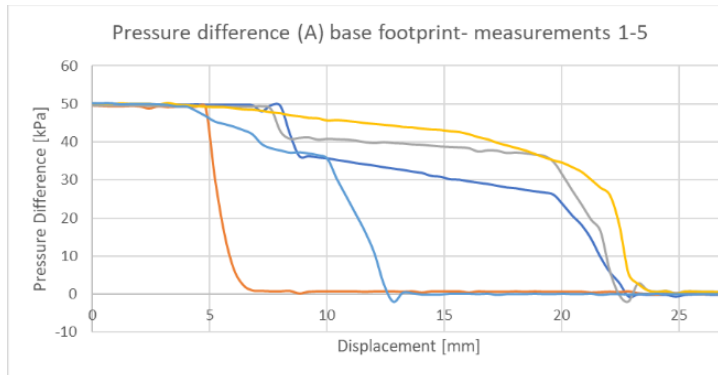
H. Experiment I graphs

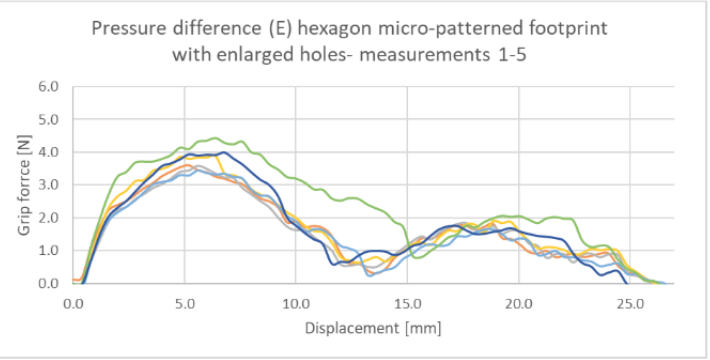
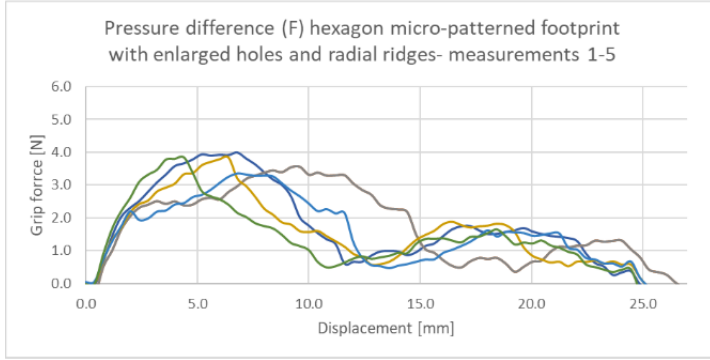
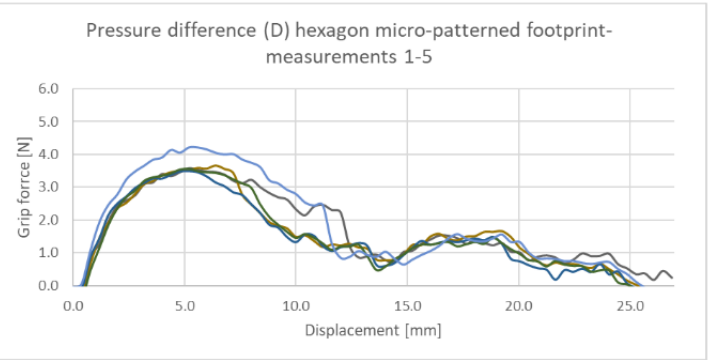
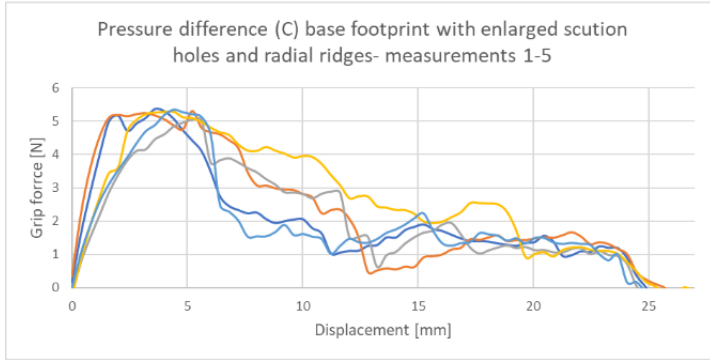
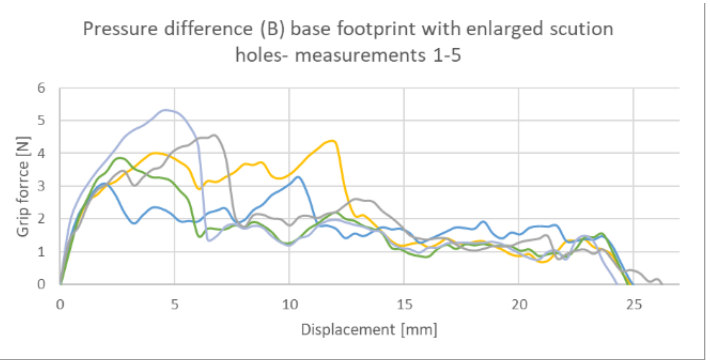
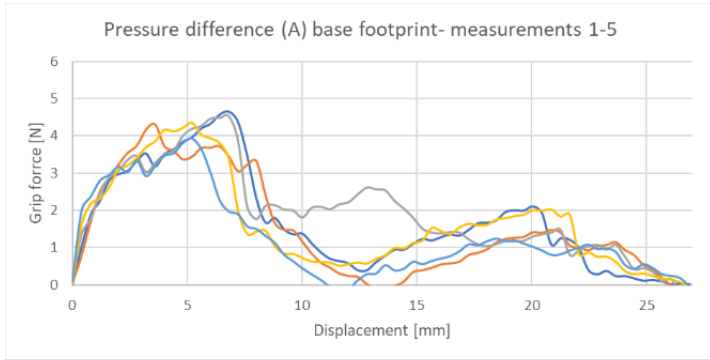






I. Experiment II graphs

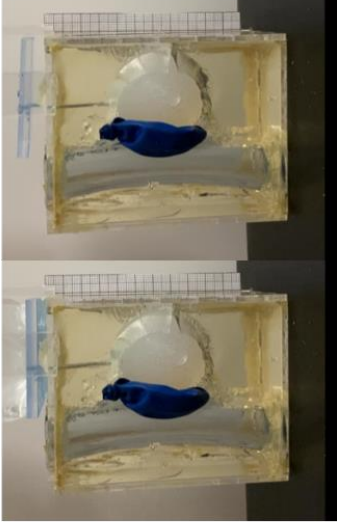




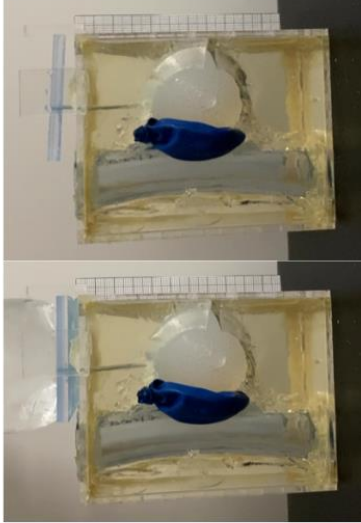
J. Experiment III graphs

No ProSTATIC

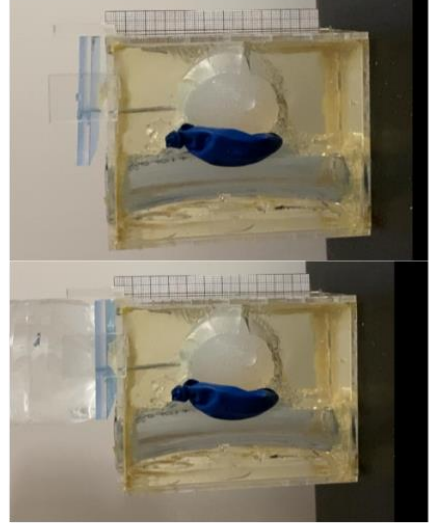
1



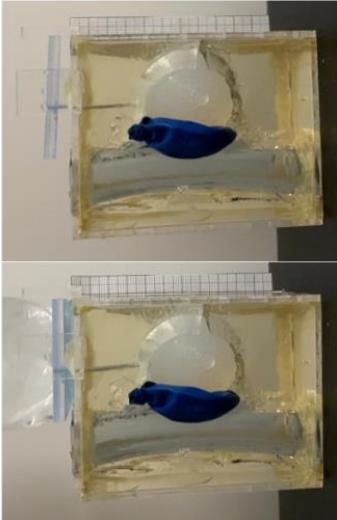
2



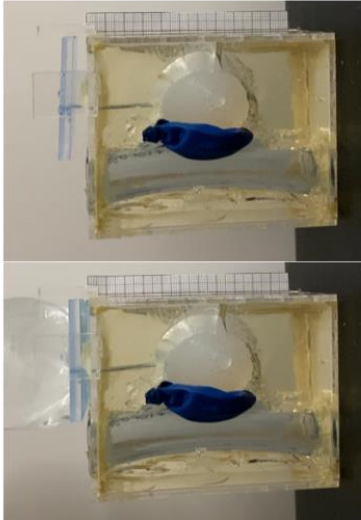
3



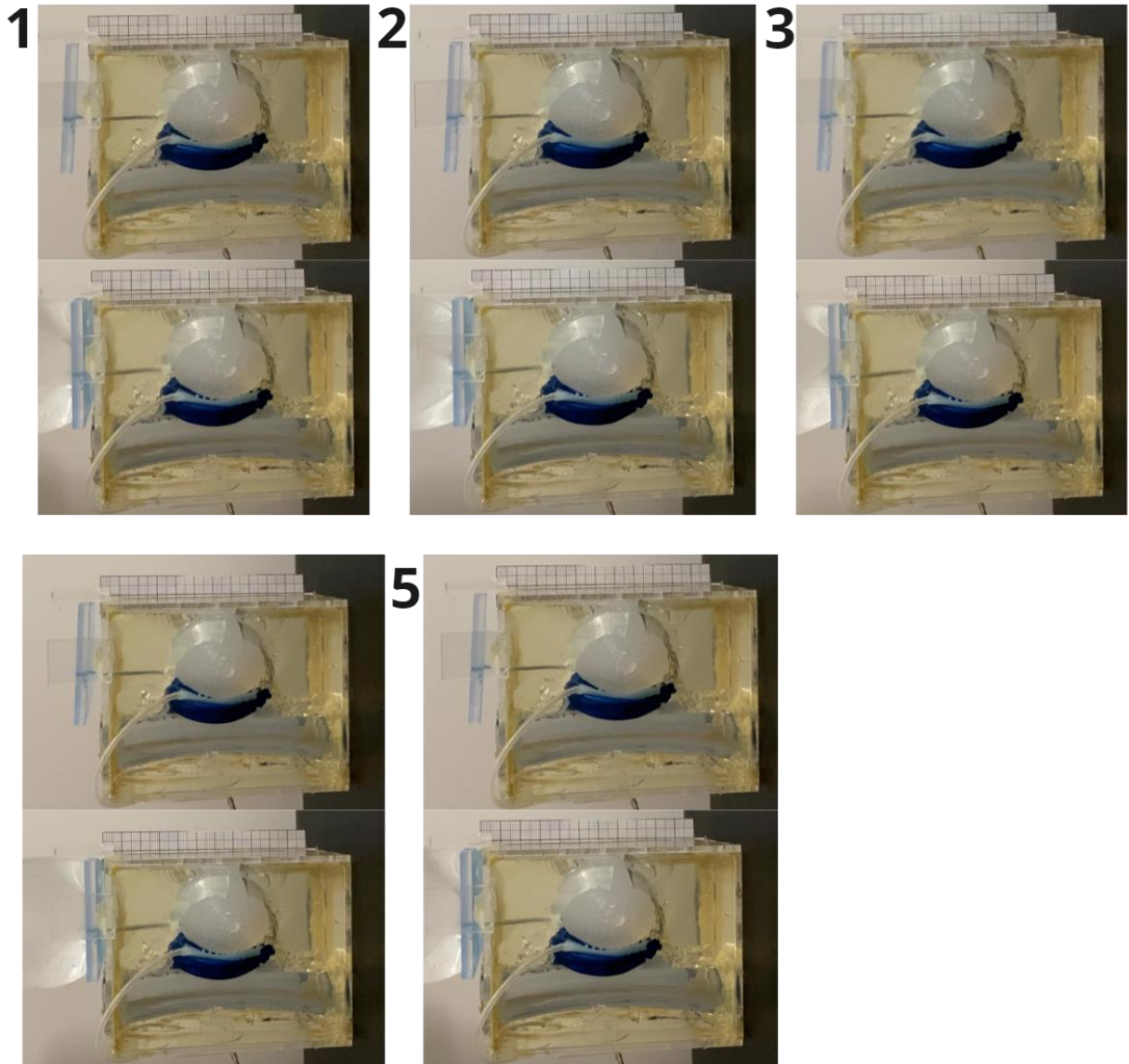
4



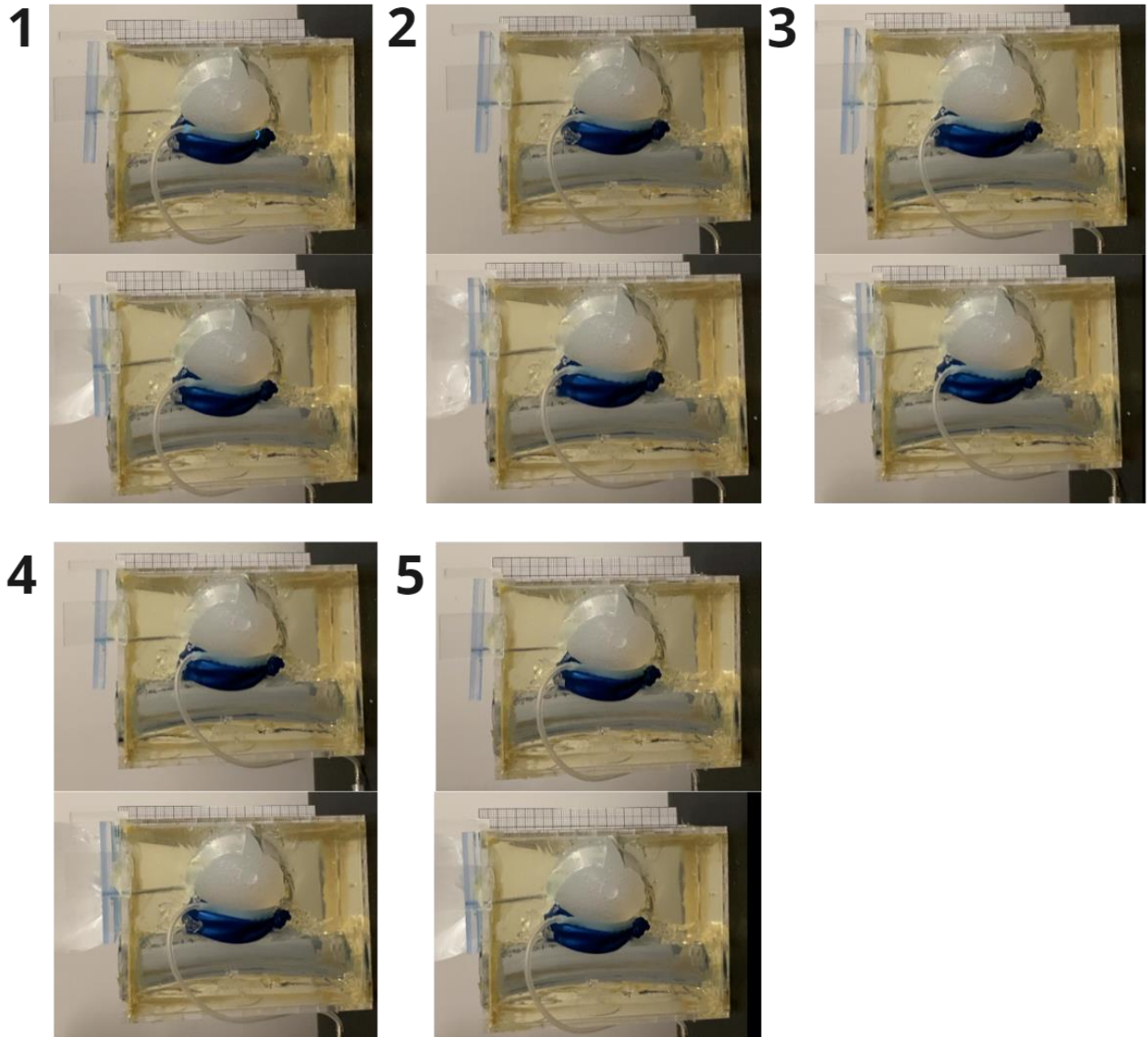
5



ProSTATIC no vacuum



ProSTATIC with vacuum



K. Normality tests

Maximum grip force data

Normality and Lognormality Tests Tabular results	A	B	C	G	H	I
	B	B+E	B+E+R	H	H+E	H+E+R
Test for normal distribution						
Shapiro-Wilk test						
W	0.9326	0.9471	0.8831	0.7436	0.8630	0.9154
P value	0.6139	0.7163	0.3235	0.0260	0.2392	0.5007
Passed normality test (alpha=0.05)	Yes	Yes	Yes	No	Yes	Yes
P value summary	ns	ns	ns	*	ns	ns
Kolmogorov-Smirnov test						
KS distance	0.2394	0.2107	0.2414	0.3546	0.2832	0.2887
P value	>0.1000	>0.1000	>0.1000	0.0389	>0.1000	>0.1000
Passed normality test (alpha=0.05)	Yes	Yes	Yes	No	Yes	Yes
P value summary	ns	ns	ns	*	ns	ns
Number of values	5	5	5	5	5	5

Prostate displacement data

Normality and Lognormality Tests	A	B	C	D
		No suction cup	No vacuum	Vacuum
Test for normal distribution				
Shapiro-Wilk test				
W		0.8810	0.8835	0.9609
P value		0.3140	0.3254	0.8140
Passed normality test (alpha=0.05)		Yes	Yes	Yes
P value summary		ns	ns	ns
Kolmogorov-Smirnov test				
KS distance		0.2305	0.3000	0.2371
P value		>0.1000	>0.1000	>0.1000
Passed normality test (alpha=0.05)		Yes	Yes	Yes
P value summary		ns	ns	ns
Number of values		5	5	5

